HIGH-THROUGHPUT ANALYSIS USING NOVEL SAMPLE PREPARATION METHOD AND DIRECT ANALYSIS IN REAL TIME MASS SPECTROMETRY

by

Wenqiang Jing

B.S., Lanzhou University, 2012

A THESIS SUBMITTED IN PARTIAL FULFILLMENT OF

THE REQUIREMENTS FOR THE DEGREE OF

DOCTOR OF PHILOSOPHY

in

THE FACULTY OF GRADUATE AND POSTDOCTORAL STUDIES

(CHEMISTRY)

THE UNIVERSITY OF BRITISH COLUMBIA

(Vancouver)

July 2020

The following individuals certify that they have read, and recommend to the Faculty of Graduate and Postdoctoral Studies for acceptance, the dissertation entitled:

HIGH-THROUGHPUT ANALYSIS USING NOVEL SAMPLE PREPARATION METHOD AND DIRECT ANALYSIS IN REAL TIME MASS SPECTROMETRY

submitted by Wenqiang Jing in partial fulfillment of the requirements for

the degree of Doctor of Philosophy

in Chemistry

Examining Committee:

David D.Y. Chen, Professor, Chemistry, UBC
Supervisor

Laurel L. Schafer, Professor, Chemistry, UBC
Supervisory Committee Member

Hongbin Li, Professor, Chemistry, UBC
University Examiner

Edward R. Grant, Professor, Chemistry, UBC
University Examiner

Additional Supervisory Committee Members:

Suzana K. Straus, Professor, Chemistry, UBC
Supervisory Committee Member

Russ Algar, Associate Professor, Chemistry, UBC
Supervisory Committee Member

Abstract

Qualitative and quantitative determination of trace compounds in complex samples is critically important in all fields of scientific research. The direct coupling of suitable sample preparation methods and direct analysis in real time mass spectrometry (DART-MS) has been shown to be a promising solution to trace analysis of compounds in complex matrices. In Chapter 1, a technical introduction of DART-MS and a review of some of the most common sample preparation techniques in trace analysis are presented. The coupling of sample preparation and DART-MS are also briefly reviewed in this chapter.

Chapter 2 presents the direct coupling of dispersive magnetic solid-phase extraction (DMSPE) to DART-MS using a metal iron probe and its application in the trace analysis of six triazine herbicides in aqueous environmental samples. The ratio of magnetic core to graphene oxide in the sorbents and other key parameters in both DMSPE and DART-MS were investigated and optimized. This developed method combined the advantages of these two analytical techniques, and good analytical performance was achieved.

In Chapter 3, a sorbent and solvent co-enhanced DART-MS method (SSE-DART-MS) was demonstrated for the determination of trace phthalic acid esters (PAEs) in water. Six common organic solvents were added on to two graphitic carbon nitride-based materials (g-C_3N_4) with different morphologies to study the enhancement effect.

In Chapter 4, nine silica-supported ionic liquids (ILs) with different hydrophobicity were synthesized. They were then used separately as coatings for the solid-phase microextraction of five PAEs followed by DART-MS analysis to study how the hydrophobicity of sorbents influence the signals of analytes in DART-MS, and further investigation is needed to verify the general trend.

In Chapter 5, the principle of deep eutectic solvent-based microwave-assisted extraction (DES-MAE) was systematically studied. The study also showed that in most cases, adding water will reduce the heating efficiency of DES under microwave irradiation, and DES containing carboxylic acid may react with cellulose, hemicellulose, and lignin to promote cell wall destruction.

Chapter 6 summarizes the work presented and provides a brief outlook for future directions.

Lay Summary

Trace analysis of target analytes in complex matrices has become increasing important in different scientific fields such as food safety, biomedical applications, and detection of environmental pollutants. This thesis mainly focuses on the development of novel analytical methods for the high-throughput analysis of analytes in complex samples. The use of dispersive magnetic solid-phase extraction with direct analysis in real time mass spectrometry (DART-MS) was achieved and successfully applied to the trace analysis of herbicides in environmental water samples. Two novel analytical methods for the analysis of phthalic acid esters, typical harmful environmental estrogens, in water samples by coupling solid-phase microextraction to DART-MS are also presented. In addition, effort has been devoted to studying the principle of deep eutectic solvent (DES), a novel ecofriendly solvent, based microwave-assisted extraction of bioactive compounds from plants, which provides valuable information for developing DES-based extraction.

Preface

The majority of the research included in this dissertation was conducted by the author, Wenqiang Jing. Chapter 2 and Chapter 3 were published previously, and they were presented in the thesis with little revision. Chapter 5 is a revised unpublished manuscript. The contribution from other collaborators and researchers are summarized in detail below.

Contribution from other researchers:

Chapter 2: the collection and filtration of environmental water samples were done by Yanying Zhou. Part of the optimization experiment was done with the help of Miao Ni. Jiaqin Wang helped analyze some experiment data. Wentao Bi and David D. Y. Chen organized the equipment, offered advice in revising the manuscript, and purchased the reagents for the experiment. The rest of research conducted in this chapter including writing the manuscript was done by me.

A version of Chapter 2 was published as:

Jing, W.; Zhou, Y.; Wang, J.; Ni, M.; Bi, W.; Chen, D. D. Y. *Anal. Chem.* **2019**, *91*, 11240-11246.

Chapter 3: the synthesis of materials and DART-MS analysis were collaboratively conducted with Yanying Zhou. Jiaqin Wang offered help in the data analysis, especially in the characterization of materials. Part of the optimization experiment was completed by Yuanfeng Zhu and Youqi Lv. Wentao Bi and David D. Y. Chen organized the equipment, conceptualized the project, offered advice in revising the manuscript, and purchased the reagents for the experiment. The rest of research conducted in this chapter including writing the manuscript was done by me.

A version of Chapter 3 was published as:

Jing, W.; Zhou, Y.; Wang, J.; Zhu, Y.; Lv, Y.; Bi, W.; Chen, D. D. Y. *Talanta* **2020**, *208*, 120378.

Chapter 4: the synthesis of materials was collaboratively conducted with Jiaqin Wang. Charaterization of materials, coating of materials, extraction of PAEs, and DART-MS analysis were conducted by me.

Chapter 5: the synthesis of DES, extraction of target analytes from rheum palmatum and discussion of principle of DES-MAE were collaboratively conducted with Jiaqin Wang. The experimental part of response surface methodology was done by Jiaqin Wang. The study of reaction between DESs containing carboxylic acids and hydroxyl groups of sugar and choline chloride was conducted by me.

Table of Contents

List of Tables

List of Figures

List of Abbreviations

AIMS	Ambient ionization mass spectrometry
AMT	Ametryn
ATZ	Atrazine
BBP	Butyl benzyl phthalate
BET	Brunauer–Emmett–Teller
DAP	Diallyl phthalate
DART	Direct analysis in real time
DEP	Diethyl phthalate
DES	Deep eutectic solvent
DHXP	Di-n-hexyl phthalate
DI	Deionized
DMSPE	Dispersive magnetic solid-phase extraction
DNOP	Di-n-octyl phthalate
DPP	Diamyl phthalate
DPT	Dipropetryn
DPhP	Diphenyl phthalate
DPrP	Dipropyl phthalate
DZN	Diazinon
EDC	1-Ethyl-3-(3-dimethyllaminopropyl) carbodiim hydrochloride
EPA	Environmental Protection Agency
FA	Formic acid
FT-IR	Fourier transforming infrared
GC	Gas chromatograph
g-C_3N_4	Graphitic carbon nitride
HS	Headspace
HBA	Hydrogen bond acceptor
HBD	Hydrogen bond donor

HRMS	High-resolution mass spectrometry
HRE	Heating reflux extraction
IL	Ionic liquid
LLE	Liquid-liquid extraction
LLME	Liquid-liquid microextraction
LOD	Limit of detection
MAE	Microwave assisted extraction
MCA	Melamine and cyanuric acid
MCE	Mechanochemical extraction
MGO	Magnetic graphene oxide
ND	Not detected
NHS	N-Hydroxysuccinimide
PAEs	Phthalic acid esters
PMT	Prometryne
PPZ	Propazine
RSD	Relative standard deviation
SEM	Scanning Electron Microscope
SMT	Simetryne
Si-ILs	Silica supported ionic liquids
SPE	Solid-phase extraction
SPME	Solid-phase microextraction
ss	Stainless steel
SSE	Sorbent and solvent co-enhanced
TGA	Thermogravimetric analysis
TM	Transmission mode
TEM	Transmission electronic microscopy
TOF	Time-of-flight
UAE	Ultrasonic-assisted extraction
UPLC	Ultrahigh performance liquid chromatography
UV	Ultraviolet

XRD	X-ray diffraction

Acknowledgements

I would like to express my sincere gratitude to my supervisor Dr. David Chen for his invaluable guidance and unconditional support throughout my PhD studies. David, your expertise, patience, and encouragement are lifetime treasures for me, and I cannot imagine having a better supervisor to work with for my PhD studies. You also provided me with more opportunities than I could ask for, which greatly expanded my horizon and made my journey toward a PhD degree enjoyable as well. It would not be possible for me to complete my PhD studies without your supervision.

I owe particular thanks to Dr. Wentao Bi from Nanjing Normal University. I consider myself as an extremely fortunate individual to have the opportunity to work with you, and your insights into analytical chemistry, continual help, and unshakable optimism have helped me grown both professionally and personally. I would like to thank UBC for offering me financial support with a four-year doctoral fellowship.

It is also a great pleasure to work with so many exceptional people. I would like to thank all my current and former colleagues in Chen Group: Akram, Cheng, Lingyu, Jess, Caitlyn, Matthew, Kevin, Jianhui, Zi-Ao, Tingting, Xianzhe, Lixian, Yuri, Adam, Julie, and Yueyang from UBC, and Haiyuan, Min, Qingsong, Xiwang, Miao, Dan, and Qian from Nanjing Normal University. Special thanks to Jiaqin Wang and Yanying Zhou from Nanjing Normal University for their generous help and being trustworthy collaborators.

Finally, I would like to express my deepest appreciation to my beloved parents and girlfriend Qing for their endless encouragement and love. Thank you for the strong faith in me and for encouraging me to pursue my dreams. For my parents, I am eternally grateful to have them

unconditionally support me both emotionally and financially. I feel truly blessed to be raised in such a wonderful family, and I will embalm your love forever.

To my parents, for their unconditional support and love.

Chapter 1: Introduction

1.1 Direct analysis in real time mass spectrometry (DART-MS)

The recent advancement of ambient ionization mass spectrometry (AIMS) technology is undeniably a breakthrough in the field of mass spectrometry (MS) by enabling the direct analysis of samples of different physical states under atmospheric conditions.[1-4] The rapid analyses by AIMS are simply accomplished by placing the sample directly in the ionization zone of the interface, whether it is in gas phase, liquid phase or solid phase. In some cases, the time-consuming sample preparation or chromatographic separation can be avoided in AIMS analysis. Among AIMS techniques, direct analysis in real time mass spectrometry (DART-MS) is one of the most established due to its commercial availability, simplicity, and robustness. The development of DART started in 2001 by Laramée and Cody with the intention of providing a safe alternative to the radioactive ion source in chemical agent monitors and industrial chemical sensors.[5] In early 2003, DART spectra were first observed when the gas stream from the prototype was directed to an atmospheric pressure interface of a MS, and a patent was filed accordingly later in the same year.[5] Since the initial publication by Cody *et al*. in 2005,[6] DART-MS has found itself enormously wide applications in various fields, such as food safety[7], quality control,[8,9] forensic,[10,11] drug development,[12] and so on.

1.1.1 Instrumentation

The general scheme of the DART-ion source is shown in Figure 1.1. The work gas (typically He or N_2) has to flow through two successive chambers in the commercial DART-ion source before it reaches the sample surface. In the first chamber, a plasma containing ions, electrons and metastable He or N_2 was produced by a direct-current glow discharge between a

needle electrode (around -3500V) and a perforated grounded electrode at atmospheric pressure.[5] Then, the metastable- containing plasma is heated in the second chamber to facilitate the thermal desorption of the analytes from the sample surface. The grid electrode near the exit of the DART-ion source is set to positive potential when the operation is in positive-ion mode and negative potential when the operation is in negative-ion mode with a low voltage. In this way, the grid electrode can prevent unnecessary ions of the opposite polarity, and electrons, from exiting the source without impeding the passage of desired metastable He or N_2, therefore reducing the signal loss by ion-ion recombination. The ceramic insulator cap at the exit of the source provides protection for the operator and sample from any high voltage.[6,13] In the commercial DART-SVP ion source (IonSense Inc., Saugus, MA, USA), the IonSense Vapur^{TM} interface is connected to a vacuum pump to maintain a proper vacuum condition and allow more ionized analytes to be detected by MS.

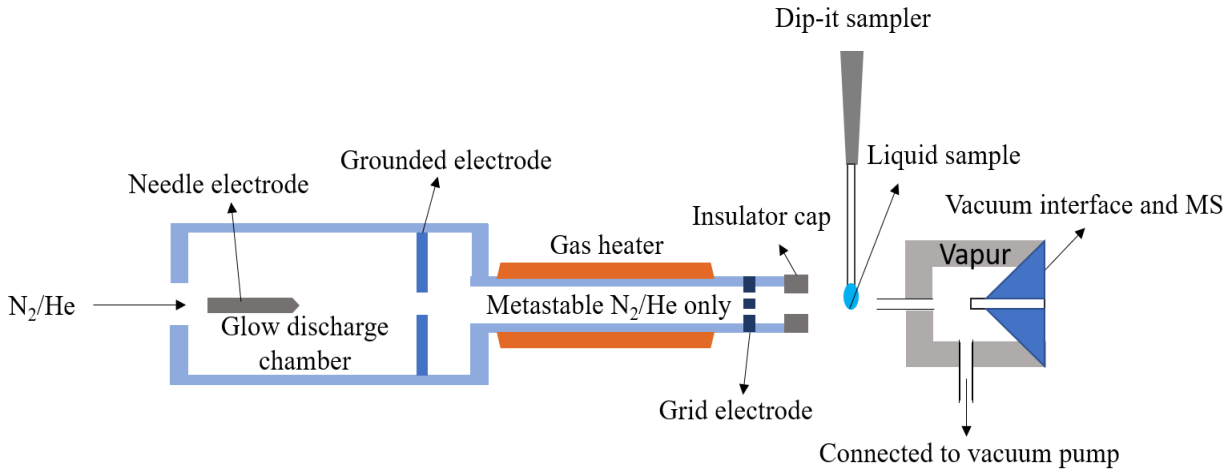

Figure 1.1 Schematic diagram of DART-ion source in the analysis of liquid sample using Dip-it sampler.

Figure 1.2 Commercial DART-SVP ion source (IonSense Inc., Saugus, MA, USA) and the analysis of liquid samples using Dip-it sampler on assembled linear rail. The white cap is the insulator cap. The heater is below the ventilation hole and the warnings for hot surface

1.1.2 Ionization mechanism

1.1.2.1 Formation of positive ions

Helium has been nearly exclusively used as DART ionization gas in DART applications, because the long-lived 2^3S excited state Helium (denoted as He* in the following text) has an internal energy of 19.8 ev,[14] which is sufficiently high to ionize common atmospheric gas and

almost all organic molecules. The He* can be generated in the DC glow discharge in the first chamber in the DART-ion source. The interaction of He* with neutral molecules (M) by Penning ionization is believed to be the initial step in the DART ionization process:

$$He^* + M \rightarrow He + M^{+\bullet} + e^- \quad (1.1)$$

where a positive ion $M^{+\bullet}$ and an electron e^- are produced.[15] For molecules with very low ionization energies, direct formation of analyte positive ions can be achieved in the above process. However, the dominating ionization mechanism for the formation of positive ions in DART involves more subsequent steps, in addition to the initial Penning ionization between He* and atmospheric water:

$$He^* + H_2O \rightarrow He + H_2O^{+\bullet} + e^- \quad (1.2)$$

$$H_2O^{+\bullet} + H_2O \rightarrow H_3O^+ + OH^\bullet \quad (1.3)$$

$$H_3O^+ + nH_2O \rightarrow [(H_2O)_nH]^+ \quad (1.4)$$

$$[(H_2O)_nH]^+ + M \rightarrow [M + H]^+ + nH_2O \quad (1.5)$$

The $H_2O^{+\bullet}$ ion formed in (1.2) participates in reactions (1.3) and (1.4) to yield pronated water clusters, which then undergo proton transfer reactions (1.5) with analyte molecule M to produce $[M + H]^+$ ion.[10,13,16]

Table 1.1 Analyte ions commonly observed in DART mass spectra in positive-ion mode.[5]

Positive ions	Origination	Analyte molecules
M^+, $M^{+\bullet}$	Penning ionization	Analytes with low ionization energies
$[M+H]^+$	Proton transfer	Polar or basic compounds. Esters, carbonyls, unsaturated hydrocarbons, and amines
$[M+NH_4]^+$	Ammoniation	Polar compounds. Esters, carbonyls, ethers, and peroxides

1.1.2.2 Formation of negative ions

In the formation of negative ions in DART, thermal electrons are supposed to produce the primary reagent ions. The electrons can be generated by Penning ionization between He* and neutrals in the gas phase (1.2), as well as surface Penning ionization between He* and the negatively biased grid electrode (S):[6]

$$He^* + S \rightarrow He + S^{+\bullet} + e^- \quad (1.6)$$

These thermal electrons are subsequently captured by oxygen in the atmosphere to produce $O_2^{-\bullet}$ ion:

$$e^- + O_2 \rightarrow O_2^{-\bullet} \quad (1.7)$$

$O_2^{-\bullet}$ ion can undergo three reactions with analyte molecules M: deprotonation (1.8), charge exchange (1.9), or formation of adduct with M (2.0):[5,13,17]

$$O_2^{-\bullet} + M \rightarrow [M-H]^- + OOH^\bullet \quad (1.8)$$

$$O_2^{-\bullet} + M \rightarrow M^{-\bullet} + O_2 \quad (1.9)$$

$$O_2^{-\bullet} + M \rightarrow [M+O_2]^- \quad (1.10)$$

For molecules with an acidic proton, deprotonation (1.8) is the dominant reaction when DART is operated in negative ion mode.

Table 1.2 Analyte ions commonly observed in DART mass spectra in negative-ion mode.[5]

Negative ions	Origination	Analyte molecules
$[M-H]^-$	Deprotonation	Analytes with an acidic proton
$[M+O_2]^-$	Anion attachment	Polarizable compounds, or compounds with hydrogen bonding.
M^-	Electron capture	Analytes with high electron affinities. Ionic liquids, or organic salts

1.1.3 Applications

1.1.3.1 Food safety and quality control

As a high-throughput, simple, and rapid analytical tool, DART-MS has been widely applied in the examination of food safety and quality control, such as detection of pesticide[18-23], melamine[24,25], mycotoxins[26-28], and characterization of food components[29-32]. Recently, a DART coupled to high-resolution mass spectrometry (HRMS) method was developed to discriminate wild-type salmon from farmed salmon.[33] 30 Major fatty acids (FAs) in salmon lipid extracts were rapidly profiled by DART-HRMS and subjected to the integration by Principal Component Analysis (PCA). The results indicated that three saturated FAs (14:0, 16:0 and 18:0), as well as unsaturated FAs with 20 or 22 carbon atoms were more abundant in wild-type salmon, while the content of three unsaturated FAs (18:1, 18:2 and 18:3) and some oxidized forms of these three FAs were found much higher in farmed salmon, which is in agreement with previous studies.

Li and coworkers proposed a DART-MS/MS method for the rapid quantification analysis of trace chloramphenicol in honey, the accuracy of which was evaluated by a validated conventional HPLC-MS/MS method.[34] Compared to HPLC-MS/MS method, DART-MS/MS showed great advantages in matrix effect reduction, time saving and cost lowering without the sacrifice of method accuracy. In this study, 52 honey samples from the local market were analyzed by both analytical methods, and the results were in good agreement suggesting that DART-MS/MS can be a powerful tool for the trace analysis of veterinary drugs in food products.

1.1.3.2 Forensics

Since the early stage of DART introduction, DART has enjoyed its great popularity in numerous forensic applications, including drugs of abuse[35-38], chemical warfare agents[39-41],

explosives[42-45], sexual assault evidence[46], and inks and dyes[47-50]. Musah *et al*. successfully performed structural studies of synthetic cannabinoids using DART with collision-induced dissociation in 2012.[51] Five different cannabinoid analogs and the mixtures of these analogs in six herbal products were identified by analysis of confirmatory structural information in DART spectra. Although DART technology has already offered forensics analysis great convenience, the on-scene analysis is still limited to some extent due to the untransportable large instrument. Brown and coworkers reported a portable DART-ion trap MS for drug analysis, providing an alternative method to carry out identifications of drugs on the scene.[52] A library of common drugs of abuse was preliminarily constructed, and actual drug samples were successfully identified in a crime laboratory and an evidence room.

1.1.3.3 Environmental analysis

Environment pollution has been gaining increasing attention of the public in modern society. The analytical methods enabling efficient, accurate and sensitive analysis of target analytes in environmental samples are in urgent need. DART-MS has proved itself a powerful tool in environmental analysis with a number of publications in this area.[53-58] Wang *et al.* demonstrated a rapid screening DART-MS based method for the determination of phenoxy carboxylic acids in water with a total analysis time around 10 min including all steps.[56] Great efforts in this thesis have also been devoted to developing high-throughput DART-MS based analytical methods in environmental analysis.

1.1.3.4 Analysis of natural product in plants

In addition to the applications of DART-MS technology in the abovementioned fields, DART-MS has also been attractive to another important field – analysis of bioactive molecules in plants, such as flavonoids[59], saccharides[60,61],alkaloids[62], and ginsenosides[63]. Ma *et al.* studied the molecular-level characterization of several different polysaccharides from six Chinese herbal medicines within seconds using a DART-HRMS method, and no sample predigestion was needed.[64] In this study, a mechanochemical extraction (MCE) was used as a sample preparation method, further accelerating the whole process. Wang and coworkers used a DART coupled with time-of-flight (TOF) MS to investigate the major components in eight traditional Chinese herbal medicines.[65] Flavonoids, ginsenosides, and alkaloids were accurately detected in these herbal medicines within seconds. Meanwhile, possible ionization mechanisms of major components in herbal medicines were discussed in the study.

1.2 Sample preparation methods

The trace analysis of metal ions and chemical compounds has been gaining increasing attention in various fields such as food safety, biomedical application, and detection of environmental pollutants. A common procedure for trace analysis usually involves sampling, sample pretreatment, separation of analytes, and quantitative and qualitative detections. Despite the recent significant advances in analytical methods and instruments, the direct introduction of samples into the instruments without any sample pretreatment may still fail to achieve satisfying results under many circumstances. The reasons for this situation are mainly due to limited sensitivity of instruments for such a low abundance and complex interferences from the background in the matrix. Besides, AIMS can only ionize analytes on sample surfaces in many

situations and may not be capable of the analysis of analytes inside samples. We hereby performed DES-based extraction to address this issue. Therefore, sample preparation plays a particularly important role in the isolation of target analytes from the complex matrix and the enrichment of target analytes. In most sample preparation techniques, a selective partitioning of solutes (S) between two immiscible phases is a fundamental process:

$$S_{phase\ 1} \rightleftharpoons S_{phase\ 2} \tag{1.11}$$

And the equilibrium constant for this partitioning is:

$$K_D = \frac{[S_{phase\ 2}]}{[S_{phase\ 1}]} \tag{1.12}$$

K_D in this equation is called partition coefficient or distribution coefficient. There is a net flow of S from phase 1 to phase 2 if the distribution coefficient K_D is large enough. To achieve an efficient selective extraction of target analytes, K_D is favored (suppose phase 2 is the extracting phase) for target analytes while unfavored for interferents. In this thesis, we focus exclusively on the extraction method when we mention sample preparation.

1.2.1 Liquid-liquid extraction (LLE)

LLE is a basic separation technique in the chemical laboratory, in which the solutes partition themselves between two immiscible liquids. The net transfer of solutes from one phase to another immiscible phase eventually leads to the enrichment of solutes. Conventional LLE can be easily performed because of the basic training of operation and easily accessible required apparatus. However, an emulsion often forms in a typical LLE procedure, and the multi-stage operation and consumption of many organic solutions make LLE not preferred by analysts in certain situations. To overcome these drawbacks, a miniaturized LLE called liquid-phase

microextraction (LPME) was developed, which uses a minimal amount of extractant. In a basic form of LPME, a syringe with a single drop of extractant (μL level) at the tip is either immersed into the sample solution or suspended onto it to enrich analytes (Figure 1.3). And there has been a growing trend towards the use of safe and non-toxic extractant in LPME, such as supercritical liquids, ionic liquids, and supramolecular solvents.[66-69]

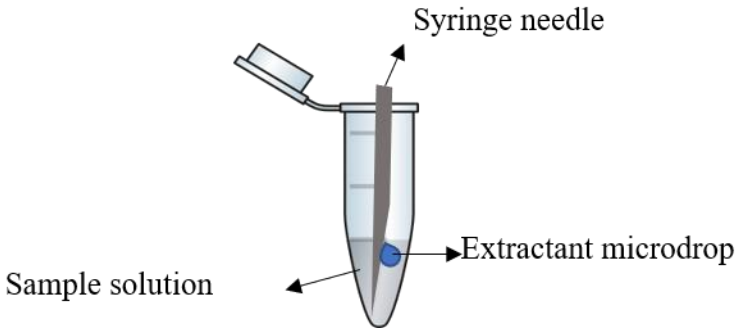

Figure 1.3 Scheme of basic form of LPME using a syringe with a single drop of extractant.

1.2.2 Conventional solid-phase extraction (SPE)

In the conventional SPE method, the adsorbent is normally packed between two frits within a cartridge. Compounds dissolved in solutions are separated on the basis of differences in their affinity to the adsorbent and the analytes of interest are retained in the solid phase (sorbents). The target analytes are then recovered for enrichment by appropriate elution. Compared to conventional LLE, a SPE method shows many advantages of being faster, easier and requires less solvent consumption.

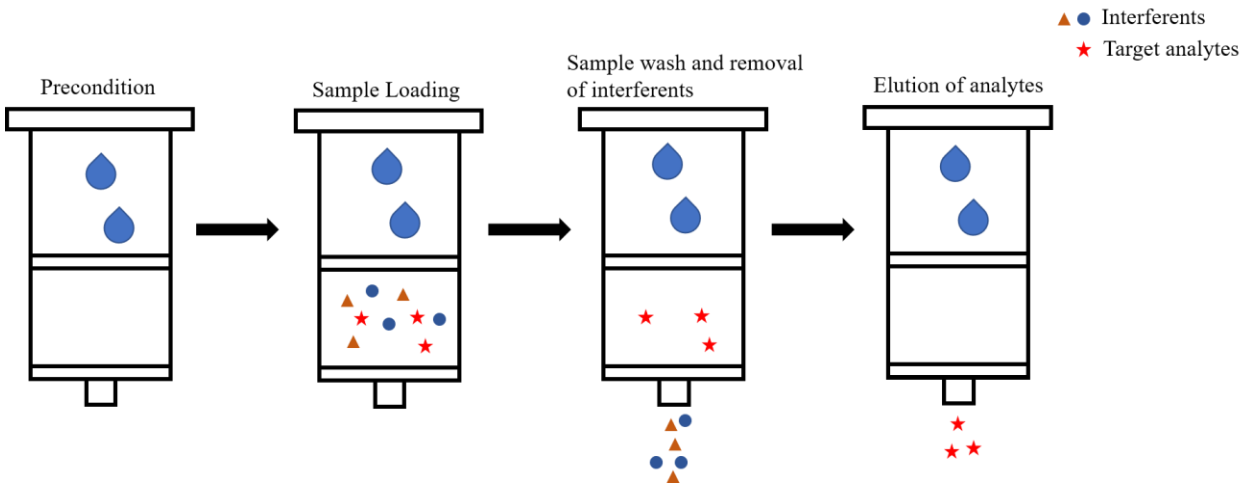

Figure 1.4 Schematic work flow of conventional SPE.

1.2.3 Solid-phase microextraction (SPME)

SPME is a promising miniaturized mode of SPE, which was first invented by Pawliszyn in 1989.[70] Generally, a fused silica of metal core fiber serves as a solid support for coatings (sorbent) with thin film in SPME. Then, a partition equilibrium of analytes can be established between the coatings on fiber and aqueous sample matrix or headspace above the sample.

There are mainly three modes of operation in SPME: direct immersion, headspace mode and membrane-protected mode.[71] The direct-immersion mode of SPME involves the direct exposure of SPME fiber to aqueous sample solution with applied agitation, and it is eminently suitable for the extraction of analytes with low volatility. When the sample matrices are too complex or contain harmful components, headspace mode is preferred which is performed by placing the SPME fiber above the sample solution with no direct contact. Compared to the direct-immersion mode, headspace mode is more appropriate for the extraction of target analytes with moderate or high volatility, and it can also be applied for extraction in gaseous phases. In a membrane-protected mode, a concentric membrane sheath is used to protect the SPME fiber from

contamination of unwanted macromolecules by allowing only the diffusion of target analytes with low molecular weight through the membrane. The membrane-protected mode enables direct contact with sample matrix with the protection of SPME fiber in analysis of real samples where the headspace mode of SPME is not applicable. In comparison to conventional SPE, SPME is a non-exhaustive, faster, portable and easily automated technique, consolidating many analytical steps such as sampling process, extraction, pre-concentration, as well as sample introduction in gas chromatography applications.

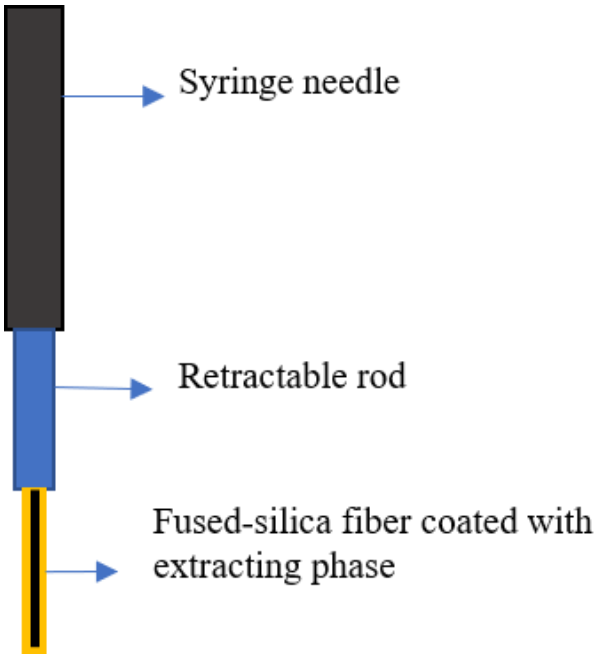

Figure 1.5 Schematic diagram of a SPME device.

1.2.4 Dispersive solid-phase extraction (DSPE)

Unlike the column-like adsorptive extraction mode in conventional SPE, a few sorbent particles are dispersed directly into the aqueous sample solutions in DSPE. After a short time of extraction, the sorbent media and solutions are usually separated by centrifugation. Subsequently,

a small volume of suitable elute is used for the desorption of target analytes. Due to the direct contact with the targeted analytes, DSPE methods usually offer high adsorption capacity, efficiency, speed and recovery.

1.2.5 Dispersive magnetic soli-phase extraction (DMSPE)

Recent years have witnessed an increasing interest in the incorporation of magnetic particles with various organic (e.g., polymers and graphene oxide) or inorganic (e.g., silica) materials as effective sorbents in SPE[72-75]. The dispersion of these magnetic sorbent composites can enhance a sufficient extraction of the target analytes. Therefore, DMSPE is essentially a type of DSPE. Nevertheless, the introduction of magnetic properties in the sorbent composites allows a more rapid, convenient, and efficient separation of sorbents with adsorbed analytes from a large volume of solution by simply applying an external magnetic field. In this way, the centrifugation or filtration steps, which are required in conventional DSPE are no longer required, which are generally considered tedious and time-consuming. Moreover, the magnetic sorbent composites have shown high selectivity and a great potential in the automation of the SPE process.[76-79]

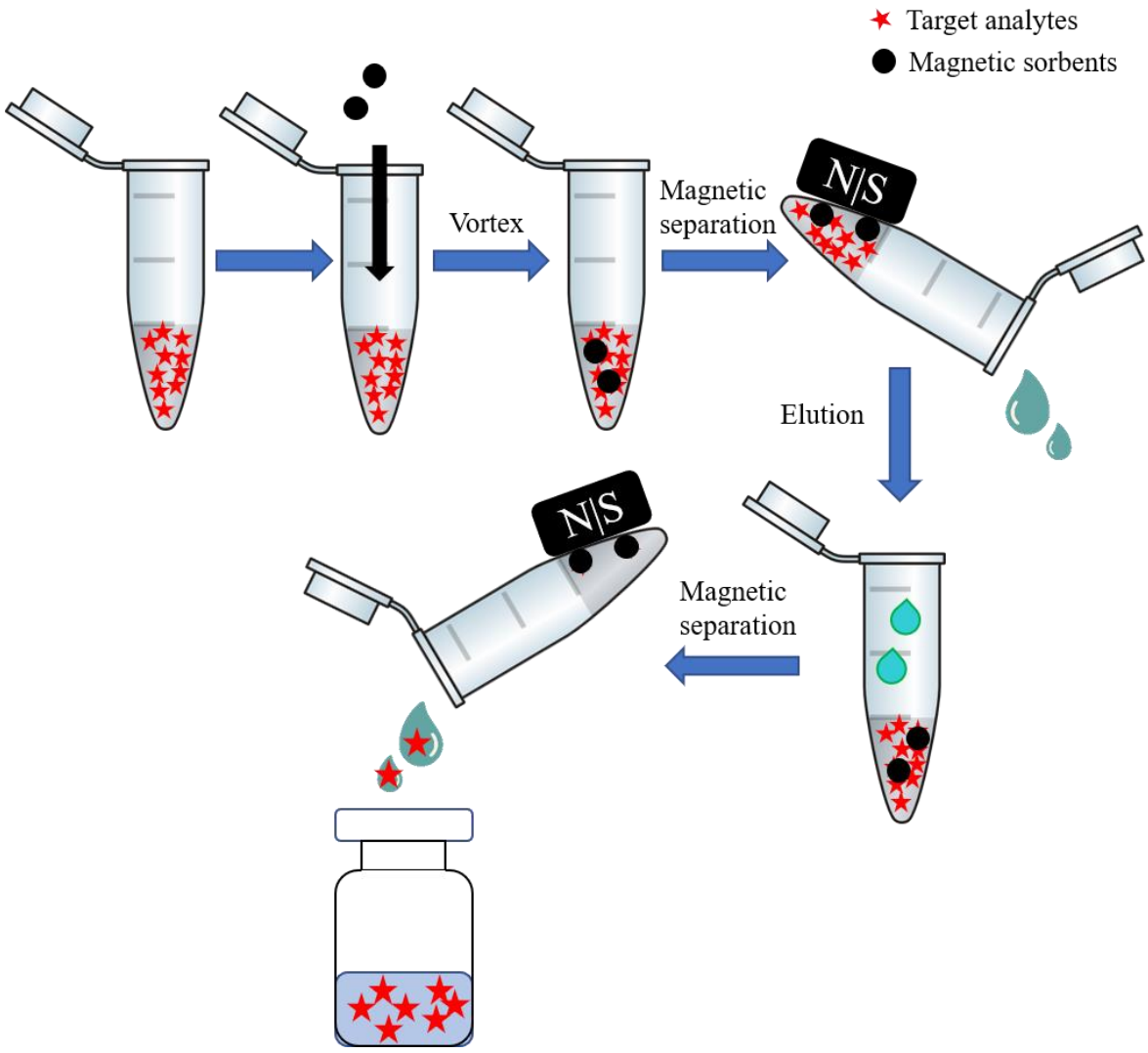

Figure 1.6 Schematic work flow of DMSPE. A few magnetic sorbents are first suspended into the sample solution. Then an external magnetic field is applied outside the vial to separate the sorbents from the solution. The eluting solvent is subsequently used to elute the analytes that are absorbed onto the sorbents.

1.2.6 Deep eutectic solvent-based extraction

Deep eutectic solvents (DESs) are an emerging type of ecofriendly solvents, that generally consist of two or more naturally occurring components including hydrogen bond acceptors (HBA, typically a quaternary ammonium salt) and donors (HBD). The hydrogen bond formation then leads to a lower melting point of DESs than any individual component. Due to their excellent

properties such as low cost, biodegradability, superior extraction efficiency, and low toxicity, they have stimulated vast interest in separation science. DESs and DESs-based materials have been widely used as efficient extraction media in many sample preparation procedures, such as LPME[80], DMSPE[81], ultrasound-assisted extraction (UAE)[82], microwave-assisted extraction (MAE)[83], and mechanochemical extraction (MCE)[84]. In Chapter 6, the principle of DES-based MAE was systematically studied and verified by extracting bioactive anthraquinones from *rheum palmatum* under optimized extraction conditions.

1.3 Coupling of sample preparation methods to DART-MS

Even though DART-MS has many advantageous features as an AIMS technique, there are still several issues that remain to be solved to improve its performance in some situations. First, in the direct analysis of real samples by DART-MS, targeted analytes usually exist at the trace amount level, and the negative background interference from complex matrix may lead to low sensitivities. Besides, some original samples are too big to be placed in the ionization zone between the gas outlet of DART and the interface, let alone achieving a high-throughput analysis. What's more, low ionization efficiency and halfway ion quenching in the air can push the sensitivity even lower without a sample preparation method. Consequently, sample preparation is necessary in many cases to improve the analytical performance of DART-MS, and many attempts have been made to the coupling of sample preparation methods to DART-MS analysis.

A single-drop liquid-liquid-liquid microextraction combined with DART-MS method was proposed by Bai *et al.*[85] for the rapid determination of multiple phytohormones in fruit juice. In this method, the acidified aqueous sample solution was firstly covered with a thin layer of organic phase (ethyl acetate and anisole, 1:1, v/v). Then a 6 μL microdroplet of diluted ammonia solution

(extracting phase) was suspended in the organic phase using a syringe during the extraction. The extraction was achieved by the equilibrium process of analytes among the sample solution, organic phase and the microdroplet. The microdroplets were finally transferred to the glass insert surface prior to DART-MS analysis.

Vaclavik and coworkers reported a modified QuEChERS method (Quick Easy Cheap Effective Rugged and Safe) for the extraction of mycotoxins from wheat and maize before quantitative analysis by DART-MS.[26] The ionization efficiencies of mycotoxins were evaluated with the DART technique initially, and accurate and sensitive analysis of toxins with good ionization efficiencies was achieved after the optimization of the QuEChERS procedure and key instrument parameters. Wang *et al.* applied a metal–organic framework MIL‐101(Cr) with large surface area in DSPE to preconcentrate triazine herbicide in aqueous samples prior to DART-MS analysis.[86] Satisfactory analytical results, including high enrichment factor, and good sensitivities and recoveries were obtained in this method. Recently, a DES-based MCE combined with DART-MS analytical protocol was developed for the high-throughput qualitive and quantitative analysis of artemisinin from aretemisia annua.[84] The entire procedure was particularly fast with a 40 s DES-based MCE and a 10~20 s DART-MS analysis for each plant sample.

The hyphenation of SPME to DART-MS is an important branch of DART-MS applications in complex samples. Generally, a SPME device is directly positioned between the DART gas exit and MS interface, and the analytes adsorbed on the SPME device are then thermally desorbed and ionized by the metastable working gas followed by MS analysis. Several modes of SPME have been successfully coupled to DART-MS depending on the geometries of SPME device: (1) conventional fiber-based SPME[87]; (2) transmission-mode (TM) SPME; (3) stir-bar sorptive extraction (SBSE)[57]; (4) in-tube (IT) SPME[88]. LaPointe and coworkers prepared two custom-made

metal fibers coated with Polydimethylsiloxane/Divinylbenzene (PDMS/DVB) and C_{18} respectively for the extraction of synthetic cathinones and relative metabolites in urine, after which the fibers were exposed to DART-MS to achieve characterization and semiquantitative analysis.[87] In addition to abovementioned modes of SPME that were coupled to DART-MS, Jastrzembski *et al.* developed a Solid Phase Mesh Enhanced Sorption from Headspace (SPMESH) coupled to the DART-MS method for the trace analysis of volatiles.[89] The PDMS-coated stainless steel meshes were prepared and used as sorbent, and this method combined the speed of DART-MS and selective extraction of SPME. The coupling of SPME to DART-MS was also explored in Chapter 3 and Chapter 4, where more details can be found.

1.4 Research objective

1.4.1 Coupling of DMSPE to DART-MS using a metal iron probe

DMSPE has been a very popular sample preparation method in analytical community for a long time, which greatly accelerates and simplifies the procedure while keeping numerous advantages of DSPE. The hyphenation of various sample preparation methods has been successfully developed to enhance the performance of DART-MS, but no attempt had been made to coupling with DMPSE before, which may synergize the superior advantages of two powerful techniques. Many aspects should be taken into serious considerations in the coupling of DMSPE to DART-MS, for instance, a proper interface, selection of appropriate sorbent, and optimization of analytical protocol. In Chapter 2, we describe the coupling of DMSPE to DART-MS using a metal iron probe for the first time and apply this novel method to the sensitive high-throughput analysis of environmental water samples.

1.4.2 Development of sorbent and solvent co-enhanced DART-MS method

As is discussed in the above, SPME has been widely used as a sample preparation method before DART-MS, nonetheless, the effect of sorbent morphology and the type of solvent on adsorption, desorption, and ionization process remains unclear in the coupling of SPME to DART-MS. And it is known that this effect significantly influences the analytical results in common sample pretreatment processes. Thus, satisfactory analytical results may be obtained by coupling SPME to DART-MS if this effect is studied in detail, which also facilitates the whole analytical process. In Chapter 3, a systematic investigation on the effect of the sorbent morphology and type of solvent in SPME-DART-MS is performed, and a novel analytical method named sorbent and solvent co-enhanced DART-MS method is developed accordingly for the high-throughput analysis of trace PAEs in aqueous samples.

1.4.3 Investigation of the effect of hydrophobicity of sorbents on DART-MS analysis

After we finished our research on the investigation of the effect of sorbent morphology and type of solvent on SPME-DART-MS, we realized that the hydrophobicity of sorbents may also influence abovementioned processes in SPME-DART-MS. The hydrophobicity of sorbents plays a key role in the adsorption capacity of sorbents, and the amount of atmospheric water near the sorbent may also vary when the hydrophobicity of sorbents is different, which may in turn influence the ionization process. In Chapter 4, we synthesized nine silica-supported ILs with similar structures but different hydrophobicity, which were used separately as coatings for the SPME-DART-MS analysis of five PAEs to study the effect of sorbent hydrophobicity on the signals of analytes in DART-MS.

1.4.4 Study of the principle of deep eutectic solvent-based microwave-assisted extraction (DES-MAE)

Due to the higher heating ability and extraction efficiency, MAE is often preferred in DES-based extraction. Despite the fact that the principle of traditional organic solvent MAE has been studied, the principle of DES-MAE remains unclear, even though it has been frequently used to enrich bioactive compounds from natural plants. Therefore, it is of great necessity that the principle of DES-MAE is systematically studied to better understand and guide the application of DES-MAE at a laboratory or industrial scale in the future. The potential coupling of DES-MAE to DART-MS analysis is also of intense interest to us. In Chapter 5, the principle of DES-MAE is investigated in detail, and the reaction between DES containing carboxylic acid and cellulose, hemicellulose, and lignin to destruct cell walls is unveiled. More efforts are being made to the coupling of DES-MAE to DART-MS.

Chapter 2: Dispersive magnetic solid phase extraction coupled to direct analysis in real time mass spectrometry for high throughput analysis of trace environmental contaminants

2.1 Introduction

Environmental pollution is one of the most significant public concerns in modern society. The analysis of trace contaminants in environmental waters allows better environmental monitoring, provides more information on the source of pollution, and makes it possible to design more effective solutions. Mass spectrometry (MS) is a powerful tool for both qualitative and quantitative determination of trace compounds in complex samples. To improve method specificity, gas or liquid chromatographic (GC and LC) techniques are usually coupled to MS for the analysis of contaminants.[90-92] However, the chromatographic processes of GC-MS or LC-MS are generally time consuming. The recent advancement in ambient ionization mass spectrometry (AIMS) enables the direct analysis of compounds under open-air conditions in their natural states by MS.[93-95] In some cases, the chromatographic separation step can be replaced by AIMS techniques.[96]

Among the AIMS ionization techniques, direct analysis in real time (DART) is one of the most widely-used due to its commercial availability, simplicity and robustness. Generally, DART-MS operates by directing a heated, electronically excited metastable gas at the sample (gas, solid or liquid) in front of the DART outlet, where the analytes are desorbed and ionized for the MS analysis.[13] DART-MS requires only a small amount of sample, has no memory effect, can be high-throughput, and has a relatively soft ionization process. When DART-MS is used alone for

complex samples, matrix effects and the lack of sensitivity can be problematic without the sample pre-concentration step. Consequently, efficient sample pre-treatments are being investigated to reduce the matrix effect and improve sensitivity. An approach by the combination of stir-bar sorptive extraction (SBSE) with DART-MS was firstly reported by Bridoux *et al.*, improving the reliability of DART-MS analysis.[57] Pawliszyn's group demonstrated the rapid determination of pesticide in food and environment samples by combining the solid-phase microextraction transmission-mode (SPME-TM) with DART-MS. The limits of detections (LODs) by this method were pushed significantly lower than that of solely using DART analysis, and the analysis time was reduced as well.[20] The use of solid-phase microextraction (SPME) with DART-MS was shown to enhance the analytical performance.[89,97-100] Significantly shorter analysis time, and better sensitivity can be achieved by combining the two processes. However, fabrication of the SPME device and possible extra coating procedures all pose challenges in real applications. Also, sometimes the need for elution of analytes increases operation steps and requires the use of organic solvent.[9,12]

Dispersive magnetic solid-phase extraction (DMSPE) is a modified form of solid-phase extraction using magnetic material as the sorbent, and has increased applications in sample pre-treatment.[101-103] Instead of using a solid phase packed cartridge, the magnetic sorbent is dispersed in the sample directly to enhance mass transfer and improve extraction efficiency. The magnetic property of the sorbent composites enables rapid phase separation by simply applying an external magnetic field. The time-consuming centrifugation or filtration steps are no longer needed, leading to faster sample preparation. This work demonstrates for the first time the use of DMSPE with DART-MS.

Usually the extracted material is recovered by an additional elution and evaporation procedure before being analyzed. However, the use of DMSPE directly with DART-MS negates this need while eliminating the matrix effect and significantly improves the sensitivity of the analysis. As for any new analytical method, many critical issues still need to be addressed for DMSPE to work well with DART-MS. The magnetic sorbent material must exhibit good adsorption efficiency toward target analytes, and the interactions between the analytes and sorbents should not inhibit the desorption and ionization processes in DART-MS. Graphene oxide (GO), which is nonmagnetic, is an efficient sorbent often used for sample preparations. In addition to its large surface area, large π conjugated system, and excellent chemical and thermal stability, GO is a superb sorbent for aqueous samples because of its rich oxygen-containing moieties, ensuring good dispersibility in water.[104] Particularly, the simple planar stack structure and excellent thermal conductivity of graphene derivatives can be used to assist in the energy transfer process from the DART gas stream to the adsorbed target molecules, facilitating the desorption and ionization process. Therefore, if incorporated with magnetic properties, GO should be a good candidate as a sorbent for DART-MS.

A magnetized probe made of an iron nail is used for collecting the sorbent of DMSPE from the water samples for DART-MS analysis in this work, showcasing the synergy between these two powerful technologies in developing high-throughput ultra-trace analytical methods for environmental contaminants. Six widely used triazine herbicides were selected as model analytes. The effect of differing ratios of magnetic cores to graphene oxide in the sorbent, and other key parameters in both DMSPE and DART-MS were systematically investigated and optimized.

2.2 Experimental section

2.2.1 Materials and chemicals

Simetryne (SMT), atrazine (ATZ), prometryne (PMT), propazine (PPZ), dipropetryn (DPT), ametryn (AMT), diazinon (DZN), 1-Ethyl-3-(3-dimethyllaminopropyl) carbodiimide hydrochloride (EDC), and N-Hydroxysuccinimide (NHS) were obtained from Aladdin Industrial Inc. (Shanghai, China). Graphene oxide was purchased from Nanjing XFNANO Materials Tech Co., Ltd. (Nanjing, China). Formic acid (FA), ferric chloride hexahydrate ($FeCl_3 \cdot 6H_2O$), anhydrous sodium acetate (CH_3COONa), glycol, sodium chloride (NaCl), and sodium hydroxide (NaOH) were purchased from Sinopharm Chemical Reagent Company Limited (Shanghai, China). All reagents were of analytical or HPLC grade and were used without further purification. Metal iron nails (length 50 mm, diameter 2.5 mm) were purchased from Meike Tools Co., Ltd. 1,6-Hexanediamine was purchased from Yonghua Chemical Technology (Jiangsu) Co., Ltd. (Changshu, Jiangsu). Three environmental water samples were collected from tap water, a pool near stadium on Nanjing Normal University Xianlin Campus, and a lake by Xianlin Hotel. Distilled water and environmental water samples were filtered by a vacuum pump and micropore filters (HA-0.45, Division of Millipore, USA) before use.

2.2.2 Sample preparation

The standard solutions of six triazine herbicides mixture (SMT, ATZ, PMT, DPT, PPZ, and AMT) at the concentration of 0.1 mg/mL were prepared in methanol and kept at 4.0 °C. These stock standard solutions were diluted with deionized (DI) water to prepare working solutions with different concentrations of six triazine herbicides mixture. The stock standard solution of internal standard DZN was prepared in methanol at the concentration of 0.1 mg/mL and stored at 4 °C. To

construct of calibration curves for quantitation with DART-MS, 6.0 μg/L DZN was spiked to all solutions with different concentrations of six triazine mixture. Triazines were individually spiked to three environmental water samples (tap water, lake water and pool water), making two final concentrations of 2 μg/L and 4 μg/L for each analyte.

2.2.3 Synthesis of MGO composite

The amino-functionalized Fe_3O_4 (Fe_3O_4-NH_2) was synthesized using a previously reported one-pot procedure.[105] In a typical batch, 1.0 g ferric chloride hexahydrate, 2.0 g anhydrous sodium acetate and 6.5 g 1,6-hexanediamine were dissolved in 30 mL glycol and the mixture was then vigorously stirred at 50 °C to form a transparent solution. Then, the solution was firmly sealed into an iron Teflon-lined autoclave and heated to 200 °C. The reaction lasted for 6 h at 200 °C and the obtained black magnetic particles were subsequently washed with deionized (DI) water and ethanol three times each with the assistance of ultrasound to remove unreacted 1,6-hexanediamine and solvent. The black magnetic powder was then dried at 50 °C for 8 hours to attain Fe_3O_4-NH_2.

Magnetic GO was prepared by the one-step covalent attachment of amino-functionalized Fe_3O_4 to graphene oxide according to the earlier reported method.[106] Three different MGOs were prepared by adjusting the feeding ratio of Fe_3O_4-NH_2 to GO ($m_{Fe_3O_4\text{-}NH_2}$:m_{GO} = 2:1, 3:1, and 4:1, denoted as M2GO, M3GO, and M4GO, respectively). In a typical synthesis of M2GO, 50 mg GO was ultrasonicated in 75 mL DI water for 1 h before the addition of 25 mg EDC and 20 mg NHS. Next, the solution was stirred vigorously for 30 min and subsequently subjected to ultrasonication for another 30 min for the formation of a homogenous suspension. Fe_3O_4-NH_2 100 mg was then added into the suspension and ultrasonicated for 30 min. Finally, the mixture was left to react at

80 °C for 2 h under mechanical stirring. The obtained MGO was washed by DI water (3 times) and freeze dried before use.

2.2.4 Characterization of MGO

X-ray diffraction (XRD) for crystal phase analysis was conducted on Rigaku D/max 2500/PC instrument. Fourier transform infrared (FT-IR) spectra (400 – 4000 cm^{-1}) were obtained on a Bruker Tensor 27 instrument using KBr pellets at the rate of 20 scans per minute. Transmission electronic microscopy (TEM) and scanning electron microscope (SEM) images were captured on a JEOL JEM-200CX and a Hitachi S-3400N II instrument respectively. BET surface areas were analyzed on a Micromeritics ASAP 2050 instrument.

2.2.5 DMSPE procedure and optimization

In a typical DMSPE process, 1.0 mg MGO was added into a solution and subjected to ultrasonication followed by vortexing for 10 min or shaking by a shaker for 10 min. The MGO with adsorbed analytes was then separated from the liquid by simply applying an external magnetic field. In the optimization of DMSPE process, 1.0 mg MGO was dispersed in 1.0 mL 2.0 μg/mL triazine standards and subjected to ultrasonication for 10 min followed by vortex for another 10 min. Then, a strong magnet was placed on the outside of the sample tube to quickly separate the sorbent from the aqueous solution. The supernatants were collected for further UPLC analysis (triplicates). Several key factors that may affect adsorption efficiency, such as salinity, temperature, and pH, were optimized. The optimizations of DMSPE were carried out for all three materials (M2GO, M3GO, and M4GO). The UPLC analysis were performed on a Thermo Dionex UltiMate 3000 UPLC system with multiple wavelength UV detection using a Luna Omega Polar

C_{18} column (2.1 × 100 mm, 1.6 μm). Ultra-pure water (A) and acetonitrile (B) were used as the mobile phase at a flow rate of 0.5 mL/min in the gradient programs: -5.0 – 0 min, 25% B; 0 – 8.0 min, 25% – 53% B; 8.0 – 8.1 min, 53 – 25%, 8.1 – 9.0 min, 25% B. The UV detection wavelength was set at 220 nm. Data from UPLC analysis were processed with Chromeleon 7.1 and Origin 8.0 software.

2.2.6 DMSPE-DART-MS method and optimization

The general scheme of DMSPE-DART-MS is presented in Figure 2.1. The DART-SVP ion source (IonSense Inc., Saugus, MA) was fitted to an Orbitrap Fusion Lumos (Thermo Fisher Scientific, San Jose, CA) mass spectrometer. Positive ion mode was used throughout the study. A web-based software (Version 5.0.5) was used to control the DART system. The DART ion source was operated with nitrogen gas in the standby mode and helium gas during analysis. The Orbitrap analyzer was used to acquire MS data under full-scan mode, and the resolution was set to 60,000. The mass range was 100 – 500 m/z. Other key MS parameters included an automatic gain control (AGC) target of 2×10^5, an ion transfer tube temperature of 300 °C, and a 100 ms injection time. The DART ion source was operated under the following conditions: wait time of heater was 5 s; the linear rail distance was optimized to 2.8 cm; the temperature of gas heater was optimized to 400 °C; contact closure delay time was set to 3.0 s; grid electrode voltage was 350 v; vacuum degree and moving speed of 12-Dip-It module on the linear moving rail was -90 kPa and 0.2 mm/s, respectively, after optimization. For the determination of LODs, single ion monitoring mode was used in the system In the study, m/z 214.1117 was used for SMT, m/z 216.1006 was used for ATZ, m/z 228.1274 was used for AMT, m/z 230.1162 was used for PPZ, m/z 242.1428 was used for PMT, m/z 256.1584 was used for DPT, and m/z 305.1074 was used for internal standard DZN

(Fig. 2.2). The LOD values were obtained based on Agilent technical note by running replicates at low concentrations, where LOD = t_α*(RSD)*(amount standard)/100%, and t_α is the Student t-test statistic using n-1 as degrees of freedom (1-α is the possibility that a measurement is greater than 0).[107] The low concentration values in estimating LODs can be found in Table A-1. The raw MS data was processed by the Xcalibur software (Thermo Fisher Scientific) and exported to Origin 8.0 (Originlab) to make the figures shown in this chapter. The measurement of each sample was repeated at least 5 times by the DMSPE-DART-MS method.

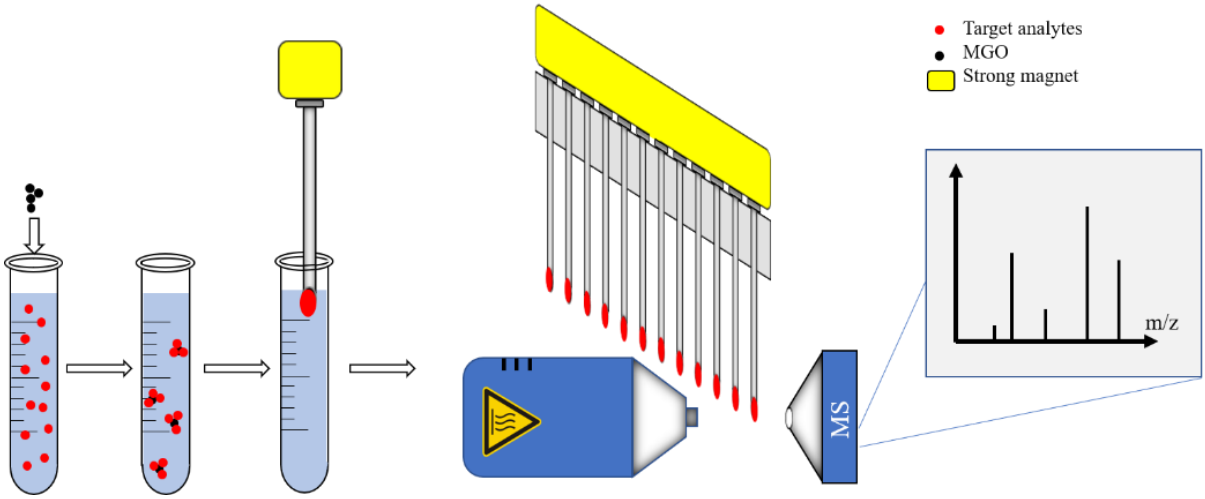

Figure 2.1 General scheme of DMSPE-DART-MS method. A small amount of MGO is added into the aqueous sample. Then the solution is subjected to ultrasonication followed by vortexing or shaking. The MGO with adsorbed analytes was then separated from the solution using the metal iron probe with a magnet before DART-MS analysis.

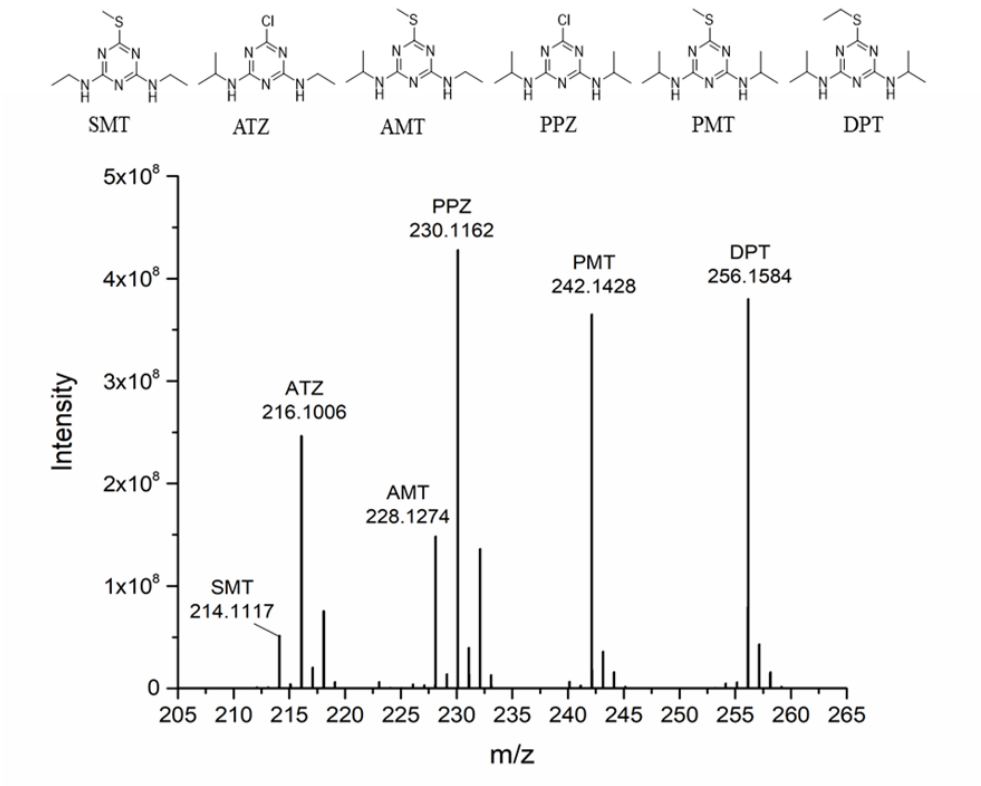

Figure 2.2 Mass spectrum of six triazine herbicides (2.0 μg/mL) obtained by DMSPE-DART-MS method under optimal conditions, and the structures of six triazine herbicides and corresponding ions are labelled.

The coupling of DMSPE to DART-MS analysis was realized by transferring MGO with adsorbed molecules onto the magnetized iron rod probe and placing magnetized probe on the commercial 12-Dip-It module for high-throughput DART-MS analysis. Typically, the probes were aligned on a 12-Dip-It module with microtiter plate spacing of DART with a strong magnet for magnetization. Then, the iron probes were inserted into the sample solutions to the depth of 0.5 cm to collect all MGO at the tip after adsorption, and the MGO at the tips was rinsed with DI water for desalination. The 12-Dip-It module with the new probes was subsequently placed on the linear moving rail assembly of DART and 5 μL 0.5% FA aqueous solution was added to MGO on each nail prior to the analysis by DART-MS.

Under the same optimal DMSPE conditions, the DART-MS signals of six triazines on M2GO, M3GO, and M4GO were compared and M2GO were selected as the magnetic sorbent in later experiments due to its slightly better results overall. To optimize key parameters of the DART ion source, 1.0 mL 2.0 μg/mL six triazine standard solutions were used in the aforementioned DMSPE-DART-MS method. In the construction of calibration curves and analysis of real water samples, 1.0 mg MGO was dispersed in 30.0 mL aqueous samples, which was spiked with 6.0 μg/L DZN as internal standard, and the mixture was ultrasonicated for 10 min followed by shaking for 10 min by an automatic shaker after the optimizations of solid to liquid ratio and extraction time, while the other steps were maintained the same as the abovementioned DMSPE-DART-MS method.

2.2.7 Validation of DMSPE-DART-MS method.

The proposed DMSPE-DART-MS method was validated by the analysis of non-spiked and spiked environmental water samples. The tap, lake, and pool water samples were individually spiked with 6.0 μg/L DZN and 2.0 μg/L and 4.0 μg/L six-triazine mixtures and analyzed by the DMSPE-DART-MS method.

2.3 Results and discussion.

2.3.1 Characterization of MGO.

The XRD pattern of GO, Fe_3O_4-NH_2, and MGO are shown in Fig. 2.3. The peak of GO at around 11.3° is attributed to the trapped water molecules between GO sheets.[108] In the XRD pattern of Fe_3O_4-NH_2, the distinct peaks at around 30.1°, 35.4°, 42.9°, 53.3°, 57.0°, and 62.6° can be assigned to crystal planes (220), (311), (400), (422), (511), and (440) respectively.[109] All the peaks

mentioned above can be found in the XRD pattern of MGO, indicating the successful binding of Fe_3O_4-NH_2 to GO sheets. The FT-IR spectra of GO, Fe_3O_4-NH_2, and MGO in the range of 400 – 4000 cm^{-1} were examined and presented in Fig. 2.3 in the Supplemental Information associated with this chapter. In the FT-IR spectrum of MGO, the assignments of adsorption peaks are listed as follows: the peak at 3430 cm^{-1} is attributed to O-H stretching or N-H stretching vibration; the adsorption peak at 1630 cm^{-1} is assigned to N-H bending vibration; peaks at 1395 cm^{-1} and 1060 cm^{-1} originate from the C-OH bending vibration and C-O-C stretching vibration on GO sheets; the adsorption peak at 574 cm^{-1} showed a Fe-O stretching vibration from Fe_3O_4-NH_2.[110-112] Accordingly, this FT-IR data suggest that the synthesis of MGO was successful. The BET specific surface areas of three MGOs were found to be 77.12 m^2/g (M2GO), 66.96 m^2/g (M3GO), and 64.33 m^2/g (M4GO). To better scrutinize the morphology and magnetic particle distribution of different MGOs, TEM and SEM images of all three MGOs were acquired. As clearly displayed on the SEM (Fig. 2.4) and TEM (Fig. 2.5) images, Fe_3O_4-NH_2 particles were densely packed onto the GO sheets. The density of Fe_3O_4-NH_2 particles on the GO sheets decrease in the order of M4GO, M3GO, and M2GO based on the TEM images of the three MGOs. These results confirmed the formation of MGO composites with different Fe_3O_4-NH_2 content.

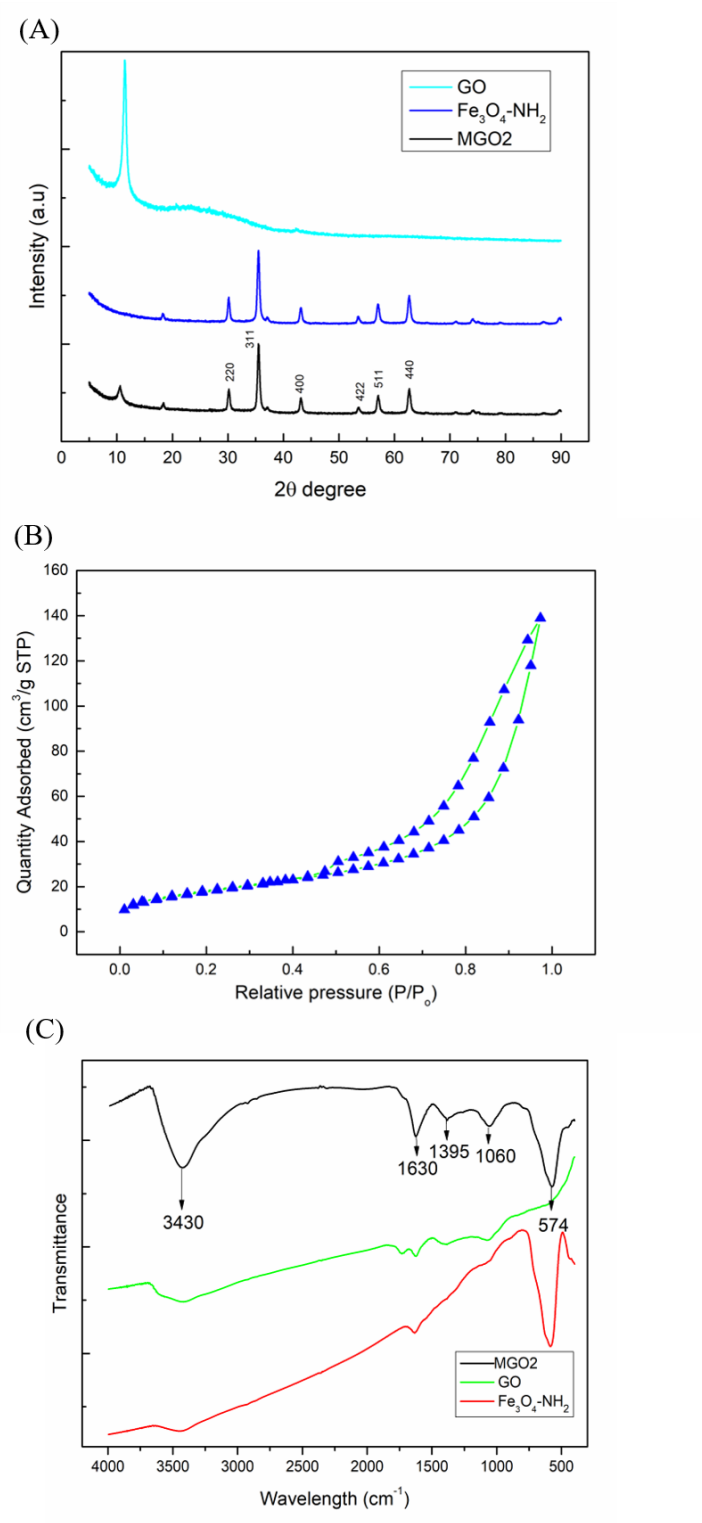

Figure 2.3 Characterizations: XRD analysis (A) of Fe_3O_4-NH_2, M2GO, and GO; BET (B) of M2GO; FT-IR spectra (C) of Fe_3O_4-NH_2, M2GO, and GO.

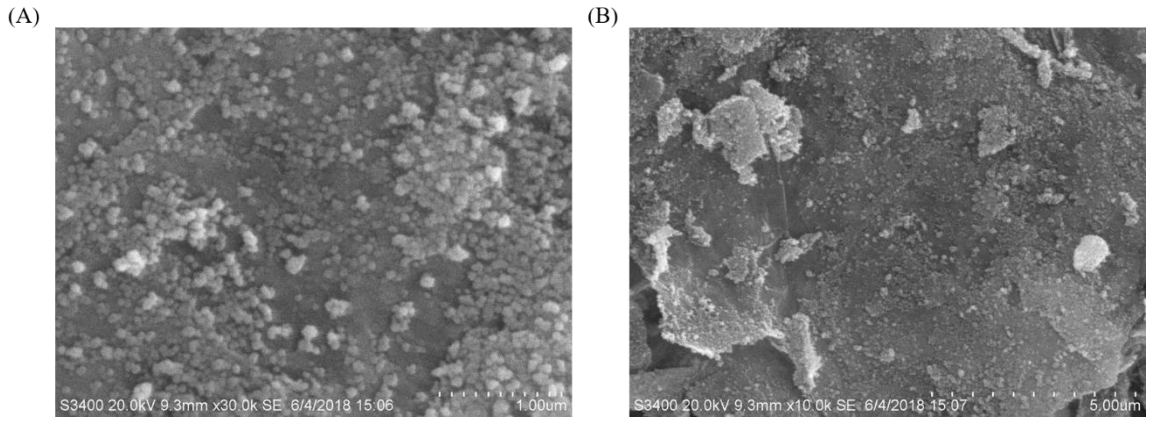

Figure 2.4 SEM images of M2GO on different scales: (A) at 1.00 µm; (b) at 5.00 µm.

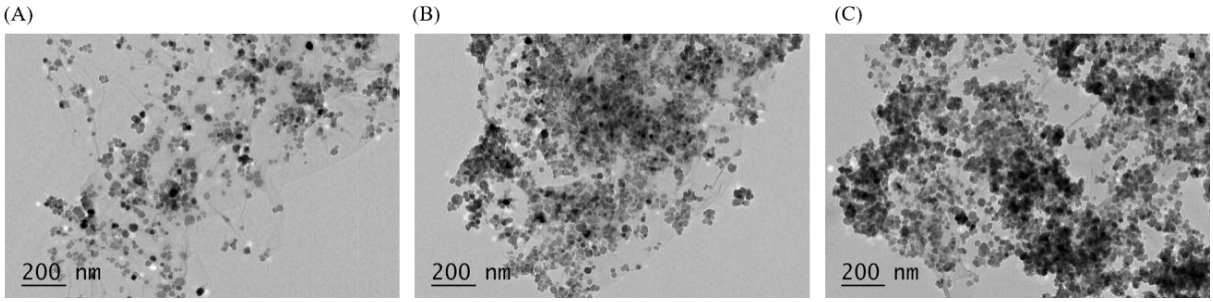

Figure 2.5 TEM images of Three different MGOs: (A) M2GO; (B) M3GO; (C) M4GO.

2.3.2 Optimization of DMSPE-DART-MS procedure.

To achieve the best possible analytical performance of the DMSPE-DART-MS method, several critical factors were systematically investigated and optimized on both the DMSPE and DART-MS procedures, using the six triazines as model analytes.

In the DMSPE process, the effect of initial concentration of standard triazine solutions on three MGOs was first examined (Fig. A-1). Standard triazine solutions (2.0 µg/mL) were used later in the optimization process. As seen in Fig. A-1, the adsorption capacity of the chlorine-containing triazines (ATZ and PPZ) was lower than the four triazines containing sulfur (SMT, AMT, DPT,

and PMT). The more electronegative chlorine atom makes ATZ and PPZ more polar than the other four triazine herbicides, which increases their solubility in water but reduces their adsorption capacities on MGO. The pH of the sample solutions is also an important factor affecting extraction efficiency because it may change the form of analytes and interactions between analytes and sorbents. The pH of the sample solutions was adjusted by adding hydrochloric acid or sodium hydroxide to access a pH range of 3.0 – 11.0. Based on the experimental results (Fig. A-2), the best adsorption was achieved under pH 7.0. Hence, pH 7.0 was used for all sample solutions in this study. Another significant factor affecting adsorption efficiency is the salinity of sample, which changes the ionic strength of the solutions. The addition of salt can introduce a salting-out effect, decreasing the solubility of organic molecules in aqueous phase and increasing their mass transfer to the sorbent. On the other hand, the addition of salt increases the viscosity of the sample media and may hinder the mass transfer in the adsorption process. The salinity of the sample solutions was adjusted by adding sodium chloride (NaCl) in the range of 5% – 30%, which is the maximum solubility. As is presented in Fig. A-3, more salt dissolved in the sample solutions leads to better adsorption efficiency. Consequently, 30% NaCl was added into each sample solution before processing. As is known, the temperature of solution can affect the interaction between analytes and sorbent, the solubility of compounds, and the viscosity of solution, which have a significant influence on the adsorption mechanism. However, no distinct difference in enrichment was observed from 25 °C to 45 °C (Fig. A-4). Therefore, all sample solutions were processed under room temperature without further optimization.

To further improve the sensitivity and analytical performance of the method, optimization of several other parameters of the DART ion source were also performed. High vacuum conditions allow more ionized molecules to be detected by MS, therefore, -90 kPa was used in the experiments

after optimization (Fig. A-5A). Because DART is a thermal desorption-based ambient ionization technique, higher temperature may facilitate the desorption process in the DART system. Compared to other temperatures used, MS signals were the highest at 400 °C (Fig. A-5B). A clear decrease in signal intensity was found with the faster moving velocity of the linear rail in the range of 0.2 – 1.0 mm/s (Fig. A-6A), hence the rail speed of 0.2 mm/s was selected. The slower linear rail speed results in longer exposure of the sorbents to the DART ion source, resulting in better MS signals. The distance from the DART ion source to the linear moving rail was varied by adjusting the linear rail distance. The largest peak areas appear to be obtained at the closest distance from the DART outlet to the sorbents (Fig. A-6B). The linear rail distance at 2.8 cm was then set for the rest of the study. Before carrying out quantification experiments and analysis of real water samples, solid/liquid ratio and extraction time were optimized in the sample solutions with a constant concentration of 3.0 μg/L. A larger sample volume contains more analyte molecules that can be adsorbed and detected, but the mass transfer rate is constrained to some extent. The best scenario was determined to be 1.0 mg M2GO in 30.0 mL sample solutions (Fig. A-7A). Thereafter, the extraction equilibrium was reached after 10 min ultrasonication and 10 min of shaking (Fig. A-7B). To explore the minimum extraction time in DMSPE-DART-MS method with the instruments in our lab, the total extraction time can be shortened to 7 min by vortex, as shown in Fig A-7C.

2.3.3 Coupling of DMSPE to DART-MS.

To couple DMSPE with DART-MS, designing a suitable sample probe is essential. The probe needs to properly fit into the moving sample introduction rail in the commercial DART ion source, and easily magnetized at low cost. Precise measurements of the 12-Dip-It module were

first obtained to establish the basic geometry of the desired interface, such as the inner diameter (ID) of the sampling position on 12-Dip-It module and the distance from the top of 12-Dip-It module to the DART outlet. Then, a metal iron nail was used as the probe with proper configurations installed (Fig. 2.6). The radius of the nail head was larger than that of the hole used to hold the sample probes in the 12-Dip-It module such that it naturally sits on the sampling rail. A magnet was placed on top of the nail head and securely held the nail in place. If the bottom of the interface is cylindrical, the materials will gather together around the bottom surface of the cylinder due to gravity and more importantly, the stronger magnetic field at the outer edge of the bottom surface, and the agglomeration of materials may hinder the contact of helium stream from desorbing and ionizing the target molecules inside the clump, reducing the desorption and ionization efficiency. Moreover, in our study, peak splitting was observed when using probes with a cylinder-shaped bottom (data not shown). In contrast, the magnetic materials are evenly distributed around the circular cone-shaped, tapered tip of the nail, and the delivery of metastable He stream to MS inlet is with much less physical blockage. Therefore, the purpose of circular cone-shaped bottom of the nail is to support enough magnetic sorbents and promote efficient ionization and desorption processes. The length of the nail body is selected to make sure that the bottom circular cone part is right in the front of the DART ion source outlet. (Fig. 2.6)

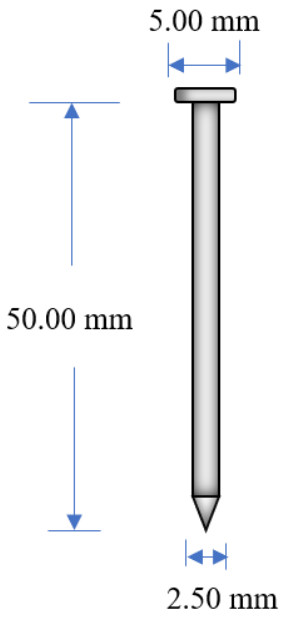

Figure 2.6 Dimensions of the metal iron nail as suitable interface.

Suitable magnetic sorbents for the triazine herbicides should be selected and used in the DMSPE-DART-MS method. First, the magnetic sorbent must exhibit enough adsorption capacity toward triazines and have good dispersibility in water. The magnetic sorbent should also have a strong magnetic property so that it is firmly attached onto the bottom of the probe. In addition, the analytes on the magnetic sorbent should be easily desorbed and ionized when exposed to the DART ion source. MGO showed good adsorption ability toward triazine herbicides and its abundant oxygen-containing groups provide good dispersibility in water. The noncovalent interaction between MGO and triazines, including π-π interactions, hydrogen bonds, and the hydrophobic effect, all make the online desorption of analytes by DART easier without sacrificing adsorption. What's more, the simple planar stack structure and excellent thermal conductivity possibly facilitate the energy transfer from the DART ion source and boost the desorption and

ionization processes. Therefore, MGO was selected as the magnetic sorbent in DMSPE-DART-MS due to its physicochemical properties.

Different ratios of GO and magnetic Fe_3O_4-NH_2 particles in MGO composites may produce different analytical results. An increased amount of Fe_3O_4-NH_2 in MGO prevents the aggregation of GO sheets and increases the magnetic strength of MGO, providing firm attachment to the iron nail probe. However, the analyte extraction and desorption/ionization efficiencies might be weakened due to the decrease in GO content in MGO. This reduced GO content may lead to a decrease in adsorption interaction and thermal conductivity of MGO, which impedes the desorption process. To evaluate the adsorption capacity between MGOs with different ratios of Fe_3O_4-NH_2 and GO, three MGOs were tested under the optimal DMSPE conditions. The minimum ratio of Fe_3O_4-NH_2 to GO in MGO was set to 2:1 to prevent the MGO from escaping the nails and entering MS. Slightly larger peak areas of the six triazine herbicides were observed on M2GO than those on M3GO and M4GO (Fig. 2.7), indicating that a higher content of GO in MGO may improve the analytical performance of DMSPE-DART-MS given the sufficient magnetization properties of MGO.

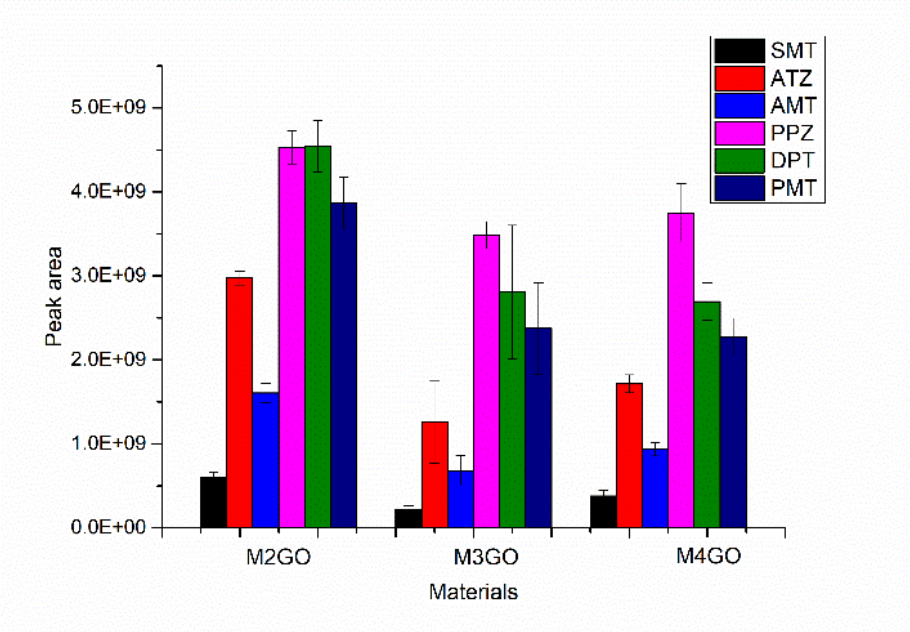

Figure 2.7 Comparison of analytical performance of M2GO, M3GO, and M4GO under optimized DMSPE conditions by DMSPE-DART-MS method. Simetryne (SMT), atrazine (ATZ), prometryne (PMT), propazine (PPZ), dipropetryn (DPT), ametryn (AMT), and diazinon (DZN).

Interestingly, the DART-MS signals of analytes were found to be different when the sorbents on the interface were dried, wetted by water, or wetted by aqueous acid solution (Fig. 2.8). The DART-MS signals from sorbents dried in air for 10 min were significantly lower than those obtained under the other two conditions, which might be explained by the ionization mechanism of DART. In a positive ionization mechanism, the heated metastable He ionizes the water molecules in the air or around the sample to form ionized water clusters. The analytes are then ionized by these ionized water clusters via proton transfer.[13] Since the number of water molecules around the sorbent decreased after drying, ionization of molecules by DART was also reduced. More ionized molecules may be carried to MS through the evaporation of water molecules in wetted samples under high temperature, resulting in stronger MS signals. Compared

to the moisturization by water, the addition of 0.5% FA aqueous solution increased the overall DART-MS signals of the six triazine herbicides. The addition of FA might weaken the ion pairing interaction between the triazines with carboxy groups on GO, thereby enhancing the desorption efficiency.[113] This DMSPE-DART-MS method not only utilizes the advantages of both techniques, but also leads to a synergy of high sensitivity and elimination of elution of extractants and separation step using organic solvents.

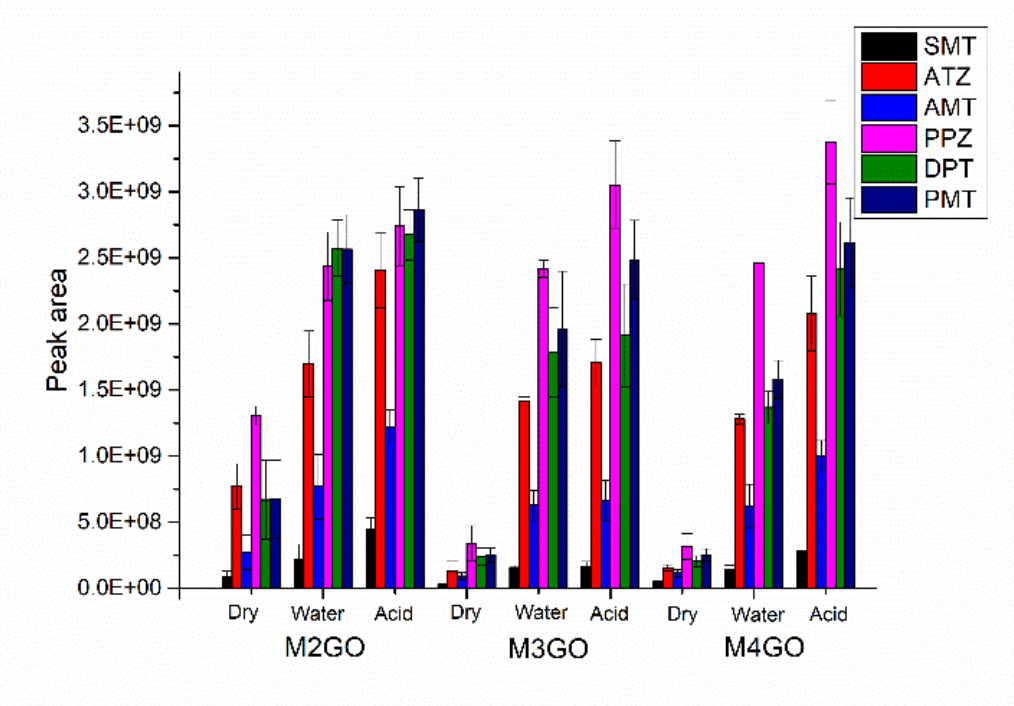

Figure 2.8 Effect of sorbent conditions on the DART-MS analysis. Three MGOs were all involved in the study of this effect. Dry, water, and acid labels on the x-axial means sorbents under dry condition, moisturized with water, and moisturized by 0.5% FA aqueous solution respectively. The samples/bars are defined as in Figure 2.7.

2.3.4 High-throughput analysis and validation of DMSPE-DART-MS.

The method of DMSPE-DART-MS were evaluated by the analysis of six triazine herbicides in both the standard solutions and in the environmental water samples under the optimized experimental conditions. The MGO sorbents were all firmly attached to the probes during the entire procedure, no significant contamination of the MS by the MGO composites was observed. The calibration curves (Fig. A-8) of the six triazine herbicides were established with good linearities ($R^2 \geq 0.99$) by plotting the average peak area ratio of analytes to IS versus the concentration of target analytes. The LODs were in the range of 1.6 –152.1 ng/L for the six triazines (Table A1). These LODs are substantially lower than the maximum allowable levels for an individual herbicide at 1 μg/L and total herbicide at 3 μg/L in surface waters required by the US Environmental Protection Agency (EPA) and the European Union (EU). [114] The present method was used to the determination of triazine herbicides in three real water samples (tap, lake, and pool water). No triazine herbicides were found in the water samples by our method except for 0.079 μg/L AMT detected in the lake water. This level conforms with EU standards for drinking water. Good recovery rates (87.5 – 115.0 %) with relative standard deviations (RSDs) between 1.9% to 10.2% were obtained in the analysis of three environmental water samples with spiked level of 2.0 and 4.0 μg/L. These findings indicated the matrix effects from complex environmental water samples were minimized with adequate precision and accuracy using the DMSPE-DART-MS method. The analytical results are summarized in Table 2.1.

Table 2.1 Summary of analytical results in the analysis of six triazine herbicides by DMSPE-DART-MS

Analytes	Spiked level (μg/L)	Tap water			Pool Water			Lake Water		
		Found average (μg/L)	Recovery (%)	RSD (%)	Found average (μg/L)	Recovery (%)	RSD (%)	Found average (μg/L)	Recovery (%)	RSD (%)
SMT	0	ND	NA	NA	ND	NA	NA	ND	NA	NA
	2	1.99	99.3	7.7	1.82	91.0	7.5	2.14	107.0	3.8
	4	4.02	100.5	8.9	4.10	102.5	1.9	4.12	103.0	2.9
ATZ	0	ND	NA	NA	ND	NA	NA	ND	NA	NA
	2	1.90	94.9	8.5	2.05	102.7	10.2	2.03	101.5	7.5
	4	4.43	110.9	6.4	4.12	103.0	5.6	3.93	98.3	3.6
AMT	0	ND	NA	NA	ND	NA	NA	0.08	NA	4.7
	2	2.04	101.8	9.3	1.97	98.2	7.7	2.21	106.2	4.1
	4	4.60	115.0	6.1	3.98	99.5	7.5	4.46	109.2	8.6
PPZ	0	ND	NA	NA	ND	NA	NA	ND	NA	NA
	2	1.98	98.8	8.8	1.89	94.3	7.6	2.25	112.5	9.8
	4	4.55	113.6	2.4	4.03	100.6	4.1	4.02	100.4	3.7
PMT	0	ND	NA	NA	ND	NA	NA	ND	NA	NA
	2	1.75	87.5	9.8	1.95	97.3	7.5	1.91	95.5	6.8
	4	4.45	111.2	5.2	4.21	105.2	7.6	4.54	113.4	8.4
DPT	0	ND	NA	NA	ND	NA	NA	ND	NA	NA
	2	2.16	108.0	10.1	2.20	110.1	3.6	1.82	91.1	9.1
	4	4.57	114.2	2.2	3.58	89.4	9.0	3.93	98.2	7.9

Note: ND: not detected; NA: not applicable. The analytical performance may vary between different batches of GO used in the method.

2.3.5 Comparison of DMSPE-DART-MS to other methods.

Previously reported analytical methods using different sample pre-treatment approaches and detection techniques for the analysis of triazine herbicides in aqueous samples are listed in Table 2.2. The lower LODs by the proposed method used in this study demonstrate the apparent higher sensitivity of the DMSPE-DART-MS in this chapter compared to those of the other methods shown in the table. In addition, the analysis time by DMSPE-DART-MS was also significantly shorter than those of the other methods due to the high-throughput analysis by DART-MS while the extraction time is comparable to those of the other methods. A point worth mentioning is that an extra elution procedure is needed in almost all other methods listed in the table. The use of organic solvents makes these methods less environmentally friendly. In contrast, the online desorption in DMSPE-DART-MS eliminates the need for an elution step, further simplifying the analytical process and making the method more efficient. Only 1.0 mg of M2GO is used in our method for the analysis of samples with a volume of 30.0 mL, which is also lower than the other methods with similar sample volumes. Consequently, the comparison with different analytical methods demonstrated that the described DMSPE-DART-MS is a green, highly efficient, and sensitive method for the high-throughput trace analysis of environmental contaminants in aqueous sample.

Table 2.2 Comparisons of DMSPE-DART-MS method with other preciously reported analytical method for the analysis of triazine herbicides in environmental water samples.

Sample preparation	Detection technique	Sample matrix	Sample Vol. (mL)	Sorbent amount (mg)	Enrichment time (min)	Analysis time (min)	LODs (ng/L)	Recoveries (%)	Precision (% RSD)	Ref.
DMSPE	DART-MS	Environmental waters	30	1	20 (shaking) 7 (vortex)	0.25	1.6 – 152.1	87.5-115.0	1.9-10.2	This work
SPE	DART-MS	Lake water	20	5	20	NA	100- 200	85.0-110.0	NA	[115]
DMSPE	HPLC-DAD	Environmental waters	250	25	20	30	25 - 40	89.0-96.2	2.2-5.6	[116]
DMSPE	HPLC-UV	Surface water	50	40	15	15	90 -150	97.0-100.8	1.6-3.8	[117]
SPME	GC-MS	Environmental waters	15	NA	20	17	50 - 100	70.0-108.0	5.1-10.2	[118]
SPDE	GC-FID	Environmental waters and juice	9	NA	NA	30	2600 - 42000	82.1-93.5	4.4-9.1	[119]

Note: SPE: solid-phase extraction; DAD: diode array detection; GC: gas chromatography; SPDE: solid-phase dynamic extraction; FID: flame ionization detector.

2.4 Conclusion.

In summary, the direct coupling of DMSPE to DART-MS was achieved for the first time, and successfully applied to the high-throughput trace analysis of six triazine herbicides in environmental samples. As for any other analytical method, the successful deployment for solving real world problems requires careful consideration of the challenges and systematic optimization. The described method not only operationally synergizes the two powerful analytical techniques, but also leads to higher sensitivity and better selectivity. A completely reusable, low-cost probe using a magnetized metal iron nail with a simple configuration to fit into the 12-Dip-It module of the DART kit, served as the interface for the coupling. MGO was easily synthesized with two steps and used as an efficient sorbent. The effect on analytical performance by altering the GO content in MGO was optimized. In addition, key parameters in both DMSPE and DART-MS were thoroughly investigated and optimized. Compared to previously reported methods, DMSPE-DART-MS has many better characteristics such as minimal usage of sorbent, high sensitivity, simple operation procedure and high-throughput. Unquestionably, the analysis of triazines by DMSPE-DART-MS as described in this study is just one use for this method. This new analytical platform shows tremendous potential and new applications in the high-throughput trace analysis of various environmental contaminants will be investigated in the future.

Chapter 3: Sorbent and solvent co-enhanced direct analysis in real time-mass spectrometry for high-throughput determination of trace pollutants in water

3.1 Introduction

Direct analysis in real time-mass spectrometry (DART-MS) is an ambient MS method developed in 2005.[6] It has been successfully used for qualitative and quantitative analysis of a broad range of analytes. It is high speed and high throughput, with good salt tolerance and can be used directly with many different types of samples.[56,120-124] A heated stream of metastable ionized gaseous nitrogen or helium atoms from the DART ion source is generated to induce Penning-type ionization of surrounding atmospheric components, which produces the reactive species, such as pronated solvent clusters including pronated water clusters. The surface of the sample in its native state is exposed to the electronically excited gas, and the dislodged analytes from the sample surface are ionized by proton transfer from the reactive species. The ionized analytes are then delivered to the MS for analysis.[13,125] Although DART-MS has many attractive features, some issues still need to be addressed when dealing with complex real samples. Because the analytes of interest often exist in a complex matrix and in trace amounts, using DART-MS alone may suffer from interference of the matrix and result in low sensitivities.[88,126-128] In addition, satisfied analytical results are not easy to obtain when the proton affinities of analytes are low, because the ionization of analytes are achieved by proton transfer from protonated solvent clusters in DART-MS. Quenching of ions in the air and the low ionization efficiency may decrease the sensitivity further.[125] Therefore, sample pretreatment steps are required under many circumstances to improve the sensitivity and reduce the matrix interference in DART-MS analysis. As a matter of fact, in

order to improve the sensitivity, one should resist the temptation of omitting the sample preparation step unless only a quick positive or negative confirmation is required.

Solid-phase microextraction (SPME), a solvent-free, and non-exhaustive extraction technique, has been widely used for preconcentration of trace analytes in environmental,[129,130] biological,[131,132] food,[133-135] and pharmaceutical samples.[136-138] In a typical SPME, a fiber coated with layers of coatings is usually used to adsorb analytes in the sample matrix. The large surface area of contact between the adsorbents and the sample enables fast mass transfer and rapid extraction.[139] Additionally, the thin layers of coatings on the fiber effectively shorten the equilibration time and facilitate the passage of the ionized molecules to the mass spectrometer.[140-143] The fibers can be easily adjusted to fit into the moving rail in the commercial DART kit box. The combination of SPME with DART-MS resulted in an excellent integration of two technologies in a simple and highly efficient analytical platform. Wang and co-workers demonstrated an online coupling of in-tube SPME to DART-MS method for the first time and successfully applied the method to the analysis of six triazine herbicides in juice and water.[88] The method was based on the coupling of the novel mode of SPME method to DART-MS. The organic eluents from the absorbing materials were analyzed by DART-MS. It is known that the types of sorbents and solvents used in the sample pretreatment process have significant influence on the analytical results [144,145]. Similarly, in SPME coupled to DART-MS, the adsorption, desorption, and ionization of the analytes are also believed to be possibly influenced by the morphology of the sorbent and the type of solvent. Therefore, good analytical results may be achieved using SPME-DART-MS if these two crucial factors, which also facilitate the whole analytical process, are optimized.

In this chapter, the effect of sorbent morphology and the type of organic solvent used on DART-MS analysis was systematically investigated and a high-throughput analytical method,

using sorbent and solvent co-enhanced direct analysis in real time-mass spectrometry (SSE-DART-MS) for the determination of trace pollutants in water, was demonstrated. Five phthalic acid esters (PAEs), which are typical harmful environmental estrogens,[146] were chosen as the analytes to evaluate the effectiveness of the SSE-DART-MS method. Graphitic carbon nitride (g-C_3N_4)-based materials were chosen as the sorbents because they have a double-sided polyaromatic scaffold with a large π-electron system that gives them a strong affinity for aromatic compounds commonly present in drugs, pollutants, and biomolecules. g-C_3N_4-based materials having two morphologies were used to systematically investigate the effects of sorbent, and six solvents were used to study the effect on the enhancement of DART-MS signals. The SSE-DART-MS method development strategy presented here can be used for the high-throughput determination of other trace analytes in liquid samples.

3.2 Experimental section

3.2.1 Materials

Melamine (purity≥99.0 %) and cyanuric acid (purity≥98.0 %) (MCA), D-glucose (purity≥99.5 %), dimethyl sulfoxide (DMSO) (purity≥99.0 %), diethyl phthalate (DEP), butyl benzyl phthalate (BBP), di-n-hexyl phthalate (DHXP), di-n-octyl phthalate (DNOP), and diamyl phthalate (DPP) were purchased from Aladdin Industrial Inc. (Shanghai, China). Tetra-deuterated internal standard of D_4-phthalate (2-) ethyl ester (D_4-DEHP) was purchased from Shanghai ZZBio CO., LTD. (Shanghai, China). Distilled water was vacuum filtered (HA-0.45, Division of Millipore, U.S.A.) prior to use. Acetonitrile, ethanol, methanol, and hexane were purchased from by Sinopharm Chemical Reagent Co., Ltd. (Shanghai, China). Kafuter Red RTV Silicone Adhesive was purchased from Guangdong Hengda New Materials Technology CO., LTD.

(Huizhou, China). All the chemicals and solvents were of Analytical Reagent Grade and were used as starting materials without further purification. The standard solutions of five PAEs mixture at the concentration of 0.1 mg/mL were prepared in methanol and kept at 4.0 °C. The stock standard solutions were diluted with deionized (DI) water to prepare working solutions with different concentrations of five PAEs mixture and stored at 4.0 °C.

3.2.2 Synthesis of g-C_3N_4 and g-C_3N_4/C

Pristine g-C_3N_4 was prepared by a modified method reported previously.[147] The precursor of g-C_3N_4, MCA, is spontaneously formed after mixing equimolar solutions of 4.00 g (31.68 mmol) melamine in 80 mL DMSO and 4.08 g (31.68 mmol) cyanuric acid in 80mL DMSO at 29 °C. After 4 hours the white solid obtained was washed by alternating ethanol and double-distilled water for 5 times. The solid was vacuum dried at 80 °C for 12 h. Upon calcining at 500 °C in a tube furnace with a heating rate of 2.3 °C min^{-1} for 4 h under argon atmosphere, MCA polymerizes to form g-C_3N_4 with the release of ammonia. g-C_3N_4/C was obtained by calcining D-glucose using a previously reported method:[147] Melamine (4.00 g, equivalent to 31.68 mmol)was dissolved in 160 mL of DMSO at 29 °C. Then 12.48 g (69.27 mmol) of D-glucose and 4.08 g (31.68 mmol) of cyanuric acid were both dissolved in 80 mL of DMSO under the same conditions. The cyanuric acid and D-glucose solutions were then slowly added dropwise into the melamine solution. The white that was generated after reaction at 29 °C for 4 h, was collected by centrifugation and washed repeatedly with ethanol and double-distilled water 5 times. After drying in a vacuum oven at 80 °C for 12 h, the sample was calcined in a tube furnace with a heating rate of 2.3 °C min^{-1} and maintained at 500 °C for 4 h under argon atmosphere, yielding black solid particles.

3.2.3 Characterization of g-C_3N_4 based materials

Scanning Electron Microscope (SEM) analysis was performed with a JSM-7600F spectrometer (Akishima-shi, Japan). Fourier Transform Infrared (FTIR) (Bruker Tensor 27) spectra were obtained between 400 and 4000 cm^{-1} at the rate of 20 scans/min using KBr pellets. Transmission electron microscopy (TEM) images were captured with an H-7650B (Hitachi, Japan) transmission electron microscope with an accelerating voltage of 80 kV. X-ray diffraction (XRD) studies were performed with a high brightness source Rigaku SmartLab 9kW instrument. Thermogravimetric analysis (TGA) was conducted with a simultaneous TG/DSC STA449C thermal analysis system (Netzsch) between room temperature and 800 ℃, at a heating rate of 10 ℃ min^{-1} in air. The specific surface area was analyzed using Brunauer-Emmett-Teller (BET) nitrogen adsorption/desorption isotherm at 77 K with a Micromeritics ASAP 2050 instrument. Element analysis (EA) was performed with a Vario EL III analyzer (Elementar. Germany).

3.2.4 Optimization of extraction process

For the optimization of extraction parameters, 1.0 mg of material was added directly to 1.0 mL of 0.5 μg mL^{-1} target solution each time. The materials were ultrasonicated for 30.0 min under 25 ℃ to achieve adsorption equilibrium. Optimum extraction conditions were: pH = 7.0, temperature at 25 ℃, and 30% salt content (NaCl). After centrifugation, the clear supernatant was collected and introduced to ultrahigh performance liquid chromatography (UPLC-UV) for further analysis. The adsorption capacity of the two materials were determined by the equation: Adsorption amount (mg/g) = (m1-m2)/m3, where m1 is the theoretical mass of the analytes in the solution, m2 is the mass of the analytes in the supernatant determined by UPLC-UV, and m3 is the mass of material added.

3.2.5 UPLC-UV analysis

The standard solutions and supernatants were injected after the extraction process into UPLC for analysis, carried out with an Ultimate 3000 UPLC (Thermo Scientific, Jose, CA, USA) system using a commercial C_{18} column (Thermo Fisher Scientific Inc., 2.1× 100 mm, 1.9 μm, China). UPLC system consisted of an HPG-3400RS pump, a WPS3000TRS autosampler, a diode array and a multiple wavelength detector. The chromatographic separation was achieved using a solvent gradient of water (A) and acetonitrile (B). The gradient programs were as follows: -5 - 0 min, 50% B at a flow rate of 0.15 mL min^{-1}; 0 - 5.4 min, 50 - 71.5% B at a flow rate of 0.28 mL min^{-1}; 5.4 - 9.0 min,71.5 - 100%B at a flow rate of 0.5 mL min^{-1} and keep up to 10.6 min; 10.6 - 14.5 min,100 - 50% B at a flow rate of 0.4 mL min^{-1};14.5 - 16.5 min, 50% B at a flow rate of 0.15 mL min^{-1}. UV absorbance detection was performed at wavelengths of 224 nm. Data processing was performed using Chromeleon 7 (Thermo Scientific, Jose, CA, USA).

3.2.6 Fabrication of sorbent-coated stainless-steel bars

An 8 cm long stainless steel (ss) bar was used to fabricate the sorbent-coated ss absorber, which was treated with aqua regia solution (HCl/HNO_3 = 3:1, v/v) for 30 min to obtain a rough surface. The ss bar was then gently washed with ultrapure water and dried in air. The dried ss bars were evenly coated with adhesive red silicone sealant by rotating ss bars slowly in a pile of red silicone sealant first, then the synthesized materials were attached firmly to the sealant coated ss bars. They were then baked in oven at 100 ^{o}C overnight to dry the silicone sealant. The sorbent-coated ss bars were rinsed thoroughly with ethanol after the bake and then were dried at 100 ^{o}C for half an hour before use. SEM was used to characterize the surface morphology of the ss bar with red silicone sealant and two different materials.

3.2.7 Analysis and quantification by DART-MS

For optimization of the key parameters of DART-MS, the sorbent-coated ss bars were immersed into the liquid samples at 1.0 cm while stirring for 30.0 min. Three real water samples: tap water, wastewater from Yueliang Lake and lake water from Xuanwu Lake, Nanjing, Jiangsu, China, were filtered with filter paper before analysis. The measurements were repeated 5 times for each sample on DART-MS.

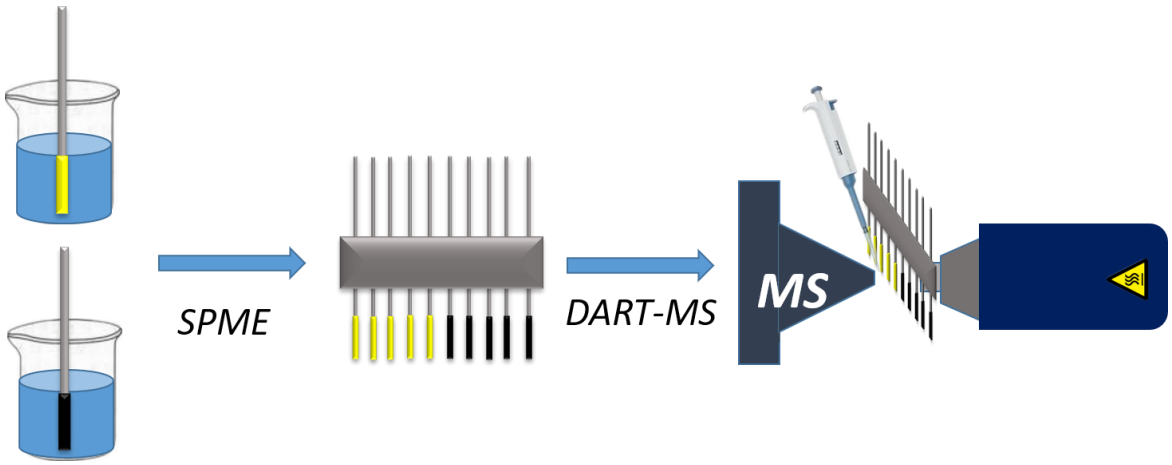

Figure 3.1 Overall scheme for the SSE-DART-MS.

The DART ion source (IonSense Inc., Saugus, MA, U.S.A.) was coupled to an Orbitrap Fusion Lumos (Thermo Fisher Scientific, San Jose, CA) mass spectrometer, with a segmented quadrupole mass filter and ion trap and Orbitrap analyzers with improved sensitivity and ion transmission. DART system is controlled by a Web-based software (DART SVP software, version 5.0.5) and the optimized DART source settings were: positive ion mode; the run temperature was 300 ℃ with He as the operation gas, grid electrode voltage was 350 V; heater wait time was 5 s ; and contact closure delay was 3 s; a 12-Dip-it glass tip linear rail that ran between the DART ion source and the ceramic tube was used to carry the samples into the source ionization region at a constant

speed of 0.2 mm s^{-1}. The distance between the DART ion source outlet and ceramic tube leading into the VAPUR® flange was maintained at 12.0 mm. The scan sequence began with an MS1 spectrum using the Orbitrap analyzer, and the related parameters included a resolution setting of 60000, mass range of *m/z* 100−500, automatic gain control (AGC) target of 2×10^5, and maximum injection time of 100 ms. The ion transfer tube temperature was 300 °C. To facilitate desorption and ionization, the ss bars were exposed to solvents, just before the analysis by DART-MS (Figure 3.1). The system was set at single ion monitoring mode for limit of detection (LOD) determination, where *m/z* 223.0965 was used for DEP, *m/z* 307.1906 was used for DPP, *m/z* 313.1436 was used for BBP, *m/z* 335.2216 was used for DHXP, *m/z* 391.2844 was used for DNOP and 395.3099 was for D4-DEHP (Figure 3.2). The LOD values were obtained based on Agilent technical note by running replicates at low concentrations, where LOD = t_α*(RSD)*(amount standard)/100%, and t_α is the Student t-test statistic using n-1 as degrees of freedom (1-α is the possibility that a measurement is greater than 0).[108] The low concentration values in estimating LODs can be found in Table B-1 and Table B-2. Orbitrap Fusion Lumos 2.0 Tune (Thermo Fisher Scientific, U.S.A.) was used for the control of the mass spectrometer. All the MS data were analyzed by Xcalibur software (Thermo Fisher Scientific, U.S.A.), and the data was exported to Origin 8.0 (Originlab, U.S.A.) to make the final plots presented in this chapter.

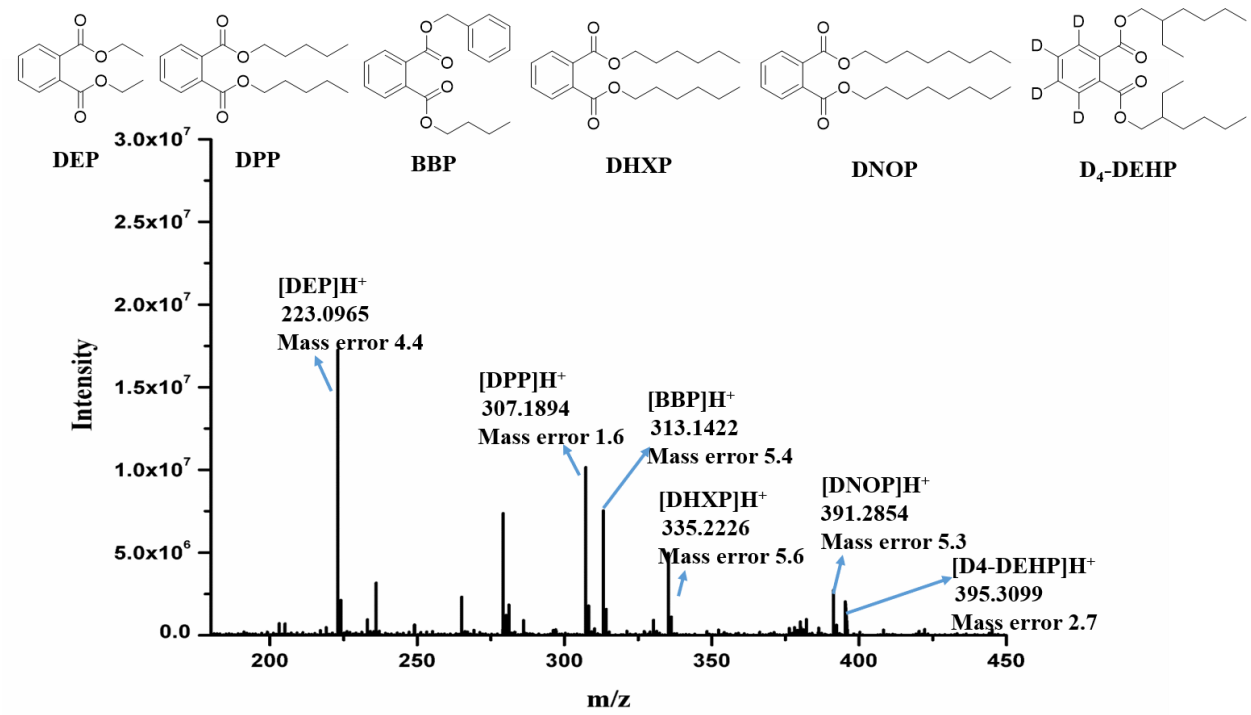

Figure 3.2 Mass spectrum of a mixture of DEP, DPP, BBP, DHXP and DNOP and internal standard D_4-DEHP; the related structures and corresponding ions are labeled. Mass errors are in ppm.

3.3 Results and discussion

3.3.1 Characterization of g-C_3N_4 and g-C_3N_4/C

Thermogravimetric analysis (TGA) of g-C_3N_4 and g-C_3N_4/C was carried out from 30 ℃ to 800 ℃ in air. Figure 3.3A shows that the TGA curves for both materials are quite similar. There was no distinct mass loss in any of the materials from 30 ℃ to 450 ℃, indicating that the two synthesized materials were thermally stable at 450 ℃. The minimal loss of weight observed in this process might be because of the evaporation of the adsorbed water and organic solvent from the surface of the materials. At 450 ℃ the two materials began to decompose, until the entire material was decomposed at 700 ℃. The percentages of mass loss in the decomposition of the two materials were 91.16% and 88.11% for g-C_3N_4 and g-C_3N_4/C, respectively.

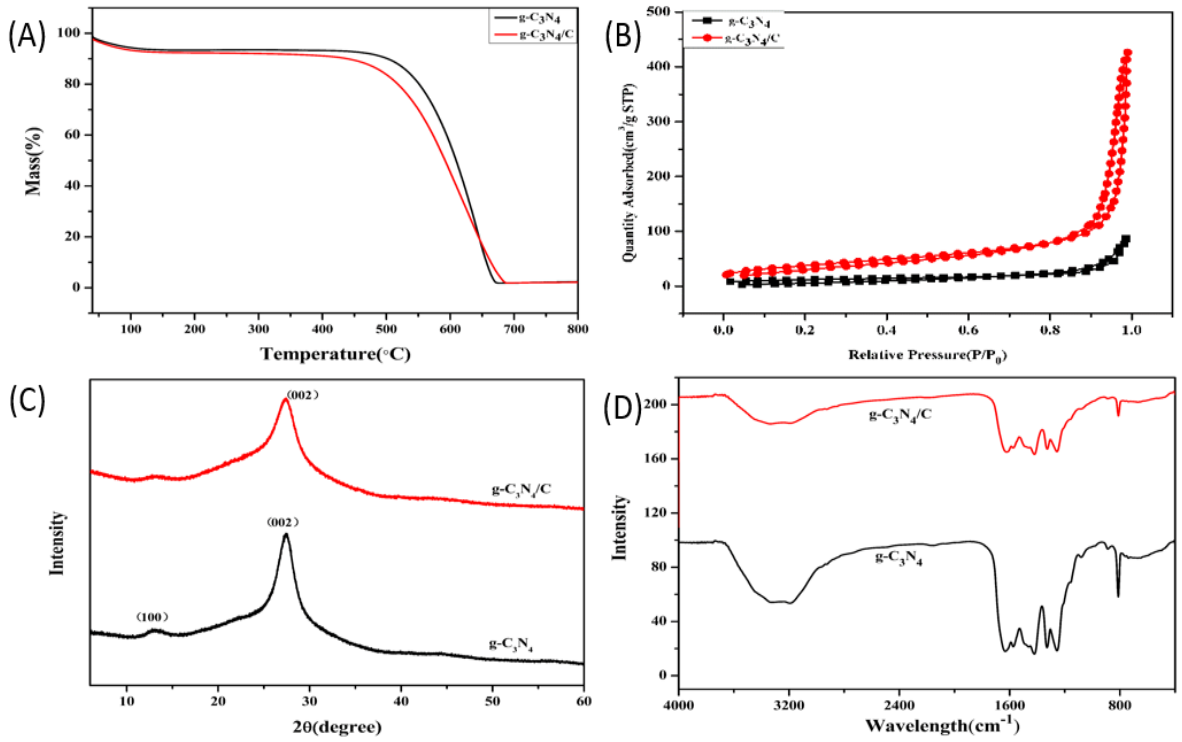

Figure 3.3 Characterization of materials. (A) TGA curves of g-C_3N_4 and g-C_3N_4/C. (B) N_2 adsorption–desorption isotherms of g-C_3N_4 and g-C_3N_4/C. (C) XRD patterns of g-C_3N_4 and g-C_3N_4/C. (D) FT-IR spectra of g-C_3N_4 and g-C_3N_4/C. line space, different from others.

N_2 adsorption–desorption isotherms of the two materials are depicted in Figure 3.3B. The Brunauer–Emmett–Teller (BET) specific surface areas of g-C_3N_4 and g-C_3N_4/C were established to be 60.5774 and 208.570 $m^2\ g^{-1}$, respectively. The evaporation of gases such as H_2O and NH_3 from g-C_3N_4 results in the formation of a large number of pores.[148] In addition to this process, the carbonization of glucose in the synthesis of g-C_3N_4/C assists in the formation of the 3D structure of g-C_3N_4/C with larger surface areas and numerous pores. The characteristic spherical 3D micropores of g-C_3N_4/C contributes crucially to its larger specific surface areas, as compared with that of g-C_3N_4.

Transmission electron microscopy (TEM) was used to study the morphologies of the two materials. According to the TEM images (Figure 3.4), g-C_3N_4 consists of 2D stacking sheets while g-C_3N_4/C possesses a spherical 3D structure with a large number of pores. The constituents of the two materials were first ascertained by element analysis. As shown in Table 3.1, C and N were the two major elements in the materials as expected, whereas the trace amount of H and was attributed to adsorption of H_2O. The C/N rations were 0.67 for g-C_3N_4, according with the chemical formula (C_3N_4). The content of C increases in g-C_3N_4/C when compared to g-C_3N_4 due to the calcination of D-glucose in the synthesis of g-C_3N_4/C. The XRD patterns of g-C_3N_4 and g-C_3N_4/C were displayed in Figure 3.3C. The two peaks at around 13.2° and 27.4° were assigned to the diffraction of (100) and (002) crystal planes in g-C_3N_4.[149] The stronger intensity of the peak at 27.4° might be ascribed to the interlayer stacking of the aromatic conjugated system. The peak at 13.2° corresponds to the triazine structure in g-C_3N_4.

Table 3.1 The content of carbon, nitrogen and hydrogen in samples by elemental analysis.

Material	N (wt%)	C (wt%)	H (wt%)
g-C_3N_4	56.78	32.53	2.429
g-C_3N_4/C	49.95	39.15	2.676

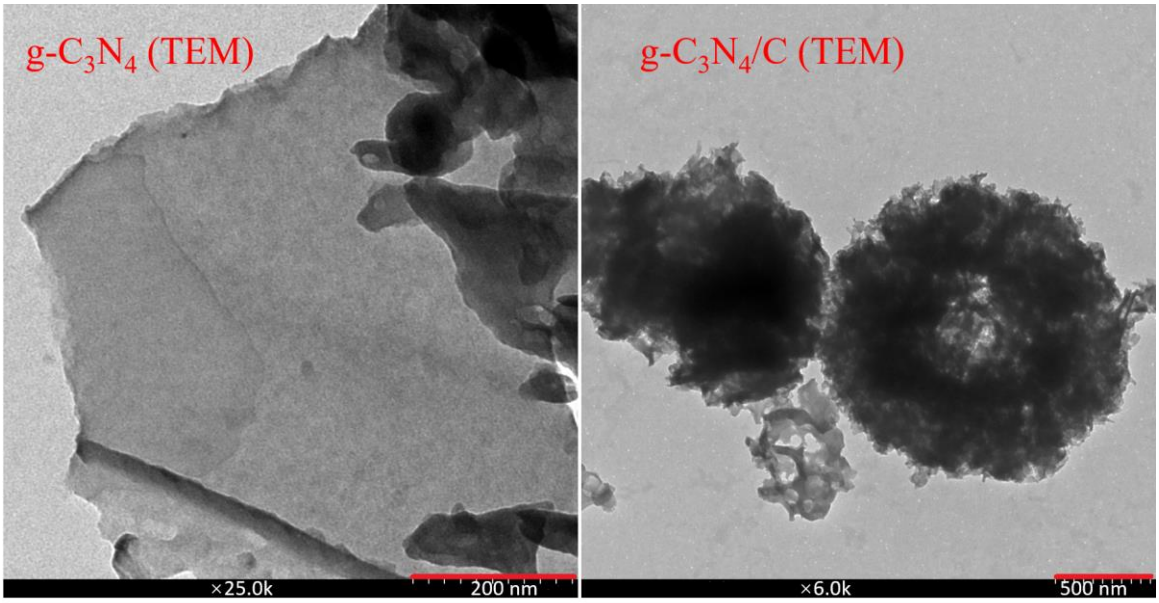

Figure 3.4 Transmission electron microscopy (TEM) images for g-C_3N_4 and g-C_3N_4/C. g-C_3N_4 consisted of a 2D stacking sheets structure while g-C_3N_4/C possessed a spherical 3D structure with plenty of pores

FT-IR was also used to characterize the structure of the as-synthesized two materials (Figure 3.3D.). The multiple bands found in 1200-1652 cm^{-1} were assigned to the stretching modes of CN heterocycles. And the adsorption band centered at 807 cm^{-1} showed the typical breathing mode of triazine units, which proved the existence of typical structure of C_3N_4.[150] The broad adsorption band at 3100-3300 cm^{-1} corresponds to the stretching modes of remaining N-H or O-H bond from uncondensed amino group and adsorbed water molecules. These characterizations clearly suggested that g-C_3N_4 and g-C_3N_4/C were synthesized successfully. Detailed SEM analysis of ss bars is presented in Supplemental information in Appendix C.

3.3.2 Optimization of extraction process

The critical factors in SPME were systematically optimized by UPLC with UV detection before further analysis by DART-MS. The adsorption capacity of the two materials were found to increase with increasing concentrations of the PAEs. The amounts adsorbed on the materials decreased in the order DHXP > DPP > DNOP > BBP > DEP, with decreasing hydrophobicity of the analytes [151,152]. PAEs (0.5 μg mL^{-1}) were chosen to study the effect of other factors on SPME (Figure 3.5). Normally, the addition of methanol would reduce the interaction at the interface of the sorbent and matrix, which would improve the dispersity of the sorbent and facilitate the adsorption of the analytes onto the surface of the sorbents. The experimental data reveals that the methanol content in 0.5 μg mL^{-1} standard solution of PAEs had no apparent effect or even negative effect on the adsorption results, indicating that the adsorption of analytes on g-C_3N_4-based sorbents occurred by both hydrophobic and π-π interactions, without sacrificing the dispersity in water. Hence, no methanol was added to the standard solution for analysis (Figure B-2).

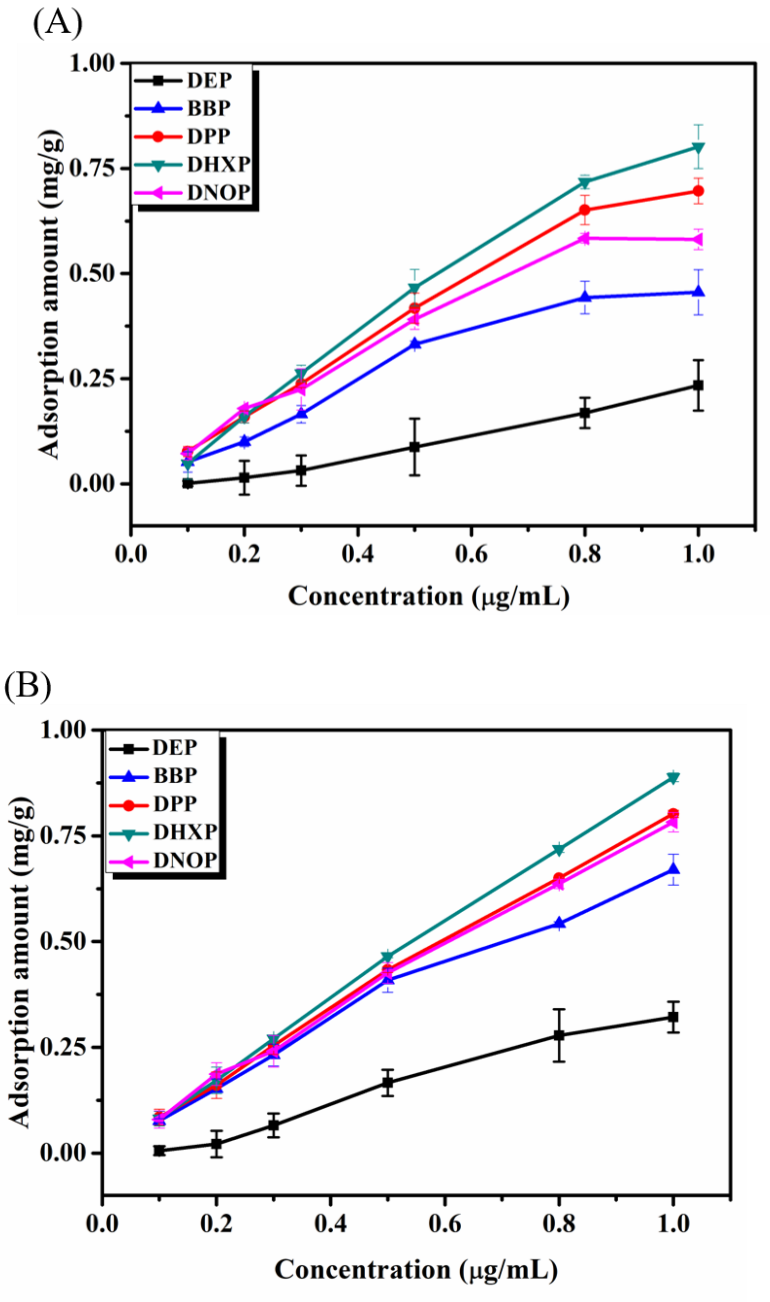

Figure 3.5 Effect of initial concentration (0.01 - 1.0 μg mL^{-1}) for (A) g-C_3N_4 and (B) g-C_3N_4/C on UPLC-UV. The error bars are standard deviations.

An optimum extraction temperature is necessary, because higher temperature may increase the diffusion of the target analytes but may also reduce the adsorption capacity simultaneously.

The adsorption did not vary significantly in the range of 25 – 30 ℃ for the both materials, except for 30 ℃, at which the adsorption of g-C_3N_4/C was significantly lower than the other temperatures. Thus, room temperature was selected for convenience (Figure B-3). The dispersity of sorbents and interaction between analytes and sorbents might be different by altering pH conditions. Hence, the effect of pH was investigated in this study. Hydrogen chloride and sodium hydroxide was added to the standard solution to adjust the pH. There was no obvious distinction in adsorption at different pH values, suggesting that adjustment of pH has no significant effect in this case (Figure B-4). NaCl was added to the standard solution to evaluate the effect of ionic strength. The adsorption capacity increases with increasing salt content, which can be explained by the salting-out effect.[153] When the content of salt was 30% (w/v), the amount adsorbed reached the maximum, and all PAEs in the standard solution were fully adsorbed on the two materials. Salt content of 30% (w/v) was chosen (Figure 3.6). Without any optimization, the adsorption capacity of g-C_3N_4/C was found to be slightly higher than that of g-C_3N_4, although the specific surface area of g-C_3N_4/C (208.570 m^2 g^{-1}) was much larger than that of g-C_3N_4 (60.5774 m^2 g^{-1}). This phenomenon might be explained by the smaller pore size of g-C_3N_4/C (41.7912 nm), as compared with that of g-C_3N_4 (148.5611 nm), and the low ratio of the effective adsorption area of g-C_3N_4/C, which makes it difficult for the analytes to enter the pores. No significant differences in the adsorption capacity of the two materials were observed after the optimization of extraction.

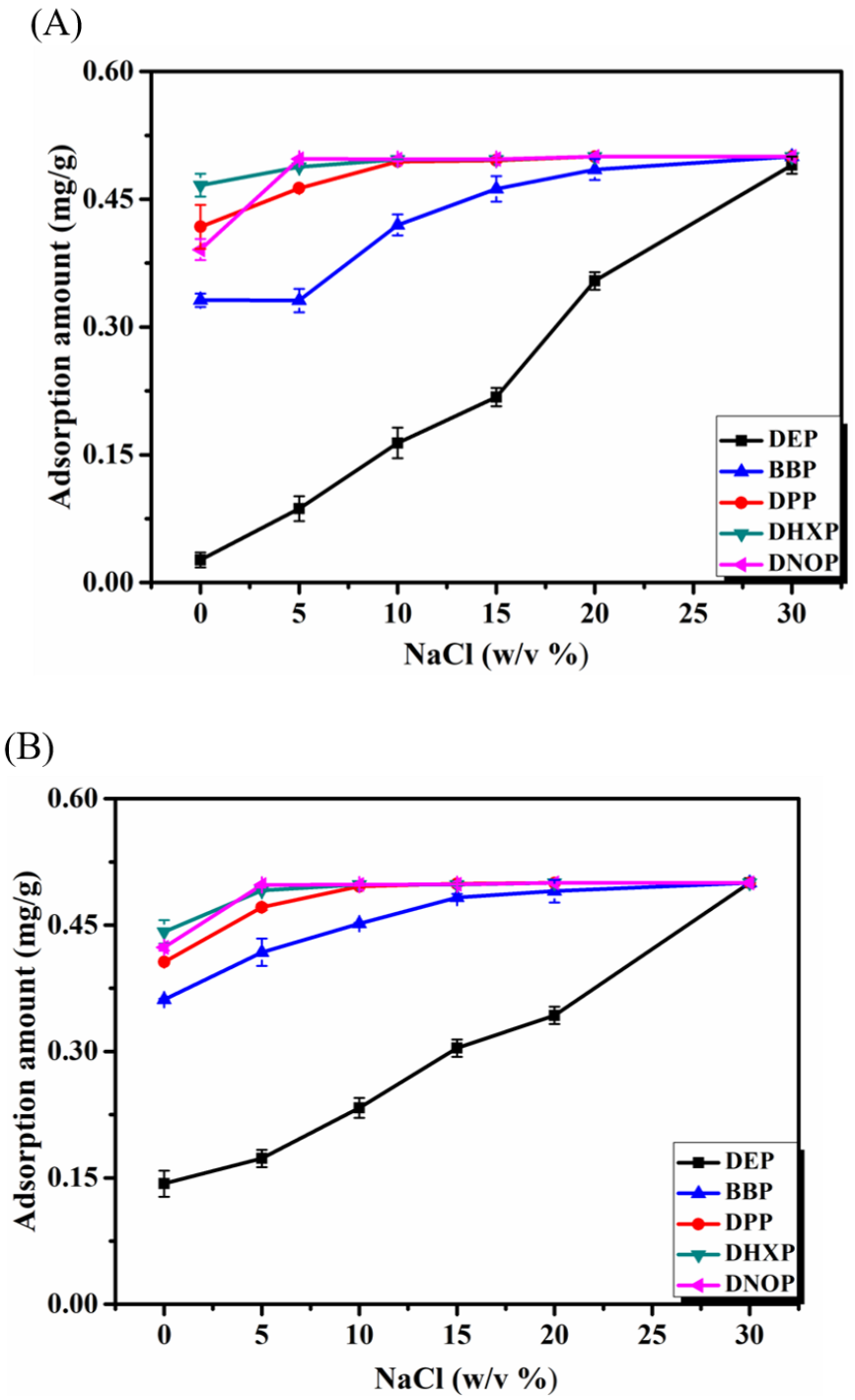

Figure 3.6 Effect of the concentration of NaCl (0, 5%, 10%, 15%, and 30% (w/v)) for (A) g-C_3N_4 and (B) g-C_3N_4/C on UPLC-UV. The error bars are standard deviations.

3.3.3 Effect of sorbent morphology and solvent on DART-MS analysis

Figure 3.7 shows that all the MS signals of the five PAEs on the planar g-C_3N_4 were stronger than the 3D g-C_3N_4/C. The simple planar morphology of g-C_3N_4 may make it easier to transfer energy and desorb and ionize the adsorbed analytes. The thermal conductivity on the porous morphology was possibly not as good, and the abundant smaller pores may prevent the desorption and ionization of the adsorbed analytes to some extent.

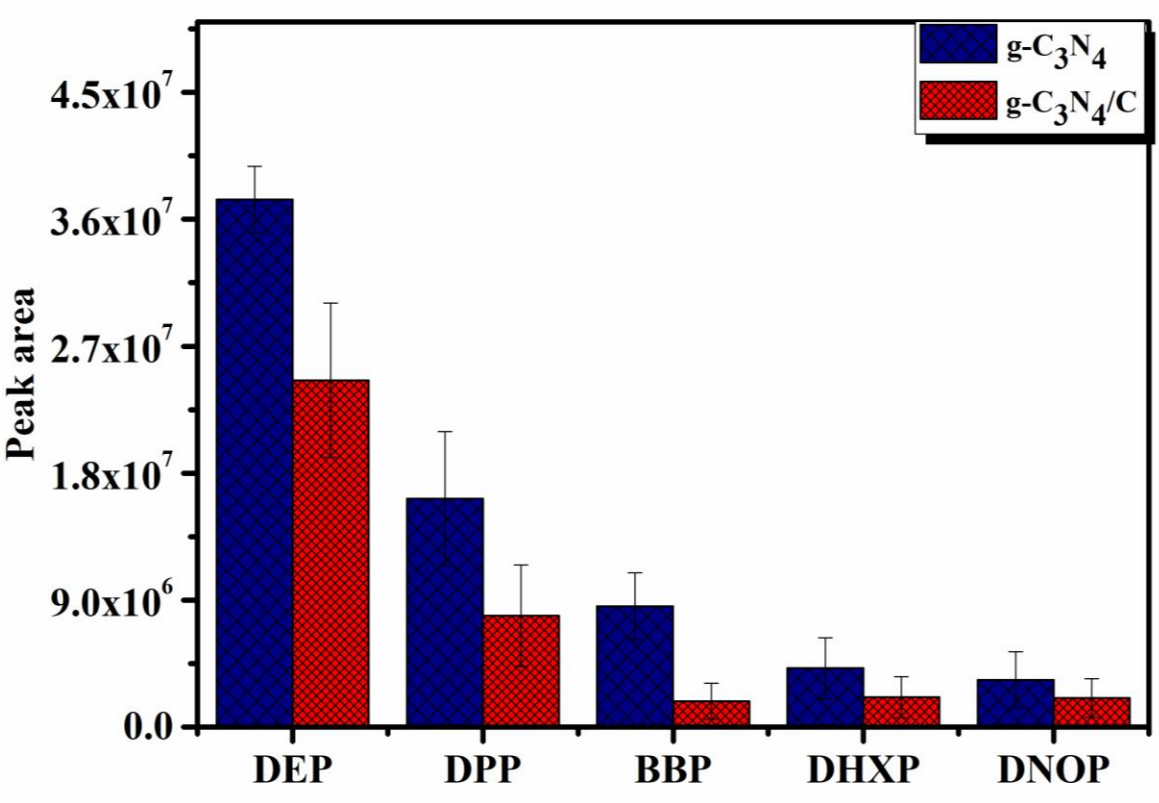

Figure 3.7 MS signals of five PAEs on g-C_3N_4 and g-C_3N_4/C under the optimum extraction conditions without addition of solvents. The error bars are standard deviations.

Figure 3.8 shows the effect on the MS signals upon the addition of six common organic solvents. It is obvious that the addition of common organic solvents remarkably enhanced the DART-MS signal, as compared with the case where no organic solvents were added. A possible

mechanism of ionization in positive-ion DART, as previously reported,[16] suggests that a transient microenvironment might be generated around the analytes by the desorption of the volatile matrix, once the analytes are in contact with the gas stream from DART. This could shield the direct ionization of the analytes by the DART gas stream. The DART gas stream would first ionize the volatile matrix of the analytes, and then these matrix ions would ionize the target molecules via gas-phase molecule/ion reactions. The ionization energies of all the organic solvents used in the experiments are lower than the energy of the excited electronic state (2^3S) of He (19.8 eV), and therefore all of them can be ionized in the DART gas stream., accounting for the significant enhancement of the MS signals for both the materials. The temperature used in these experiments was above the boiling points of these organic solvents and hence, all were vaporized. Significant differences in the MS signals were observed for g-C_3N_4 when four different organic solvents were used separately. Ethanol seemed to offer the highest overall enhancement (especially for DEP). The enhancement was mainly assessed by the ionization efficiencies of the organic solvents, because the simple planar structure of 2D g-C_3N_4 already rendered the adsorption easy. The dominant ionic forms of ethanol, methanol, and acetonitrile were their protonated dimers.[16] The proton affinity of these dimers slightly decreased in the order ethanol (910 kJ mol^{-1}) > acetonitrile (909 kJ mol^{-1}) > methanol (891 kJ mol^{-1}),[16] predicting a relatively better enhancement in the presence of ethanol. The enhancements for the 2D g-C_3N_4 were lower when two organic solvents were mixed, than when they were used separately. This was because the two organic solvents might compete for the ionization of the analytes and suppress it in the blended matrix.

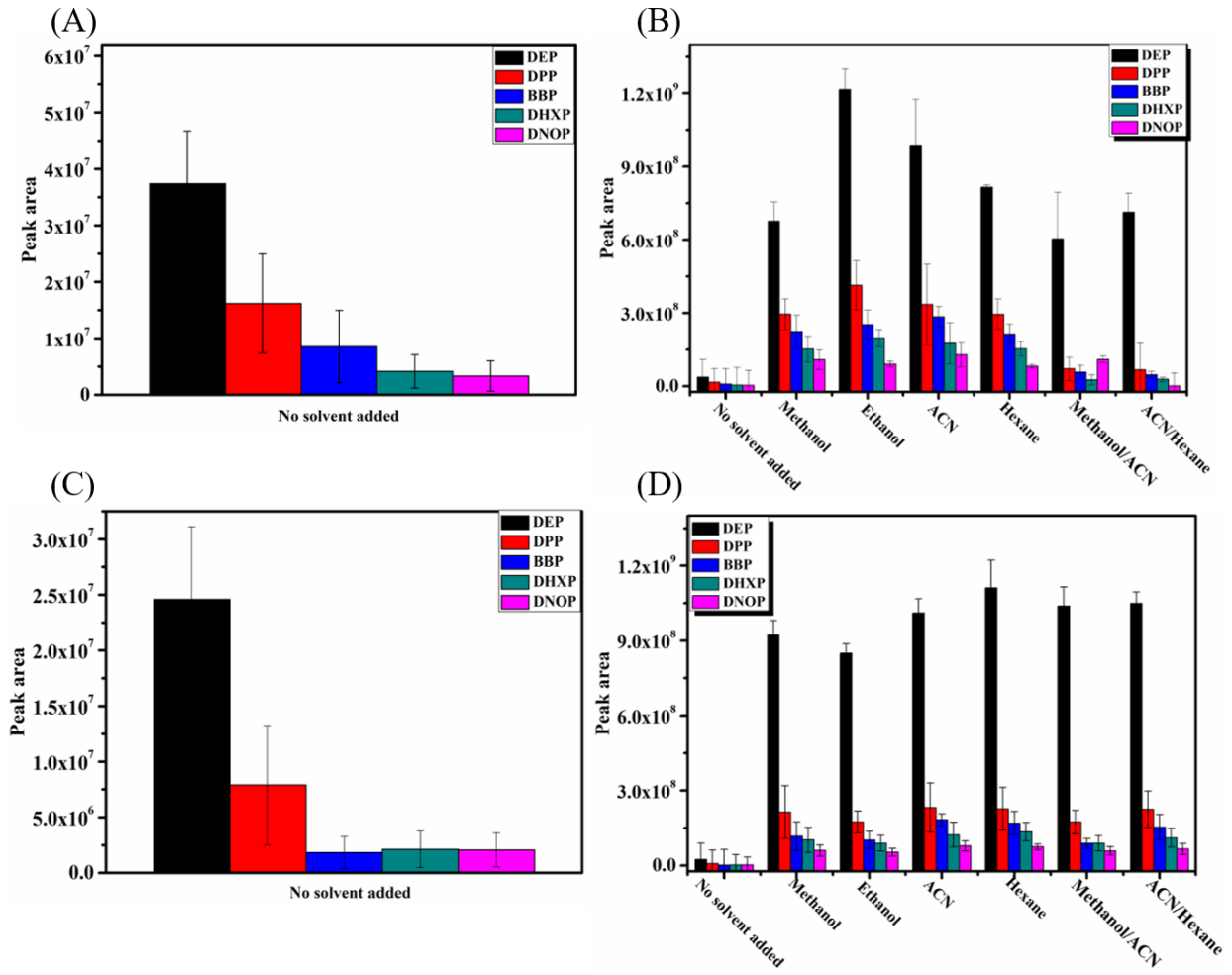

Figure 3.8 MS signals of five PAEs on g-C_3N_4 (A) and g-C_3N_4/C (C) when no solvent was added onto sorbent, respectively. MS signals of five PAEs on (B) g-C_3N_4 and (D) g-C_3N_4/C after addition of 6 different solvents (methanol, ethanol, acetonitrile, hexane, methanol/ acetonitrile (v: v=1:1), and acetonitrile/ hexane (v:v=1:1)) separately. The error bars are standard deviations.

There was no significant difference on the enhancement of MS signals of five PAEs in the six organic solvents (whether mixed or separately) on g-C_3N_4/C. Due to the complex porous surface of 3D g-C_3N_4/C, the dominant factor was assumed to be the desorption of the analytes inside the smaller pores. Since PAEs can be dissolved in all these organic solvents, they are sufficiently

suitable to desorb the analytes continuously, with no apparent distinction on enhancement of MS signals.

3.3.4 Optimization of key parameters in DART-MS

To further improve the sensitivity of DART-MS, several key parameters were optimized. The thickness of the ss bar was optimized first. The best results were obtained when the diameter of the ss bar was 1.0 mm, which was the thinnest among all ss bars (Figure 3.9). The linear rail moving rate was tested from 0.2 mm s^{-1} to 0.6 mm s^{-1} (Figure B-5), and it was found that larger peak area was accompanied by slower rates of movement for both the materials, allowing longer contact time with the excited metastable He to achieve a higher extent of completion of the desorption and ionization of analytes. The vacuum was adjusted by tuning the valve on the dry vacuum pump, and -90 kPa was selected for both materials to obtain the best ion transfer efficiency (Figure B-6). There was a clear downward trend of peak area with increasing distance of the DART ion source outlet to MS inlet, and a distance of 6.0 mm was used for both the materials (Figure B-7). The temperature of the excited metastable He did not have much influence on the peak area of the analytes, but a temperature of 300 ℃ for the excited metastable He appeared to be the most suitable for g-C_3N_4/C. The temperature of excited metastable He was then set to 300 ℃ for the two materials (Figure B-8). The extraction time in SPME also affected the MS signal. The highest peak area for g-C_3N_4 was obtained when the extraction time was 45 min, while the highest peak area for g-C_3N_4/C was obtained when the extraction time was 30 min (Figure B-9). Appropriate amount of organic solvents added on the ss bar results in the best analytical performance, since excess solvent would probably impede the energy transfer process and insufficient solvent would reduce the desorption and ionization efficiency. The results suggested that 5 and 7 μL of the

solvents were the best for g-C_3N_4 and g-C_3N_4/C, respectively (Figure B-10). The determination of LODs and recoveries of all the analytes from environmental water on the two materials were performed under the optimized conditions mentioned above.

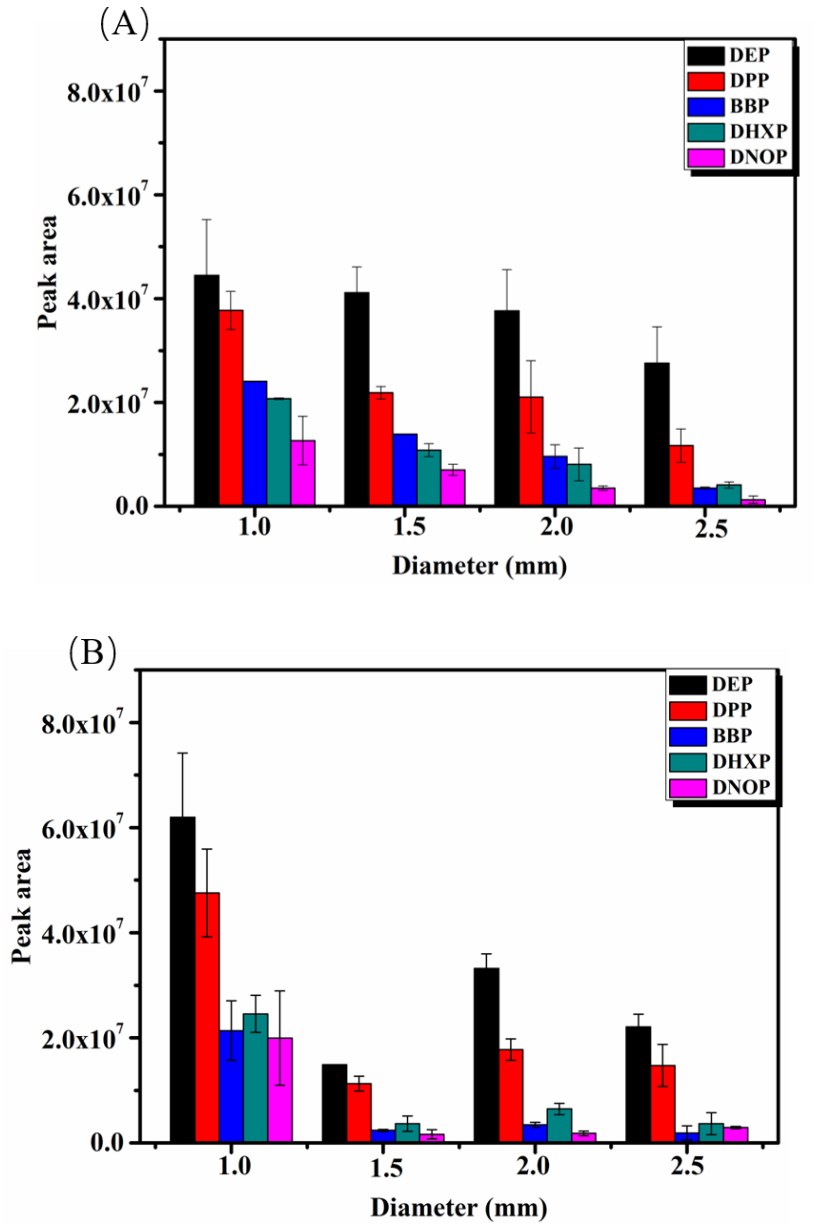

Figure 3.9 Effect of diameter of ss bar (1.0, 1.5, 2.0, and 2.5 mm) for (A) g-C_3N_4 and (B) g-C_3N_4/C on MS signals in SSE-DART-MS method. The error bars are standard deviations.

3.3.5 Quantification and validation of SSE-DART-MS method

The analytical performance of SSE-DART-MS method was evaluated under the optimum conditions for both materials. Ethanol and acetonitrile were used to enhance the MS signals for g-C_3N_4, and g-C_3N_4/C, respectively. The LODs of SSE-DART-MS ranged from 0.07 - 0.94 ng L^{-1} for g-C_3N_4 and 5.23 – 10.29 ng L^{-1} for g-C_3N_4/C, respectively. The calibration curves were established by analyzing samples of 50 mL water spiked with various known concentrations of PAEs. D_4-DEHP (32 µg L^{-1}) was used as the internal standard. The horizontal axis shows the concentrations of PAEs, and the vertical axis is the ratio of the relevant peak areas of the target analytes over the internal standard in the extracted ion chromatogram.

For g-C_3N_4/C, R^2 values were in the range of 0.9915 – 0.9978 for PAEs in different concentration ranges (0.1 – 12.0 µg L^{-1} for DEP, DPP, and BBP; 0.1 – 16.0 µg L^{-1} for DHXP and DNOP). For g-C_3N_4, R^2 values were in the range of 0.9915 – 0.9983 for all the five PAEs in the concentration range of 0.1 – 72.0 µg L^{-1} (Figures B-11 and B-12). Finally, three real water samples (tap water, wastewater and lake water) were collected, and used to evaluate the potential application of the SSE-DART-MS method on the real samples. BBP, which is found in lake water, was successfully detected by both the sorbent materials; no other PAEs were detected by the described methods. The water samples (50.0 mL, n = 5) were spiked with 20.0 µg L^{-1} and 50.0 µg L^{-1} of each of the five PAEs for g-C_3N_4 and 4.0 and 10.0 µg L^{-1} of each of the five PAEs for g-C_3N_4/C and analyzed. Good recoveries in the range of 82.8 – 119% were found for g-C_3N_4, with relative standard deviations (RSDs) between 2.45% and 9.79%, while good recoveries in the range of 83.1 – 120% were found for g-C_3N_4/C, with RSDs between 1.01% and 9.69% (Table 3.2 and 3.3). Thus, the SSE-DART-MS method described in this study, with the synergistic effect of

sorbent and solvent, showed great potential for the high-throughput trace analysis of pollutants in water.

Table 3.2 Recoveries obtained by g-C_3N_4 on DART-MS for PAEs in spiked samples from different areas (n = 5).

Analytes	Con (μg L^{-1})	Tap water			Wastewater			Lake water		
		C	R %	RSD %	C	R %	RSD %	C	R %	RSD %
	0	ND			ND			ND		
DEP	20	18.0	90.0	6.7	23.6	118	2.9	19.0	95.0	2.5
	50	46.3	92.6	9.8	51.5	103	3.4	48.4	96.8	3.0
	0	ND			ND			ND		
DPP	20	19.3	96.5	3.3	22.4	112	3.7	17.1	85.3	4.8
	50	58.8	118	6.3	54.7	109	3.9	54.5	109	8.5
	0	ND						3.69		
BBP	20	23.2	116	3.4	21.2	106	2.9	24.4	103	3.5
	50	55.9	112	9.2	43.7	87.4	6.2	54.5	102	5.3
	0	ND			ND			ND		
DHXP	20	18.3	91.5	9.8	17.8	89.0	5.7	18.9	94.5	7.3
	50	52.4	105	4.2	41.4	82.8	7.2	50.9	102	4.7
	0	ND			ND			ND		
DNOP	20	20.2	101	8.9	16.6	83.0	4.7	20.9	105	5.3
	50	59.3	119	8.6	51.2	102	4.2	43.6	87.2	7.7

Table 3.3 Recoveries obtained by g-C_3N_4/C on DART-MS for PAEs in spiked real samples from different areas (n = 5).

Analytes	Con (μg L^{-1})	Tap water			Wastewater			Lake water		
		C	R %	RSD %	C	R %	RSD %	C	R %	RSD %
	0	ND			ND			ND		
DEP	4	3.91	97.8	7.1	4.01	100	3.4	3.62	90.5	3.5
	10	9.27	92.7	8.6	9.85	98.5	6.5	9.22	92.2	4.3
	0	ND			ND			ND		
DPP	4	4.25	106	8.5	3.71	92.8	5.3	3.41	85.3	5.4
	10	8.38	83.8	6.3	8.35	83.5	4.7	9.35	93.5	4.5
	0	ND			ND			2.77		
BBP	4	3.65	91.3	3.0	3.99	99.8	5.9	6.64	96.8	5.3
	10	9.12	91.2	6.9	8.53	85.3	3.8	11.1	83.1	4.2
	0	ND			ND			ND		
DHXP	4	3.43	85.8	1.4	3.34	83.5	9.7	3.70	92.5	4.4
	10	8.62	86.2	5.2	11.1	111	2.7	9.67	96.7	5.0
	0	ND			ND			ND		
DNOP	4	4.17	104	4.0	4.42	111	3.6	4.79	120	8.0
	10	9.17	91.7	7.9	10.6	106	2.1	8.80	88.0	1.0

Note: Con: concentration of spiked compound (μg L^{-1}); C: concentration of found target (μg L^{-1})； R: recovery; RSD: relative standard deviation.

The described method was compared with previously reported analytical method[152,154-156] for the determination of PAEs in terms of extraction time, analytical time, LODs, linear range, RSD and recoveries. As listed in Table 3.4, the LODs of PAEs using the SSE-DART-MS method were the best and significantly lower than those obtained by other methods. The superior sensitivity of the SSE-DART-MS method can be attributed to the synergistic effect of the sorbent and solvent acting together. The analysis time for the SSE-DART-MS methodology is overwhelmingly less than that of the other methods. The RSD, extraction time, linear range and recoveries were comparable to the other methods. The ss bars used in this method were inexpensive (approximately $0.15 each) and reusable. Since there was little organic solution required and no additional elution step, the SSE-DART-MS method is environmentally friendly as well. These comparisons suggest that the method reported in this work is indeed highly sensitive, environmentally friendly, and cost-effective way for high-throughput analysis of PAEs in complex environmental compounds.

Table 3.4 Comparison of analytical performance of SSE-DART-MS with other methods on analysis of PAEs.

Sample Prep.	Analytical Methods	Sample	Material	Extraction time (min)	Analytical time (min)	Linear Range (μg L^{-1})	LOD (ng L^{-1})	RSD (%)	Recovery (%)	Ref
HF-LPME	HPLC	Juice milk	Graphene	30	32	3.0-1000	200-5000	<7.6	81.0-108.0	154
SPME	GC-FID	Drinking water	SiO_2–PDMS-MWNTs	>32	20	0.1-300	10-20	<12.2	85.3-109.3	155
SPE	GC/IT-MS	Alcoholic drinks	XAD-2	>45	-	1.0-800	200-2000	<5.5	88-102	156
MSPE	HPLC-UV	Water	g-C_3N_4/Fe_3O_4	>15	15	0.1-50	50-100	<3.8	79.4-99.4	152
SSE	DART-MS	Water	g-C_3N_4	45	0.25	0.1-72	0.07-0.94	<9.8	82.8-119	This work
SSE	DART-MS	Water	g-C_3N_4/C	30	0.25	0.1-16	5.23-10.29	<9.7	83.1-120	This work

3.4 Conclusion

SSE-DART-MS method was successfully established for high-throughput determination of trace PAEs in water samples. The enhancements were observed using organic solvents to assist the desorption and ionization of analytes on both the 2D g-C_3N_4 and 3D g-C_3N_4 in DART-MS analysis. Six common organic solvents were added on to the 2D g-C_3N_4 and 3D g-C_3N_4 to study the enhancement effect. The sorbent with 2D morphology exhibits better performance compared to 3D morphology in the proposed SSE-DART-MS method. Key parameters in the SSE-DART-MS method were systematically investigated and optimized. The SSE-DART-MS method proved to be highly efficient and can be used to improve the sensitivity of DART-MS significantly. This study not only presented a reliable method for the analysis of one group of water contaminants, but also demonstrated a systematic approach to the study of other sample pretreatment techniques and provided significant insights into improving the high-throughput analysis of pollutants by DART-MS.

Chapter 4: Study on the effect of sorbent hydrophobicity on SPME-DART-MS analysis

4.1 Introduction

Direct analysis in real time mass spectrometry (DART-MS) is one of the most popular AIMS techniques nowadays due to its numerous remarkable features, such as high speed, soft-ionization, high salt tolerance, minimal sample preparation and no memory effect.[125] Typically, a heated stream of metastable helium gas is generated inside the DART ion source to desorb and ionize molecules from surfaces of the sample, which could be gas, liquid, or solid. The detailed ionization mechanisms can be found in previous articles and book chapters.[5,13,125] Although, one major advantage of DART-MS lies in the great reduction of total analysis time by the elimination of sample preparation steps, there is an analytical trade-off between the simplification of experimental procedure and improvement of analytical performance when dealing with trace analytes in complex matrices. For instance, direct analysis of real-world samples by DART-MS may sometimes produce very complex mass spectra, posing a challenge in data processing. Additionally, in sole analysis of real samples by DART-MS, low sensitivity is a critical issue when target analytes exist in trace-level and complex matrices. The inherent low ionization efficiencies of AMS and half-way ion quenching in the air can worsen the situation if no sample preparation is involved. Therefore, necessary sample preparation is frequently needed prior to DART-MS analysis to address the abovementioned issues under many circumstances.

Solid-phase microextraction is a mini version of SPE, preserving all the merits of SPE while reducing the required consumption of organic solvent. Since the pioneering work by Cajka and coworkers in 2010,[157] the combination of SPME and DART-MS has become an effective

approach to improve the selectivity and sensitivity of DART-MS analysis. In a typical fiber-based SPME-DART-MS method, a fiber coated with sorbent is placed between the DART ion source and MS inlet after extraction of analytes, after which the analytes on SPME fiber are thermally desorbed and ionized by the metastable He gas from DART for further analysis by MS. In addition to all the advantages SPME owns as a superior sample preparation method, the thin layer of sorbent coating can facilitate the passage of ionized molecules, and the fibers can be easily adjusted to fit in the sampling module in the commercial DART kit box. Very recently, the Pawliszyn group reported the first use of SPME-TM coupled to DART-MS for small-volume analysis.[158] The drugs of abuse were rapidly quantified in oral fluid and blood droplets (15 μL and 25 μL) with very low detection limits. The successful detection of nicotine in a 15 μL oral fluid from a male smoker proved the applicability of this method in real life. It is commonly believed that the hydrophobicity of sorbent has a great influence in the dispersibility of sorbent and partition equilibrium, which could ultimately influence the extraction efficiency.[159,160] Beside being inspired by the systematic investigation of effect of sorbent morphology and the type of organic solvent used on SPME-DART-MS analysis in Chapter 3, it is reasonable to speculate that sorbent hydrophobicity may also play a significant role in the SPME-DART-MS analysis. In a previous work of our group, it was found that the weaker the interaction between the sorbents and analytes, the easier it is for the analytes on the sorbent to be desorbed and ionized in SPME-DART-MS analysis.[58] Hence, the analytical performance of SPME-DART-MS can be improved if the effect of sorbent hydrophobicity on SPME-DART-MS is systematically studied.

In this Chapter, a systematic research on effect of sorbent hydrophobicity on SPME-DART-MS was performed. Ionic liquid (IL) was chosen as a remarkable candidate in this study because of its high selectivity, good extractability, and especially good tunability, which offers

custom-designed properties. Nine silica supported ionic liquids (Si-ILs) with similar structures but different hydrophobicity were successfully synthesized and coated on SPME fibers, which were then used in SPME-DART-MS analysis of four phthalic acid esters (PAEs) in aqueous solutions. Several key parameters in the SPME process were optimized before the evaluation of analytical performance of nine Si-ILs in DART-MS. However, based on the experimental results we acquired by comparing the analytical performances of nine Si-ILs in SPME-DART-MS analysis of four PAEs, a clear relationship between the sorbent hydrophobicity and analytical results in SPME-DART-MS has not been confirmed so far, and more efforts are required to unveil this effect.

4.2 Experimental section

4.2.1 Chemicals

Diphenyl phthalate (DPhP), bis(methylglycol) phthalate (DMEP), dipropyl phthalate (DPrP), diallyl phthalate (DAP), 3-chloropropyltrimethoxysilane, silica gel (40 – 45 μm), potassium hexafluorophosphate (KPF_6), sodium fluoroborate ($NaBF_4$), 1-ethylimidazole, and 1-butylimidazole were purchased from Aladdin Industrial Inc. (Shanghai, China). Anhydrous toluene, methanol, acetone and ethanol was purchased from Sinopharm Chemical Reagent Co., Ltd. (Shanghai, China).1-octylimidazole was obtained from Shanghai yuanye Bio-Technology Co., Ltd. Kafuter Red RTV Silicone Adhesive was purchased from Guangdong Hengda New Materials Technology CO., LTD. (Huizhou, China). All the chemicals and reagents were of analytical grade and used without purification. The standard solutions of four PAEs (DPhP, DMEP, DPrP, and DAP) were prepared in methanol at the concentration of 0.1 mg/mL. Other standard PAEs solutions with lower concentrations were prepared by diluting the 0.1 mg/mL stock solution with deionized (DI) water. All standard solutions were stored in the refrigerator at 4 ℃.

4.2.2 Synthesis of nine Si-ILs

The synthesis of nine Si-ILs were based on previously reported literature with a few modifications.[161] The activation of silica was first achieved by immersing silica in hydrochloric acid for 24 h and then washed with DI water. The activated silica was dried at 100 ℃ for 8 h. Then, 6.0 g of dry activated silica was suspended in 60 mL anhydrous toluene followed by the addition of excessive 3-chloropropyltrimethoxysilane (6.0 mL). The suspension was gently stirred and refluxed for 24 h. After the reaction was cooled to room temperature, the modified silica was washed in turn with toluene, DI water, and finally methanol to obtain chloropropyl silica, which was subsequently dried at 60 ℃ for 10 h.

The obtained chloropropyl silica was then reacted with 1-ethylimidazole, 1-butylimidazole, and 1-octylimidazole, respectively. Briefly, 5.0 g of dry chloropropyl silica was added into reaction flask containing 50.0 mL anhydrous toluene and an excess of imidazoles (5.0 g). The mixture was then stirred and refluxed for 24 h. When the mixture was cooled to room temperature, the modified silica was thoroughly washed in turn with toluene, ethanol, and methanol, after which the imidazolium-bonded silica was dried at 60 ℃ for 10 h. In this step, Si-ILs with Cl^- as anion was obtained, and one more step is needed to yield Si-ILs with BF_4^- or PF_6^- as anion[162]: the obtained Si-ILs with Cl^- as anion was then anion-exchanged by stirring it with KPF_6 or $NaBF_4$ in acetone at room temperature for 3 days. There were nine Si-ILs synthesized using the abovementioned method, and they were denoted as $[C_2MIM][Cl]$, $[C_4MIM][Cl]$, $[C_8MIM][Cl]$, $[C_2MIM][BF_4]$, $[C_4MIM][BF_4]$, $[C_8MIM][BF_4]$, $[C_2MIM][PF_6]$, $[C_4MIM][PF_6]$, and $[C_8MIM][PF_6]$. (The subscript number 2, 4, and 8 means starting materials of 1-ethylimidazole, 1-butylimidazole, and 1-octylimidazole respectively.)

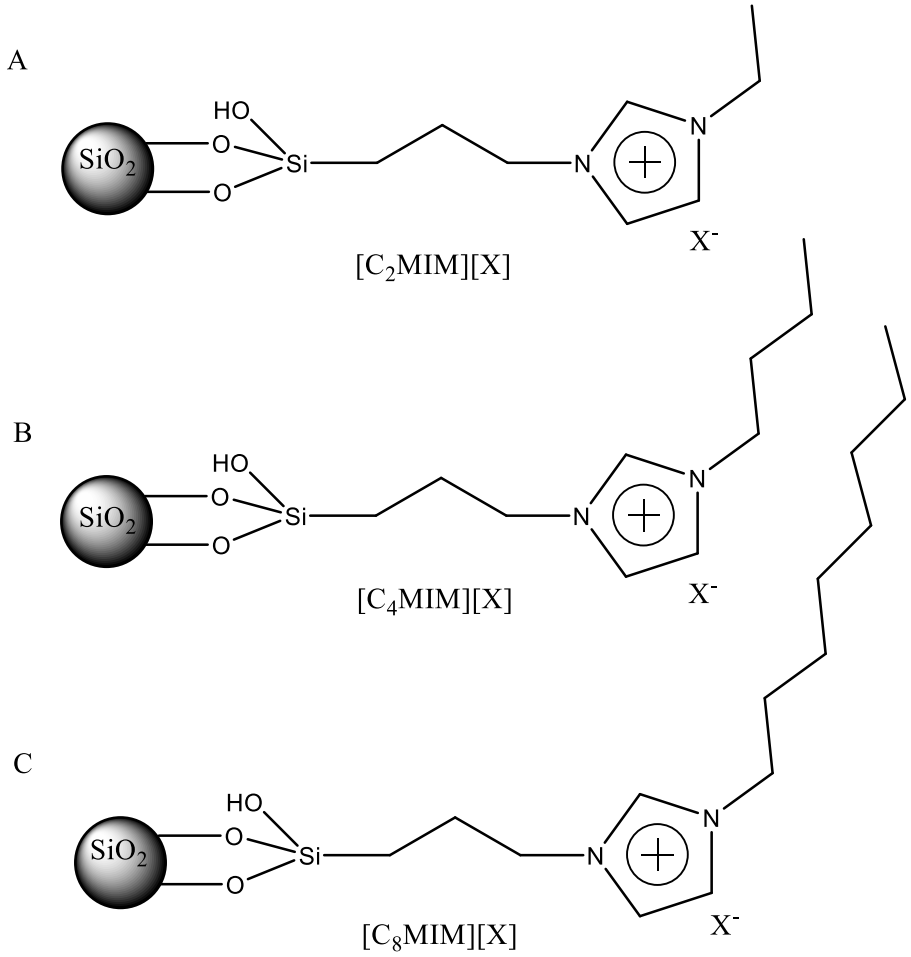

Figure 4.1 Structures of Si-ILs synthesized in this chapter. (A), (B) and (C) are the structures of ILs with cations as $[C_2MIM]^+$, $[C_4MIM]^+$, and $[C_8MIM]^+$, respectively. The anion X^- is Cl^-, BF_4^- or PF_6^- depending on the anion exchange procedure.

4.2.3 Characterization of nine Si-ILs

Fourier Transform Infrared (FTIR) (Bruker Tensor 27) spectra were obtained between 400 and 4000 cm−1 at the rate of 20 scans/min using KBr pellets. Scanning Electron Microscope (SEM) analysis were performed with a JSM-7600 F spectrometer (Akishima-shi, Japan).

4.2.4 Preparation of Si-ILs coated SPME fiber

The sorbent-coated SPME fiber was fabricated by an eight cm long stainless-steel fiber, which was treated with aqua regia solution (HCl/HNO3=3:1, v/v) for 30 min to generate a rough surface. The fiber was then gently washed with DI water, and dried in air. The tips of dried fibers (about 2 cm) were evenly coated with adhesive red silicone sealant by rotating ss bars slowly in a pile of red silicone sealant first, then the synthesized materials were attached firmly to the sealant coated fibers. They were then baked in oven at 90 °C overnight to dry the silicone sealant. The sorbent-coated SPME fibers were rinsed thoroughly with ethanol after the bake and then were dried at 90 °C for half an hour before use.

4.2.5 Optimization of SPME process

For the optimization of extraction parameters, 1.0 mg of material was added directly to 1.0 mL of 3.0 μg mL^{-1} target solution each time followed by ultrasonication for 30.0 min under 25 °C to achieve adsorption equilibrium. Optimum extraction conditions were: pH = 7.0 and temperature at 25 °C. After high-speed centrifugation, the clear supernatant was collected and introduced to ultrahigh performance liquid chromatography (UPLC-UV) for further analysis. The adsorption capacity of the two materials were determined by the equation: adsorption amount (mg/g) = (m_1-m_2)/m_3, where m_1 is the theoretical mass of the analytes in the solution, m_2 is the mass of the analytes in the supernatant determined by UPLC-UV, and m_3 is the mass of sorbent added.

4.2.6 UPLC-UV analysis

The UPLC-UV analysis were carried out with an Ultimate 3000 UPLC (Thermo Scientific, Jose, CA, USA) system using a commercial C18 column (Thermo Fisher Scientific Inc., 2.1×100 mm, 1.9 μm, China). UPLC system consisted of an HPG-3400RS pump, a WPS3000TRS autosampler, a multiple wavelength detector as well as a diode array. The chromatographic

separation was achieved using a solvent gradient of water (A) and acetonitrile (B). The gradient programs (same as the gradient program used in Chapter 3) were as follows: 5 - 0 min, 50% B at a flow rate of 0.15 mL min^{-1}; 0–5.4 min, 50–71.5% B at a flow rate of 0.28 mL min^{-1}; 5.4–9.0 min,71.5–100% B at a flow rate of 0.5 mL min^{-1} and keep up to 10.6 min; 10.6–14.5 min,100 - 50% B at a flow rate of 0.4 mL min^{-1};14.5–16.5 min, 50% B at a flow rate of 0.15 mL min^{-1}. UV absorbance detection was performed at wavelengths of 224 nm. Data processing was performed using Chromeleon 7 (Thermo Scientific, Jose, CA, USA). triplicates

4.2.7 DART-MS analysis

The DART ion source (IonSense Inc., Saugus, MA, U.S.A.) was coupled to an Orbitrap Fusion Lumos (Thermo Fisher Scientific, San Jose, CA) mass spectrometer, with a segmented quadrupole mass filter and ion trap and Orbitrap analyzers with improved sensitivity and ion transmission. DART system is controlled by a Web-based software (DART SVP software, version 5.0.5) and the optimized DART source settings were: positive ion mode; the run temperature was 300 ℃ with He as the operation gas, grid electrode voltage was 350 V; heater wait time was 5 s ; and contact closure delay was 3 s; a 12-Dip-it glass tip linear rail that ran between the DART ion source and the ceramic tube was used to carry the samples into the source ionization region at a constant speed of 0.2 mm s^{-1}. The distance between the DART ion source outlet and ceramic tube leading into the VAPUR® flange was maintained at 12.0 mm. The scan sequence began with an MS1 spectrum using the Orbitrap analyzer, and the related parameters included a resolution setting of 60000, mass range of m/z 100−500, automatic gain control (AGC) target of 2×10^5, and maximum injection time of 100 ms. The ion transfer tube temperature was 300 ℃. In the analysis of four PAEs, m/z 247.0970 was used for DAP, m/z 251.1282 was used for DPrP, m/z 283.1742 was used for DMEP, and 319.0971 was for DPhP. Orbitrap Fusion Lumos 2.0 Tune (Thermo

Fisher Scientific, U.S.A.) was used for the control of the mass spectrometer. All the MS data were analyzed by Xcalibur software (Thermo Fisher Scientific, U.S.A.), and the data was exported to Origin 8.0 (Originlab, U.S.A.) to make the final plots presented in this chapter.

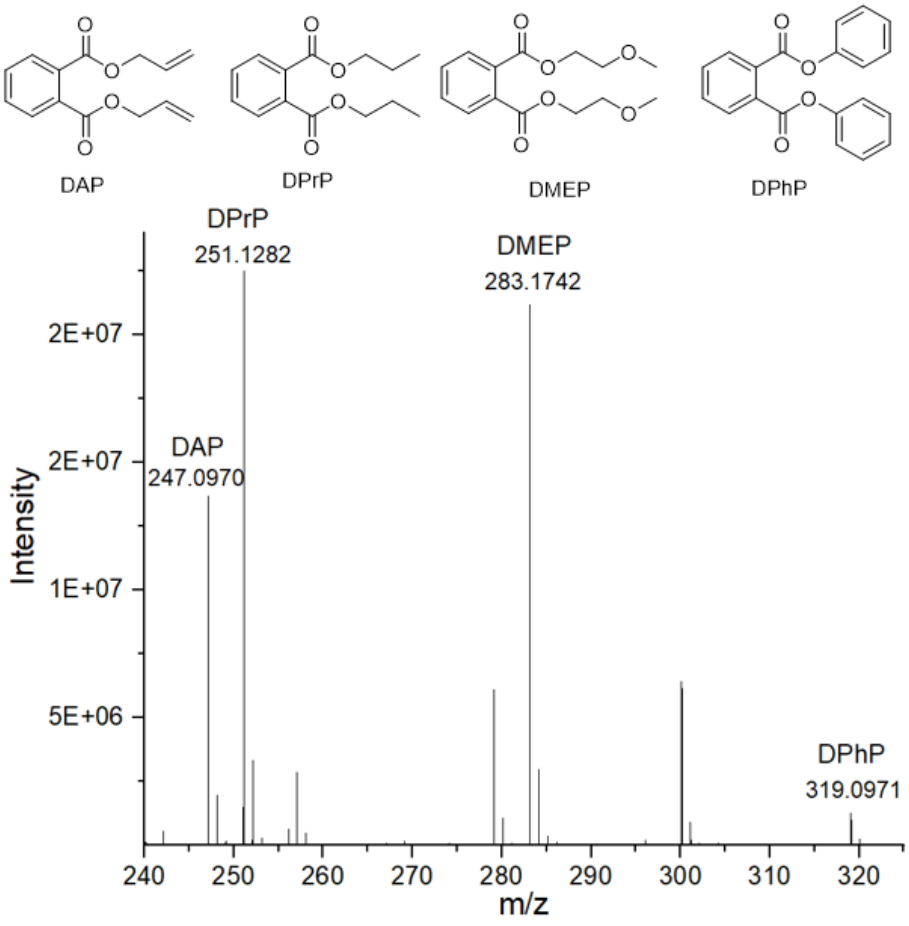

Figure 4.2 Mass spectrum of four PAEs obtained by DART-MS. The structures of four PAEs are shown, and corresponding ions are labelled.

4.3 Results and discussion

4.3.1 Characterization of nine Si-ILs

The morphological characteristics of Si-ILs and fiber coated with Si-ILs were captured by SEM images (Figure 4.2). As is shown in the SEM images, the surface of Si-ILs was rough and

Si-ILs were evenly coated onto SPME fiber. The morphology characteristics of Si-ILs were in accordance with these in previously reported literature.[163]

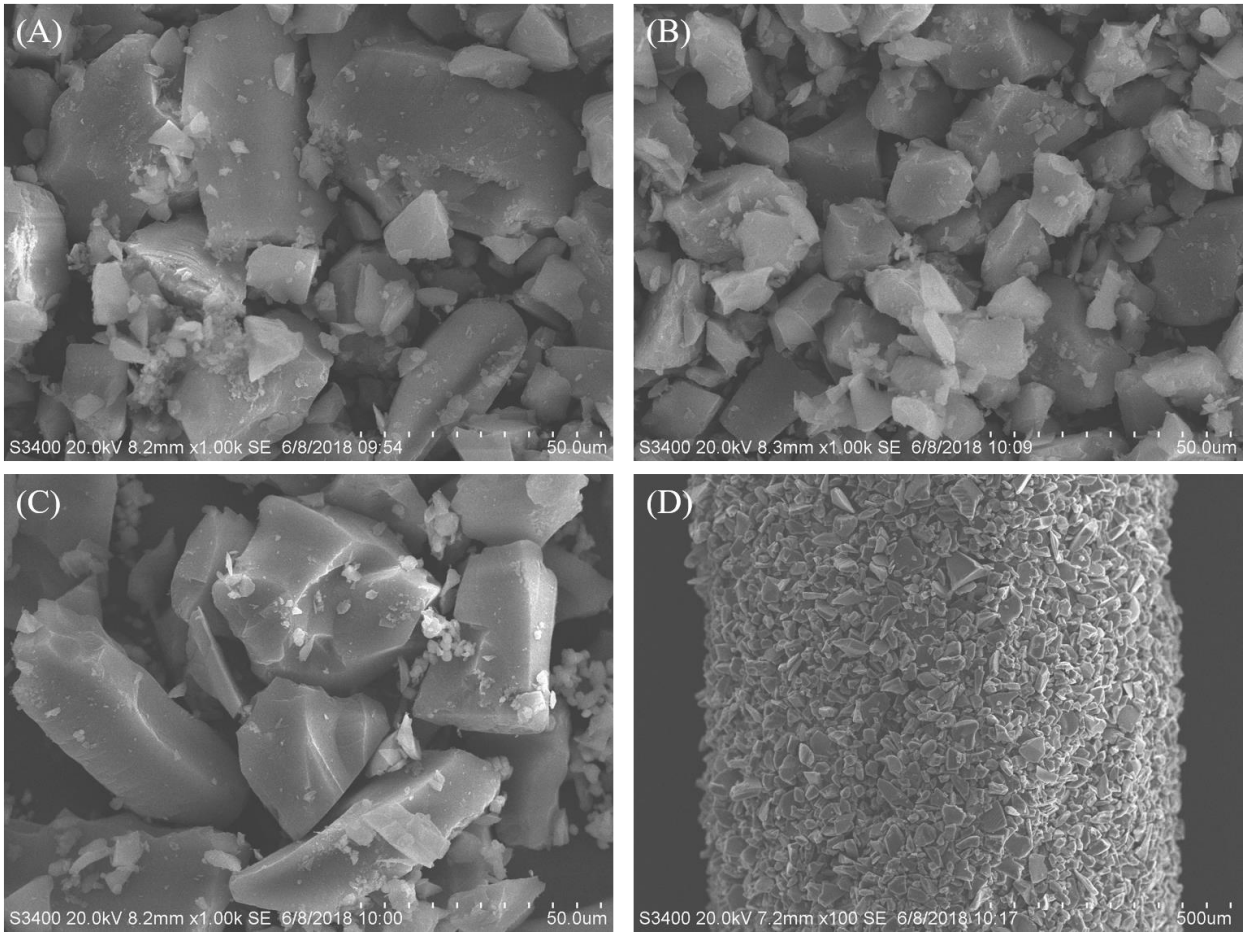

Figure 4.3 SEM images of Si-ILs and SPME fiber coated with Si-ILs: (A) [C_2MIM][Cl]; (B) [C_2MIM][BF_4]; (C) [C_2MIM][PF_6]; (D) SPME fiber coated with [C_2MIM][Cl].

Infrared spectroscopy has been a useful technique for the characterization of chemical compounds. In the FT-IR spectrum of Si-ILs, the assignments of adsorption peaks were marked accordingly, and they were in accordance with these in previously reported literature[163-165]: the large peak at 3450 cm^{-1} is attributed to O-H stretching or N-H stretching vibration; the adsorption

peak at around 1090 cm^{-1} is the typical peak of Si-O-Si; the small peaks ranging from 1500-1600 cm^{-1} correspond to finger print region of C-N vibration, confirming the successful bonding of imidazoles; the adsorption peak at around 700 cm^{-1} means the presence of C-Cl; the adsorption peak at around 550 cm^{-1} is from PF_6^-, and the presence of BF_4^- is indicated by the adsorption peak at around 769 cm^{-1}. The synthesized Si-ILs with same anion but imidazoles of different alkyl chains showed similar profiles. The above information clearly shows the successful synthesis of nine Si-ILs.

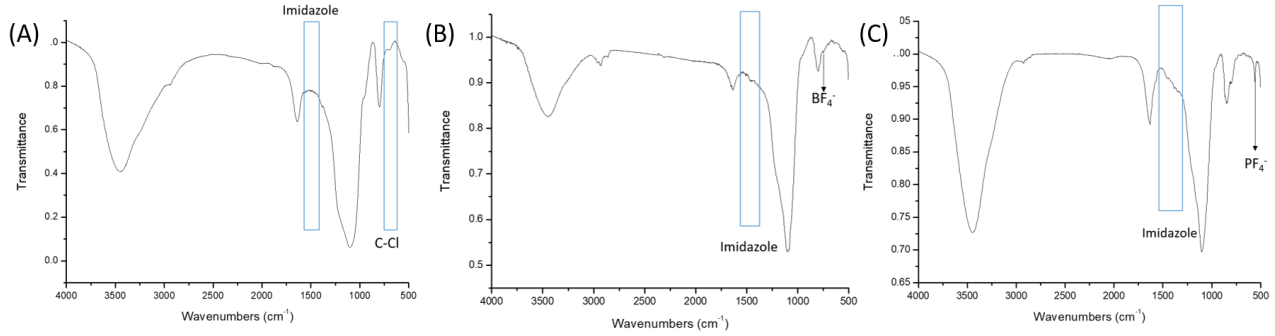

Figure 4.4 FT-IR spectra of as-synthesized Si-ILs: (A) [C_2MIM][Cl]; (B) [C_2MIM][BF_4]; (C) [C_2MIM][PF_6].

4.3.2 Optimization of SPME process

To achieve an optimal extraction efficiency, the extraction temperature and pH were optimized with PAEs standard solutions of 3 μg/mL (Figure C-1, C-2, and C-3). Although higher temperature may increase the mass transfer in the solution, the adsorption capacity may be reduced at the same time. Based on the results we obtained (Figure 4.4), the adsorption efficiency of some Si-ILs did not vary too much, while there was a downward trend of adsorption efficiency with the increase of temperature in the range of 25 ℃ - 65 ℃. Therefore, the extraction was carried out in room temperature. The effect of pH on the extraction process was also studied, because it may

influence the dispersity of sorbents. Sodium hydroxide and hydrogen chloride were added into the solutions to adjust pH. However, no obvious distinction of adsorption capacity was observed in the pH ranging from 5 to 9. Thus, the pH of sample solution was not adjusted in the extraction process for convenience.

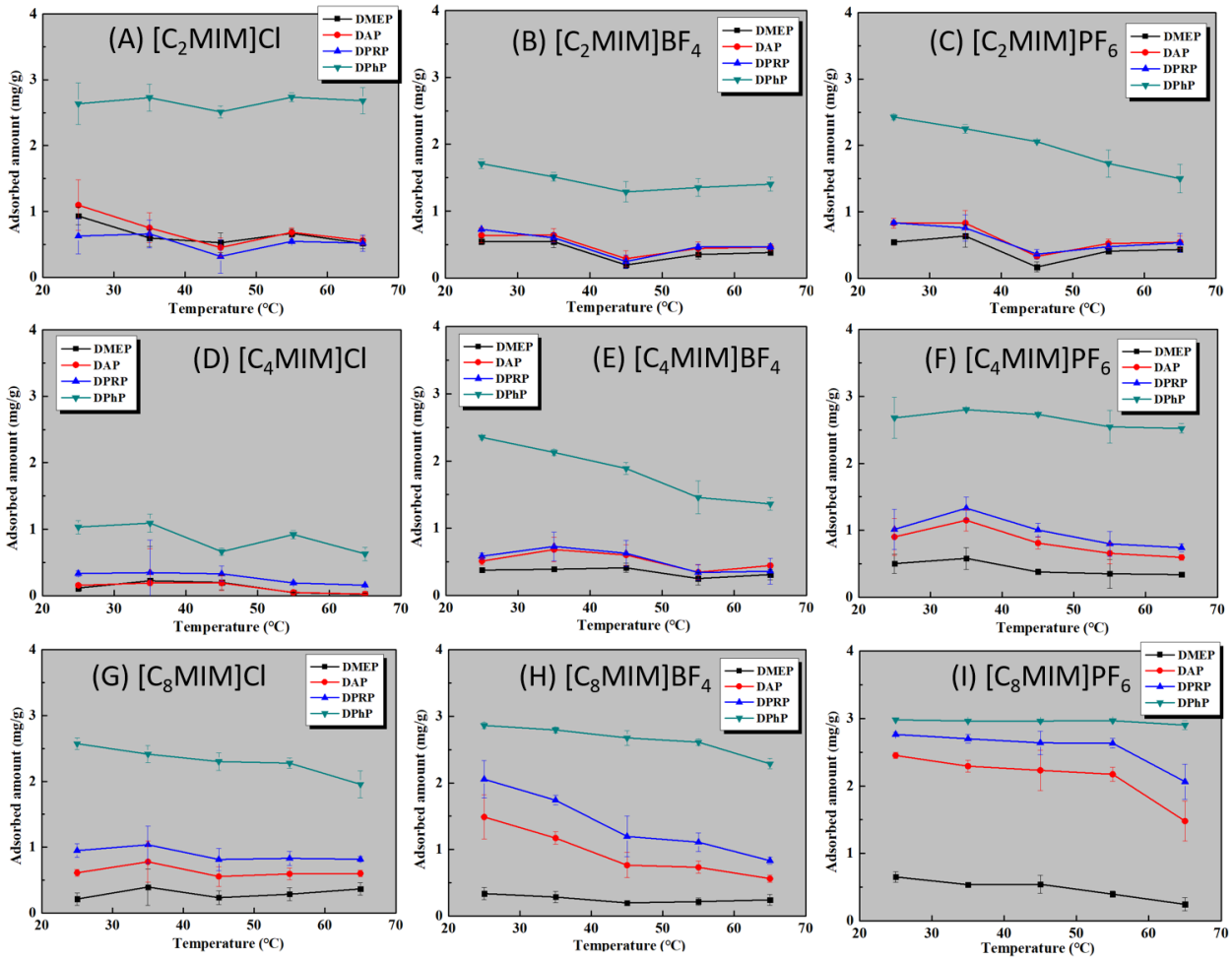

Figure 4.5 Effect of temperature on SPME process: (A) [C_2MIM][Cl]; (B) [C_2MIM][BF_4]; (C) [C_2MIM][PF_6]; (D) [C_4MIM][Cl]; (E) [C_4MIM][BF_4]; (F) [C_4MIM][PF_6]; (G) [C_8MIM][Cl]; (H) [C_8MIM][BF_4]; (I) [C_8MIM][PF_6].

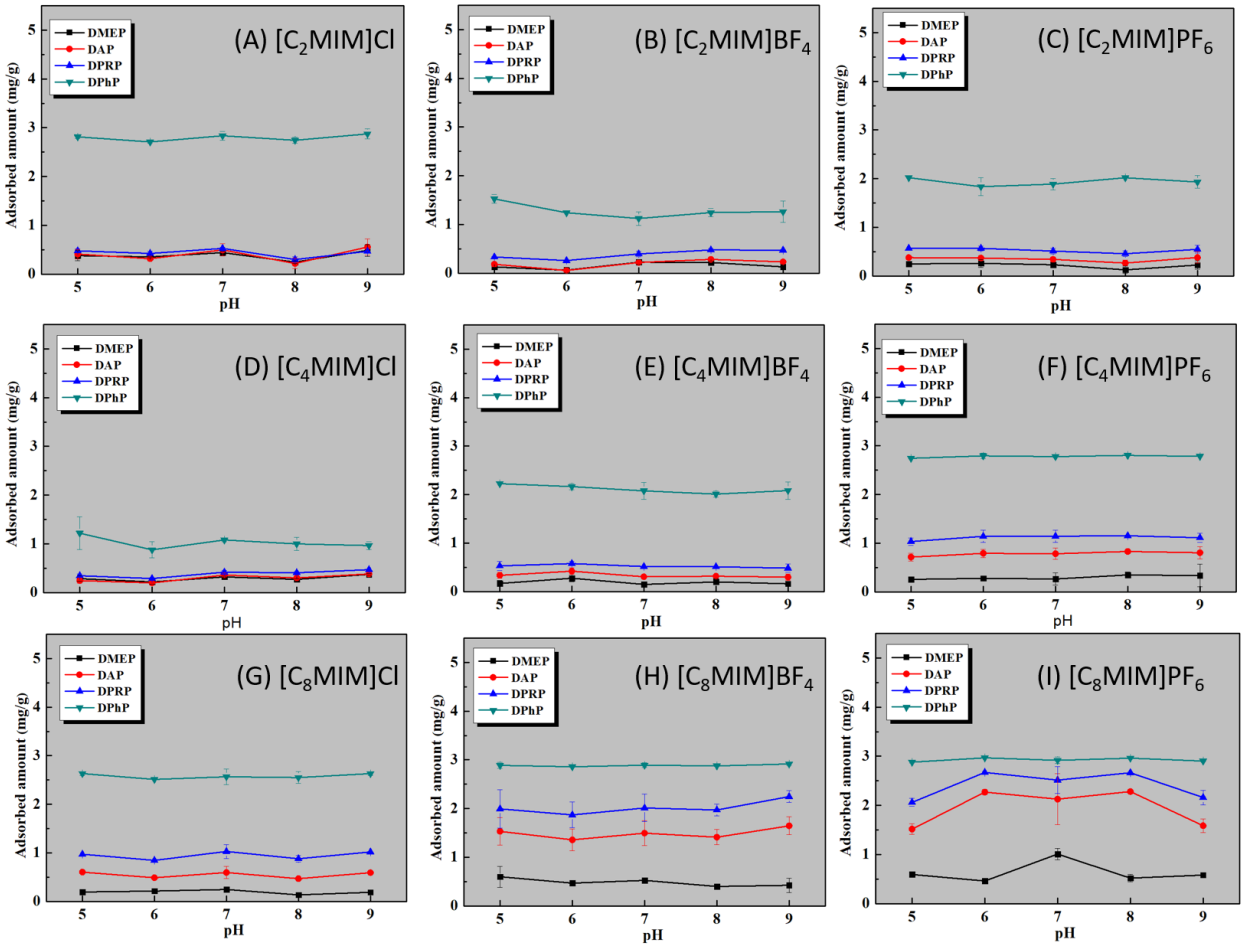

Figure 4.6 Effect of pH on SPME process: (A) [C_2MIM][Cl]; (B) [C_2MIM][BF_4]; (C) [C_2MIM][PF_6]; (D) [C_4MIM][Cl]; (E) [C_4MIM][BF_4]; (F) [C_4MIM][PF_6]; (G) [C_8MIM][Cl]; (H) [C_8MIM][BF_4]; (I) [C_8MIM][PF_6].

4.3.3 Effect of sorbent hydrophobicity on SPME-DART-MS analysis

The relative hydrophobicity of nine Si-ILs prepared in this study was determined by the length of alkyl chains in the imidazoles and counter anions.[166,167] The hydrophobicity of Si-ILs with same counter anion increases with longer alkyl chains in the imidazole. When the length of alkyl chains in imidazoles is the same, the difference in hydrophobicity of Si-ILs is determined by counter anion, and the hydrophobicity increases in the order of Cl^-, BF_4^-, and PF_6^-. Therefore, the

comparison of hydrophobicity of nine Si-ILs can be summarized in the following table. The hydrophobicity increases from top to bottom in each column and increases from left to right in each row. This trend can also be verified by comparing the adsorption capacity of nine Si-ILs in each row or column in Figure 4.4 and Figure 4.5. Because PAEs are hydrophobic analytes, sorbents commonly showed better adsorption with higher hydrophobicity. As were shown in Figure 4.4 and Figure 4.5, there were clear trends that the adsorption capacity increased from top to bottom in each column and increases from left to right in each row, except the rows or columns involving $[C_2MIM]Cl$. In this study, the effect of sorbent hydrophobicity was compared only within each column or row.

	Hydrophobicity increases →		
Hydrophobicity increases ↓	$[C_2MIM]Cl$	$[C_2MIM]BF_4$	$[C_2MIM]PF_6$
	$[C_4MIM]Cl$	$[C_4MIM]BF_4$	$[C_4MIM]PF_6$
	$[C_8MIM]Cl$	$[C_8MIM]BF_4$	$[C_8MIM]PF_6$

Table 4.1 Comparison of hydrophobicity of nine Si-ILs.

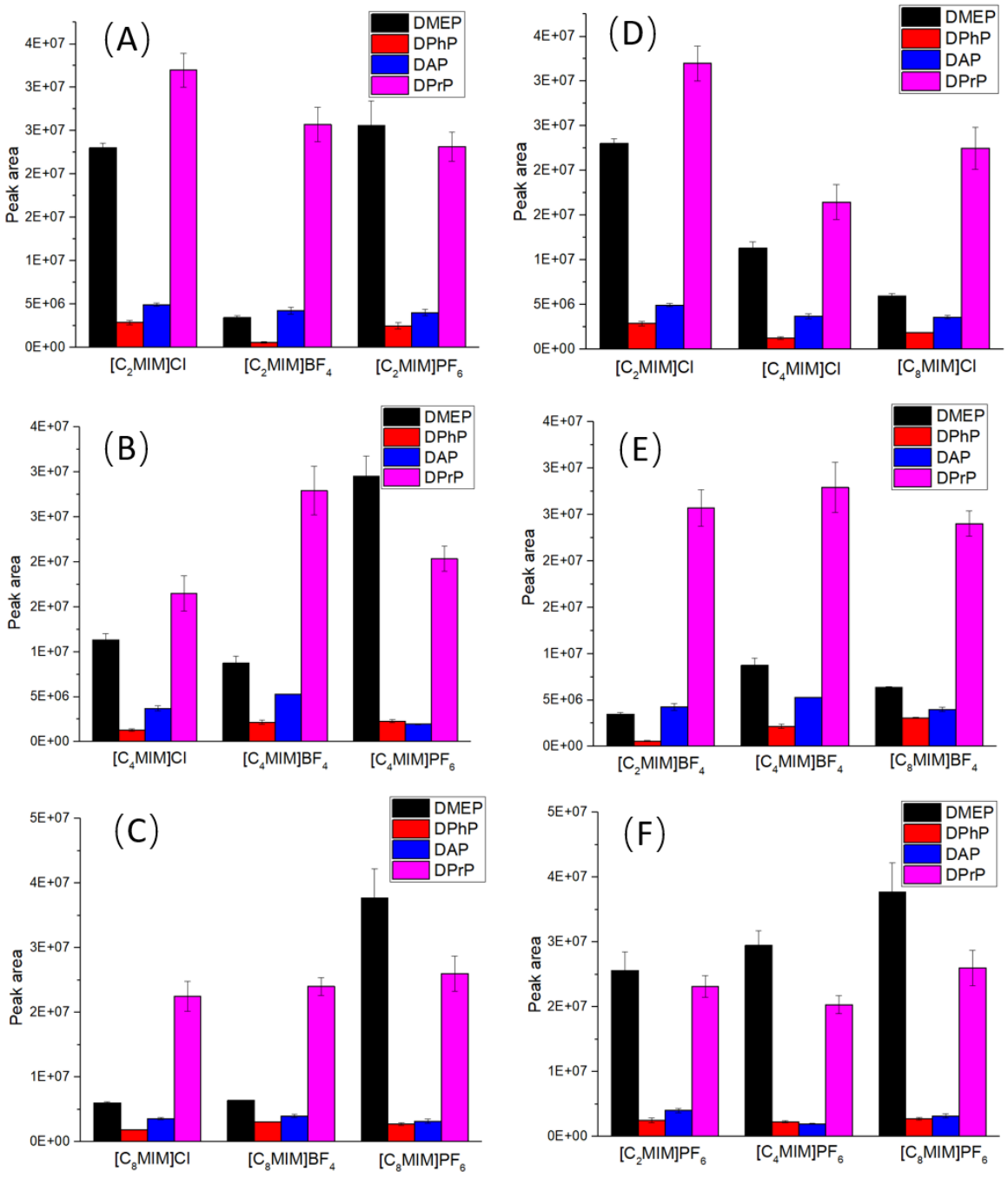

Figure 4.7 Comparison of nine Si-ILs in SPME-DART-MS analysis: (A) Si-ILs with ethylimidazole and different anions; (B) Si-ILs with butylimidazole and different anions; (B) Si-ILs with octylimidazole and different anions; (D) Si-ILs with Cl^- as anion and imidazoles of different alkyl chains; (E) Si-ILs with BF_4^- as anion and imidazoles of different alkyl chains; (F) Si-ILs with PF_6^- as anion and imidazoles of different alkyl chains.

All ILs were found to be hygroscopic to a certain degree[168], and the water sorption increases at higher temperature.[169] As presented in Chapter 2, the moisturization of sorbents can enhance DART-MS signals when they are exposed to DART outlet by improving the ionization efficiency. And SPME-DART-MS can benefit a lot from this unique characteristic using Si-ILs as sorbent, because the hydrophobicity of Si-ILs at low temperature can increase the adsorption capacity of hydrophobic analytes (PAEs in this study are hydrophobic) in SPME process, while the water sorption ability of Si-ILs at high temperature may facilitate the ionization of analytes on the Si-ILs in DART-MS analysis. As displayed in Figure 4.6, the DART-MS signals on nine Si-ILs were examined and compared within each column or row in Table 4.1. In Figure 4.6C, it is evident that the peak area of analytes increased with the increasing hydrophobicity of Si-ILs. However, there was no clear relationship between the sorbent hydrophobicity and analytical performance in SPME-DART-MS based on other figures in Figure 4. Therefore, the effect of sorbent hydrophobicity on SPME-DART-MS remains unclear based on the experimental results shown in this chapter.

4.4 Conclusion

Inspired by our work in Chapter 3, an attempt to uncover the effect of sorbent hydrophobicity on SPME-DART-MS was described in this chapter. Nine custom-designed Si-ILs with different hydrophobicity were used in the SPME-DART-MS analysis of four PAEs. Two key parameters in SPME process were optimized. The analytical results of SPME-DART-MS using nine Si-ILs as sorbents were systematically divided into six groups for comparison. Nonetheless, it was obvious that more efforts or new strategies are needed to provide insights on the effect of sorbent hydrophobicity on SPME-DART-MS.

Chapter 5: Investigation of deep eutectic solvent-based microwave-assisted extraction and efficient recovery of natural products

5.1 Introduction

In recent years, interest in bioactive compounds (such as phenolic acids, ginsenosides, rutin and flavonoids) contribution to human well-being has increased dramatically.[170-173] In addition to reported anti-inflammatory, anti-microbial and anti-enzymatic benefits, bioactive compounds are vital for the development of new medicines.[174] Organic solvents have previously been used to extract such bioactive compounds from various sample matrices.[175] However, the use of traditional, often toxic and volatile, organic solvents increases the environmental burden. Therefore, as a replacement for traditional organic solvents, deep eutectic solvents (DESs) were developed as a "greener" alternative.[176] DESs are usually produced through the complexation of a hydrogen bond acceptor (HBA), such as a quaternary ammonium salt (e.g., choline chloride) and a hydrogen bond donor (HBD).[177] DESs have a low production cost, are non-toxic in nature, are simple to prepare and have good biodegradability, making them an ideal alternative solvent for the extraction of natural products from plants.[178] Previous studies have experimented with DESs and developed a variety of methods for extracting natural products from plants.[80,179,180] These extraction methods include, heating reflux extraction (HRE), ultrasound-assisted extraction (UAE) and microwave-assisted extraction (MAE).[181,182] An increased extraction temperature is often required due to the high viscosity of DESs. Thus, due to their heating component, HRE and MAE are the most widely used methods for DES-based extraction in both experimental and industrial

settings. However, MAE is usually preferred due to its higher heating and extraction efficiency.[183-185]

During MAE, polar solvent molecules interact with microwaves, resulting in heating via ionic conduction and dipole rotation.[186,187] This may occur either via just one of these mechanisms, or via both simultaneously. MAE can thus be applied to extract natural products from plants. In dried plant material, the heating target is minute traces of moisture that are present even in desiccated plant cells. Microwave heating of this intracellular moisture results in evaporation, generating tremendous pressure on the cell wall, leading to cell rupture.[184] Thus, exudation of the active constituents of the ruptured cells occurs, increasing the yield of phytoconstituents. Even higher yields can be obtained by increasing the extraction temperature, which facilitates faster penetration of the solvents into cell walls. Although the principle of traditional organic solvent MAE has been studied, the principle of DES-MAE is still not clear, even though this technique has been used to extract bioactive compounds from several plants.[84,188,189] Therefore, the principle of DES-MAE should be further studied to better understand and guide the application of DES-MAE in laboratories and on an industrial scale in the future.

To systematically study DES-MAE methodology, *rheum palmatum* was selected as a model plant matrix. The constituents of *rheum palmatum* include flavonoids, polyphenols, dianthrones, anthocyanins and anthraquinones. Anthraquinones, such as aloe-emodin, emodin, chrysophanol and physcion (Figure D-1), are the major bioactive components of interest in *rheum palmatum*, which has proven antimicrobial, antibacterial and anti-inflammatory functions.[190-192] Therefore, anthraquinones were selected as the target bioactive compounds to evaluate the extraction performance of DESs under MAE. It is essential that the thermal behavior of DESs during MAE is studied, as MAE also results in heating of the solvent. An increase in the

temperature of the DES should be conducive to improved extraction efficiency due to increased solvent fluidity and solubility. To investigate DES thermal behavior, three types of DESs with different HBDs (acids, amines and alcohols) were used. Cell morphology was also studied after the DES-MAE process, as MAE usually results in cell morphology changes. Other factors affecting extraction were also investigated by using optimizing by response surface methodology (RSM). These methodologies allowed us to compare the well-known principle of MAE with that of DES-MAE to enable optimum extraction performance in further studies. To complete the natural product extraction process from *rheum palmatum*, phenyl (PHE-SIL), octyl (C_8-SIL) and amino groups (NH_2-SIL) were modified to the surface of silica to recover the targets from DES extracts. By comparing the adsorption effects of these sorbents, some possible interactions and effective functional groups were presented. This information would be useful for the design of future efficient sorbents for the recovery of targets from DES extracts. In the next plan, we hope to use DART-MS for the high-throughput analysis of these DES extracts.

5.2 Experimental section

5.2.1 Chemicals and materials

Aloe-emodin, emodin, chrysophanol and physcion (analytical standard), choline chloride (≥ 98.0%), glycerol (≥ 98.0%), glycol, 1,4-butanediol (≥ 98.0%), methylurea (≥ 98.0%), acetamide (≥ 98.0%), urea (≥99.5%), malonic acid (≥98.0%), citric acid (≥ 98.0%), malic acid (≥98.0%), trimethoxyphenylsilane (>98.0%), (3-aminopropyl)trimethoxysilane (97.0%), trimethoxy(octyl)silane (97.0%), and silica gel (37-54 μm) were obtained from Aladdin Industrial Inc. (Shanghai, China). Ethyl acetate, acetone, methanol, ethanol and cyclohexane were supplied by Sinopharm Chemical Reagent Co., Ltd (Shanghai, China). Distilled water was vacuum filtered

(HA-0.45, Division of Millipore, USA) prior to use. The *rheum palmatum* (dried) were purchased from local market. The applied regents in this study were all in HPLC or analytical grade and used without further purification. Stock solutions of aloe-emodin, emodin, chrysophanol and physcion (0.1 mg mL^{-1}) were prepared in methanol and were placed in vials and kept at 4 °C before use.

5.2.2 Synthesis of DESs

The preparation of DESs was conducted as described previously.[84] Briefly, different molar ratios (1:1, 1:3) of HBA (choline chloride) and HBDs were mixed in a round-bottomed flask and heated to 80.0 ℃ with constant stirring until a homogeneous liquid formed. In brief, they are referred as DES-1 (glycerol based), DES-2 (glycol based), DES-3 (1,4-butanediol based), DES-4 (methylurea), DES-5 (acetamide based), DES-6 (urea based), DES-7 (malonic acid based), DES-8 (citric acid based), DES-9 (malic acid based), respectively.

5.2.3 Investigation of heating rates of DESs

In order to investigate the heating rate, mixture of different DESs with 0, 20, 40, 60 and 80 wt% of water (20.0 mL) were added into a 50 mL beaker and heated for 0.5, 1.0, 1.5, 2.0 and 3.0 min under microwave irradiation (WBFY-201, Gongyiyingyu Instrument Co., Ltd., China) at the power of 80 W.

5.2.4 Extraction of anthraquinones from rheum palmatum

Dried *rheum palmatum* was first smashed into powders with a grinder (FW100, Taisite Instrument Co., Ltd., China). The powder (0.12 g) was added to a 50 mL round-bottomed flask containing 10.0 mL DES solution and then the flask was subjected to the microwave irradiation at 80 W for 16.5 min. Key factors influencing the MAE including solid/liquid ratio (0.005 -

0.045 g mL^{-1}) and the extraction time (1.0-20.0 min) were optimized. After MAE, suspensions were centrifuged (Centrifuge H-1650, Xiangli Centrifuge Co., Ltd., China) at 10000 rpm for 5.0 min. The supernatant was collected and diluted with 50% water prior to UPLC-UV analysis.

5.2.5 Comparison of different extraction methods and solvents

Conventional extraction methods including HRE and UAE were used for the comparison with DES-MAE method. *Rheum palmatum* powder (0.12 g) was extracted with 10.0 mL solvent by the three extraction methods, respectively. UAE (ultrasonic cleaner KQ-400 KDB, Nanjing David Instrument Co., Ltd., China) and HRE were performed with two solvent systems of DES-8 (HBA/HBDs = 1:1, mol/mol, 80 wt%) aqueous solution and methanol. In addition, five organic solvents including ethyl ether, acetone, methanol, ethanol and cyclohexane were used for MAE and compared with DES-8. The extracts (supernatant) were quantified by UPLC-UV after centrifugation at 10000 rpm for 5.0 min.

5.2.6 Synthesis of three sorbents for recovery

Silica was first immersed in hydrochloric acid for 24.0 h and then washed with DI water and dried at 100 ℃ for 8.0 h. The activated silica (6.0 g) was suspended in 60.0 mL of dry toluene and then excess trimethoxyphenylsilane (6.0 g), trimethoxy(octyl)silane (6.0 g), and (3-aminopropyl)trimethoxysilane (6.0 g) were added, respectively. The suspension was stirred and refluxed for 24.0 h. After refluxing, the reaction was stopped and the modified sorbents were cooled to room temperature, and washed with toluene, and ethanol in turn. The obtained sorbents functionalized with phenyl, octyl, and amino groups were named as PHE-SIL, C_8-SIL, and NH_2-SIL, respectively. The sorbents were finally dried at 60.0 ℃ for 6.0 h.

5.2.7 Recovery of anthraquinones from DES extract

The extract was then diluted to 40 % DES solution with water to break the hydrogen bonds in the DESs. Then sorbent (20.0 mg) was added and subjected to ultrasonication (1.0 min) (Scientz Ultrasonic Cleaner SB-3200DTN, Ningbo Co., Ltd., China), and vortexing (5.0 min) (The US SCILOGEX Cyrus Czech MX-S Adjustable Mixer) were used for assisting adsorption at room temperature with adding 5 % (*w/v*) of NaCl. The sorbents were separated from the extract by centrifugation (TGL-16M desktop high speed refrigerated centrifuge, Xiangli Centrifuge Co., Ltd., China). The sorbents were then transferred into a tube and dried in oven, and the adsorbed target compounds were eluted with 0.4 mL of ethanol with ultrasonication. The final eluent was separated from the sorbents by centrifugation. Finally, the eluent was analyzed by UPLC-UV (Thermo UltiMate 3000 Series).

5.2.8 Other experimental details

Other experimental details including instruments used in this chapter (similar to those used in former chapters), experimental design of response surface methodology (RSM), and characterization of three sorbents for recovery were listed in Supporting Information.

5.3 Results and discussion

5.3.1 Study on principle of DES-MAE

During MAE, the heating efficiency of the DES affects its fluidity, viscosity, and the solubility of the target compounds. In addition, the elevated temperature of the solution may weaken hydrogen bonds within the cell wall, therefore promoting the dissolution and destruction of the

cell wall by the DES and improving extraction efficiency. Therefore, the heating efficiency of different DESs was first studied. As the HBD used has a great influence on the properties of DESs, the DESs were classified into three groups (alcohol-based, amide-based and acid-based) according to their HBD types. Choline chloride (ChCl) was used throughout as the HBA. (Table 5.1).

Table 5.1 Abbreviations and components of DESs used in the experiments

Abbreviation	HBA	HBD	Mole ratio
DES-1	Choline chloride	Glycerol	1:1, 1:3
DES-2		Glycol	1:1, 1:3
DES-3		1,4-Butanediol	1:1, 1:3
DES-4		Methylurea	1:1, 1:3
DES-5		Acetamide	1:1, 1:3
DES-6		Urea	1:1, 1:3
DES-7		Malonic acid	1:1, 1:3
DES-8		Citric acid	1:1, 1:3
DES-9		Malic acid	1:1, 1:3

In the case of alcohol-based DESs (DES 1-3), the solvent temperature increased as the time of microwave irradiation increased (Figure 5.1). We also observed that the heating rates of the alcohol-based DESs with a molar ratio of 1:3 (HBA:HBD) were slightly higher than those of the alcohol-based DESs with a molar ratio of 1:1 (HBA:HBD). The addition of the alcohol-based HBDs leads to an increase in OH moieties in the solution, which are excited by microwave frequency. Thus, water was added into the DESs to further increase the number of polar moieties

in the system to verify this effect. However, the heating rate decreases with the increase of water content. According to a previous report, the molar heat capacities of the binary mixtures of DESs and water increase with increasing DESs mole fraction,[193] which is contradictory to the experiment results here, meaning more factors need to be considered besides the molar heat capacity. The addition of water may destroy the existing hydrogen bonds between the initial constituents,[194] and this change of the nature of hydrogen bonds existing in the solution may be the possible reason for the observed phenomenon. Consequently, more microscopic information of the DESs-water binary mixtures is needed before the mechanism is well understood.

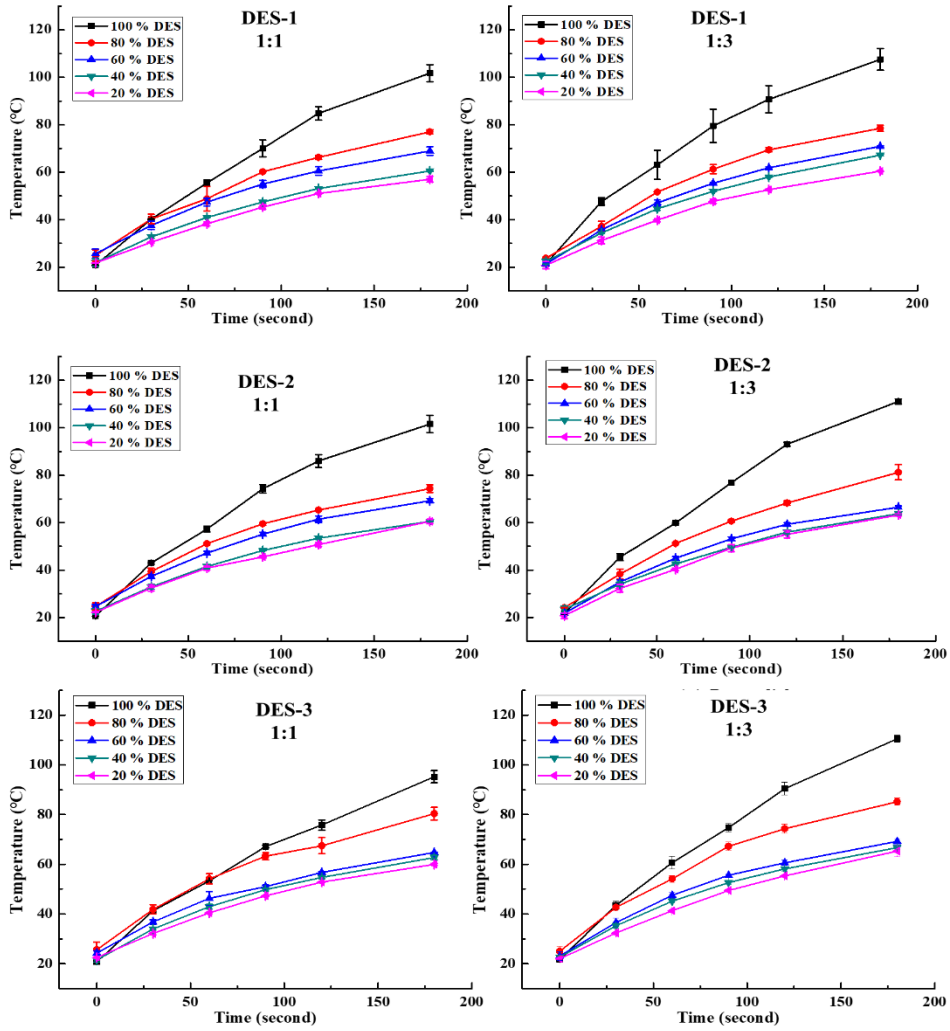

Figure 5.1 The heating rates of DES-1 to DES-3 and their aqueous solutions with HBA/HBD molar ratio of 1:1 and 1:3.

Similarly, in the case of the amide-based DESs, as microwave radiation time increases, the temperature of the solvent also increases (Figure 5.2). The heating rate of all the amide-based DESs slightly increased as the HBD content increased, except in the case of pure DES-4 with no addition of water. This may be attributed to the relatively weak polarity of methylurea. As the microwave absorption capacity of the whole system decreased with the increasing content of methylurea, and therefore so did the heating rate. With the increase of water content, the heating rate of the binary DESs-water mixture also decreased.

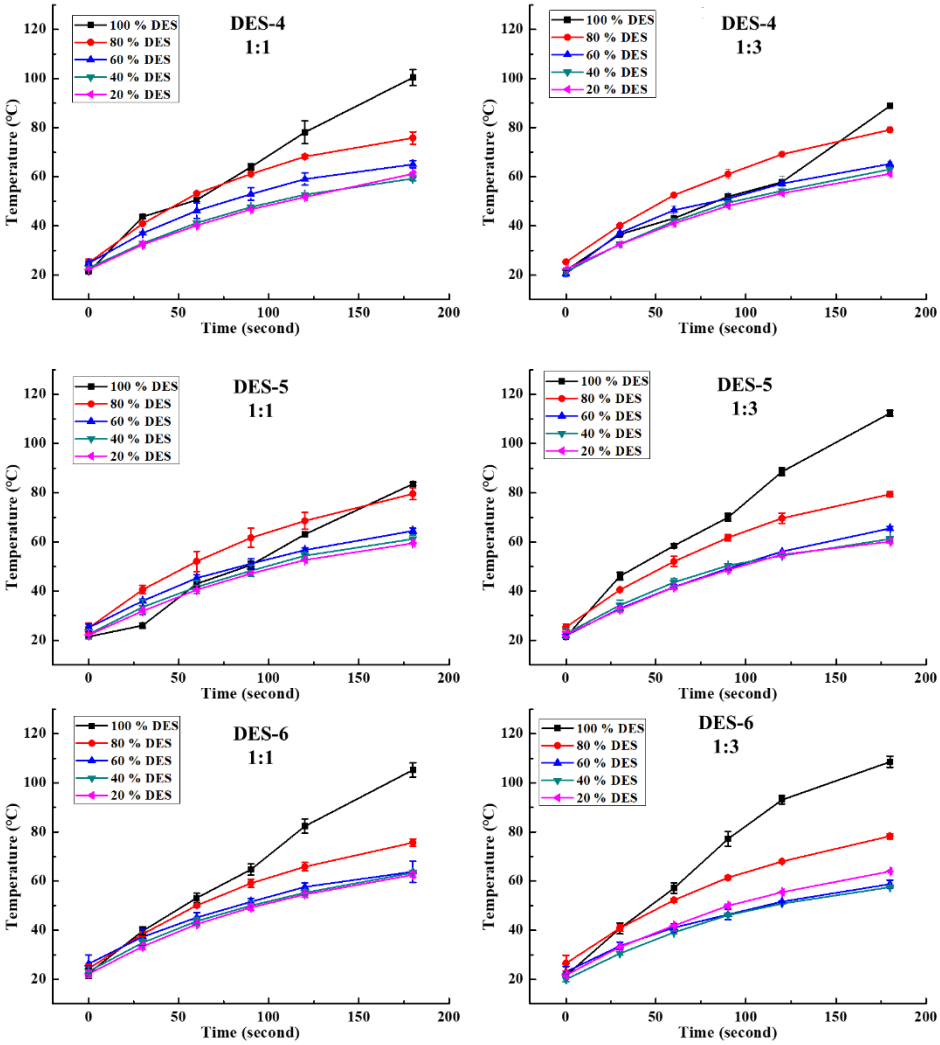

Figure 5.2 The heating rates of DES-4 to DES-6 and their aqueous solutions with HBA/HBD molar ratio of 1:1 and 1:3.

The heating rates of acid-based DESs did not differ greatly from those of the alcohol and amide-based DESs (Figure 5.3). Only DES-8 had a different heating rate curve from all other DESs. The heating rate of pure DES-8 was even lower than that of DES aqueous solution with 80% water content. This is an unusual phenomenon, which possibly could be attributable to DES-8's citric acid functional groups. Citric acid contains three carboxyl groups and one hydroxyl

group. These carboxyl groups can form many hydrogen bonds, both with ChCl, and with itself, and these crosslinked hydrogen bond networks possibly make the system more rigid.[84] DES-8 also presents as a hard solid material at room temperature, and this may make it difficult for the microwaves to act on the molecules in order to heat the system. In addition, DES-8's solid state conceivably makes heat transfer less efficient and reduces the microwave's penetration ability.

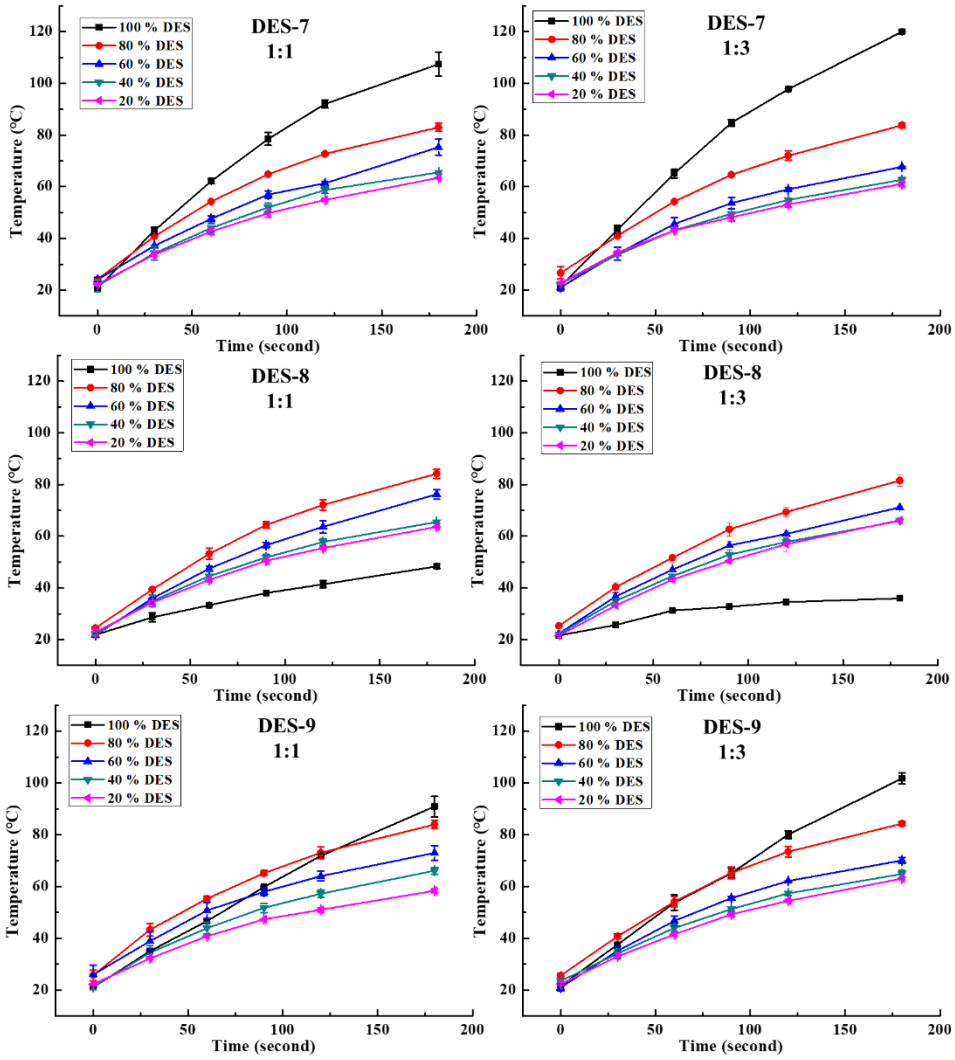

Figure 5.3 The heating rates of DES-7 to DES-9 and their aqueous solutions with HBA/HBD molar ratio of 1:1 and 1:3.

As MAE with traditional solvents usually results in destruction of the plant cell wall, it is of interest to study the effect that the alternative DES-MAE has on cell walls. To study this, the morphology of the plant matrix before and after extraction was characterized using SEM. As Figures 5.4 and D-4 show, the sample's cell wall was partially destroyed and dissolved after MAE with water. However, when using methanol as the solvent, this effect is reduced. This finding is consistent with results reported in previous literature.[84,188] When DESs were used as the solvents for MAE, plant cell wall destruction and dissolution was far greater than that for extraction using water. The cell walls of most samples were destroyed and dissolved when DESs were used. Amide-based DESs were more efficient at cell wall destruction than alcohol-based DES. One of the reasons may be the stronger hydrogen bonding between amide-based DESs and cell walls (typically cellulose). Additionally, recent studies have demonstrated that DESs showed a driving force for the formation of micelles,[195-197] which can destruct the lipid bilayers of cell wall and therefore may improve extraction efficiency. Unexpectedly, the destruction and dissolution of the cell wall by acid-based DESs were better than that of other solvents, demonstrated by the silky-smooth surface shown in the SEM images. DESs and glucose were used as models to investigate this phenomenon. Therefore, DESs were mixed with glucose under microwave irradiation for 3.0 minutes. These solutions were then analyzed using an ultraviolet-visible spectrophotometer. An absorption peak between 250 and 300 nm was observed only in the DES-7, 8 and 9 solutions containing glucose (Figure 5.4 and D-5). The results suggest that the carboxylic acid in the DESs may interact or react with glucose. To further verify whether DESs react with glucose, the products of the DES-8 and glucose solution, heated by microwave irradiation, were analyzed via liquid chromatography-mass spectrometry. The results in Table 5.2, and Figure 5.4, D-6 and D-7 show that the ionic peaks of the esterification products of citric acid and glucose were observed in both

the positive and negative ion modes. Unexpectedly, the esterification products of ChCl and citric acid as well as ChCl, citric acid and glucose were found in the mass spectrometry data. This indicates that the carboxylic HBDs can react with the hydroxyl groups of glucose and ChCl, or other similar hydroxyl groups on cell wall under microwave heating (Figure 5.5). This also suggests that the hydroxyl groups on the plant cell wall may react with the carboxylic acid and that the cellulose, hemicellulose and lignin in the washed residue may not be reconnected by hydrogen bonds, thus resulting in the silky flowing surface seen in the images of Figure 5.4. However, the detailed mechanisms of these reactions remain unclear as they cannot be explained by the organic chemistry we have acquired so far. Thus, we will seek help from some experts in organic chemistry to understand the mechanism of these reactions in the future.

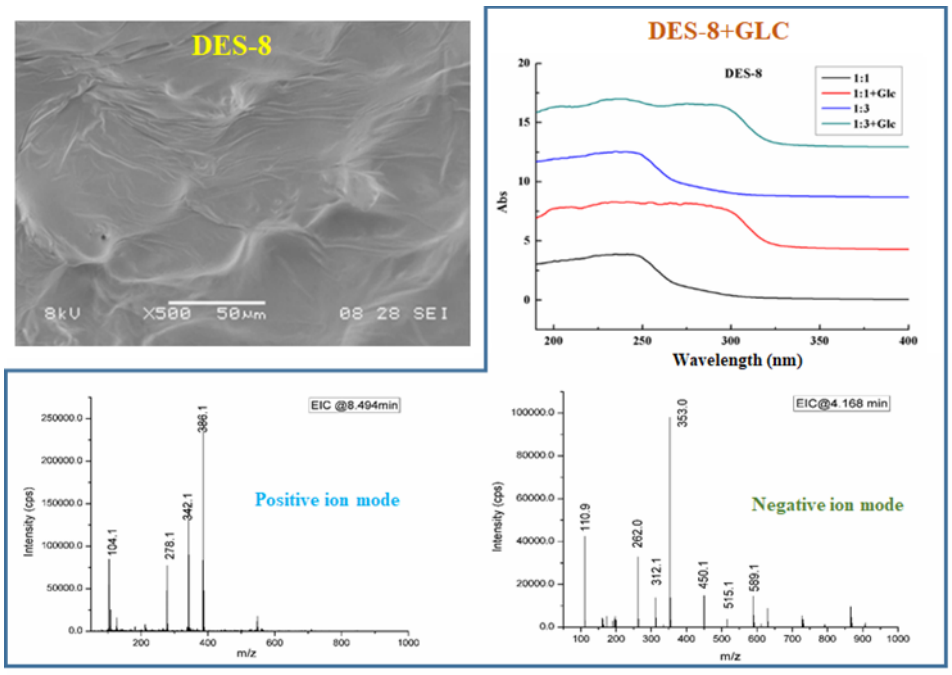

Figure 5.4 SEM image of residue after DES-MAE, and UV-Vis and LC-MS data of reaction products of DES-8 and glucose.

Table 5.2 Data from LC-MS analysis.

Negative ion mode			
RT (min)	Proposed composition and ion forms	Measured *m/z* value	Accurate *m/z* value
4.168	$[CC+CA-H_2O-H]^-$	312.1	312.09
4.168	$[Glu+CA-H_2O-H]^-$	353.0	353.08
4.168	$[2Glu+CA-2H_2O-H]^-$	515.1	515.12
4.435	$[CA-H]^-$	191.0	191.02
5.167	$[Glu+2CA-2H_2O-H]^-$	527.0	527.09
8.682	$[Glu-H_2O-H]^-$	160.9	161.05
Positive ion mode			
RT (min)	Proposed composition and ion forms	Measured *m/z* value	Accurate *m/z* value
8.494	$[Glu+CA-H_2O-2H_2O+Na]^+$	342.2	342.06
8.494	$[Glu+CC+CA-2H_2O-CH_2OH-COOH-2H_2O+Na]^+$	386.1	386.10

5.3.2 Plant anthraquinone extraction

To verify how DES-MAE acts on the extraction of plant samples, this method was used to extract anthraquinones from *rheum palmatum.* To investigate their extraction abilities, the three groups of DESs (HBAs:HBDs of 1:1 and 1:3) were used to extract four anthraquinones from *rheum palmatum.* Because pure amide-based and acid-based DESs are gelatinous, their fluidity cannot be improved further even if about 10% water is added. Although heating can improve their fluidity, once cooled, the solution becomes gelatinous again, which is not conducive for subsequent treatment. To compare the effect of water addition on the extraction efficiency, 20 wt% and 80 wt% water were added to DESs for extraction. Because 20 wt% water could not be mixed with DES-8 (HBA:HBD=1:3), this DES was not used for extraction. As shown in Figure 5.6, the extraction efficiencies of 80 wt% DES solutions were much better than those of 20 wt% DES solutions. This may be because the heating rates of 80 wt% DESs was better than that of 20 wt%

DESs. With respect to the extraction efficiency of 80 wt% DES solutions, acid-based DESs exhibited better performance than the others. Acid-based DESs can destroy and dissolve the cell wall better, which is one of the reasons for the increased extraction efficiency. DES-8 with an HBA:HBD molar ratio of 1:1 exhibited the best extraction performance, and the water content in DESs significantly influenced the extraction efficiency. Thus, the extraction performance of 10-80 wt% DES-8 aqueous solutions was further investigated. As shown in Figure D-8A, the amounts of anthraquinones extracted decreased rapidly with increasing water content in DES-8. This may be attributed to the fact that the heating rate rapidly decreased when the water content in DES-8 increased, thereby slowing down the destruction process of cell wall and reducing solubility of the target compounds.

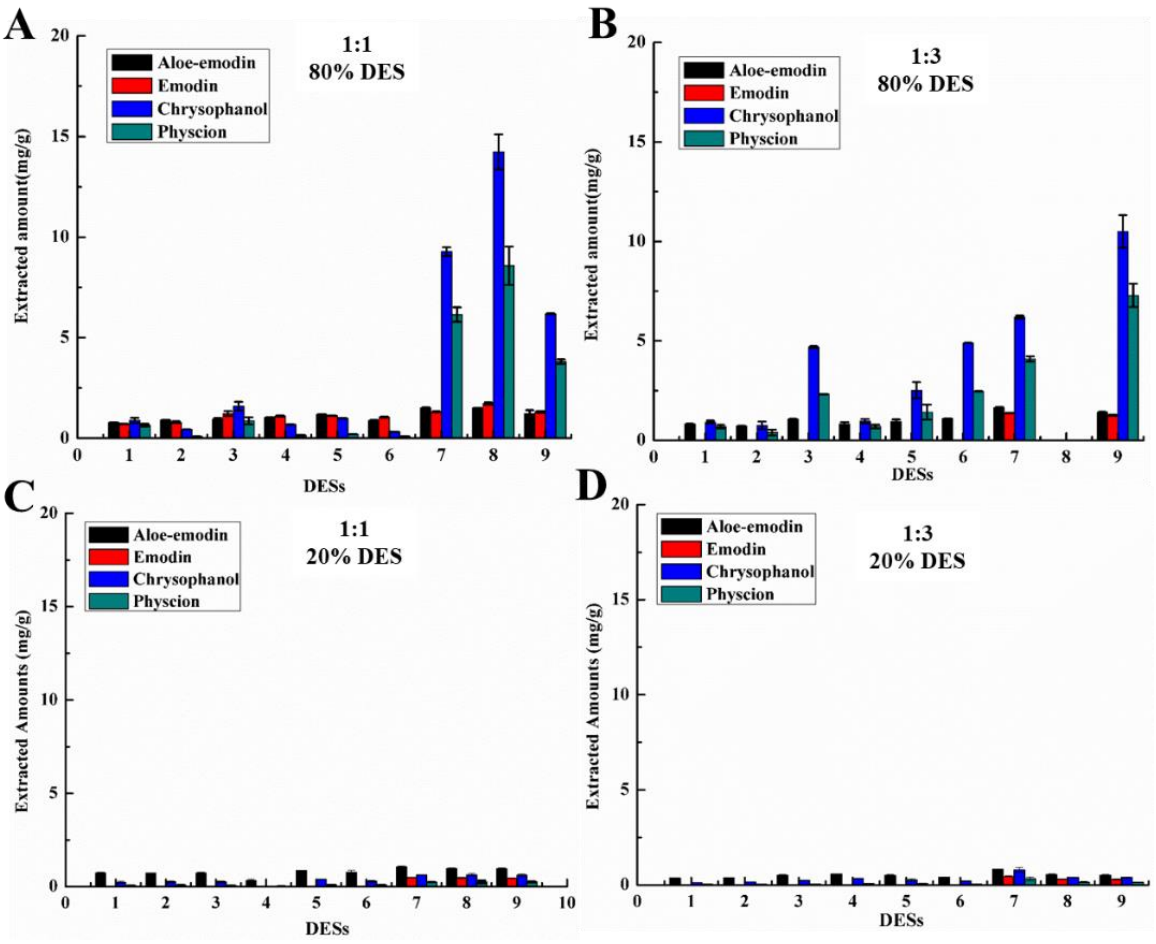

Figure 5.5 Extracted amount of four anthraquinones from rheum palmatum: (A) 80 wt% DES (HBA:HBD=1:1, mol/mol), (B) 80 wt% DES (HBA:HBD=1:3, mol/mol), (C) 20 wt% DES (HBA:HBD=1:1, mol/mol), (D) 20 wt% DES (HBA:HBD=1:3, mol/mol).

In addition, the solid/liquid ratio and extraction time have also been investigated. For *rheum palmatum* concentrations ranging from 0.005 to 0.045 g mL^{-1}in 80% DES-8 solution, the extracted amounts increased slightly from 0.005 to 0.015 g mL^{-1} and then decreased rapidly in the range 0.015-0.045 g mL^{-1} (Figure D-8B). Therefore, a solid/liquid ratio of 0.015 g mL^{-1} was selected for the following optimization. For the purpose of optimizing the extraction time, extractions were performed for 1, 5, 10, 15, and 20 min. From Figure D-8C, it is evident that the extracted amounts

increased with increasing duration of extraction from 1 to 15 min and decreased thereafter. Therefore, 15 min was selected as the extraction time for the rest of the experiments.

5.3.3 Optimization of DES-MAE by using RSM

Through previous single-factor experiments, the range of DES-8 content in the extraction solution (60-80 wt%), solid/liquid ratio (0.01-0.02 g mL^{-1}), and extraction duration (10.0-20.0 min) were selected for RSM optimization.

After fitting the experimental data (Table D-2) to the quadratic polynomial model, as shown in Table D-3, the analysis of variance (ANOVA) of extracted amounts of anthraquinones indicated that the coefficients of determination (R^2) of the experimental data were 0.9836 for aloe-emodin, 0.9898 for emodin, 0.9861 for chrysophanol, and 0.9880 for physcion using the calculated model, without any significant lack of fit (0.0546-0.0668). ANOVA of the quadratic polynomial model showed that the model was satisfactory, as evidenced from the *F*-test with a very low probability value. The coefficients of determination, the adjusted coefficients of determination (R^2_{Adj} = 0.9625 for aloe-emodin, 0.9767 for emodin, 0.9683 for chrysophanol, and 0.9725 for physcion), and the coefficient of variation (CV = 2.99 for aloe-emodin, 3.91 for emodin, 12.96 for chrysophanol, and 10.39 for physcion) suggest that the accuracy and general availability of the polynomial model were sufficient. A signal to noise ratio greater than 4 measured by "Adeq. Precision" is normally desirable, and a value of 19.510-24.022 indicates that this model can be used to navigate the design space.

The significance of each coefficient was checked by using an *F*-test and by determining the *p* value (Table D-4). The regression equation was graphically represented by a 3D response surface. From the 3D response surface curves shown in Figure D-9, the effects of independent variables

and their mutual interactions on the amounts of anthraquinones extracted from *rheum palmatum* can be observed. According to the *p* values and the 3D response curves, it is clear that the content of DES-8, the solid/liquid ratio, and the extraction time for anthraquinones were all significant, with the exception of the extraction time for aloe-emodin. This may be due to aloe-emodin having the lowest content in *rheum palmatum*. When two variables were fixed, the adsorption trends with a single variable showed similar trends to those observed in previous single-factor optimizations. On the other hand, the interaction parameter of X_1X_3 was significant, which indicated that the interactive effect between DES-8 content and time had a significant effect on the amounts of anthraquinones extracted. It could be that the interactive effect between DES content and extraction time affected the heating of the solution, thus affecting the extraction efficiency. Because the solid/liquid ratio had no effect on the heating of the solution, the interactive effect with DES content (X_1X_2) or time (X_2X_3) is not significant.

Taking these factors into consideration, the conditions were optimized for maximal extraction of the four anthraquinones. The software predicted the optimum content of DES-8, solid/liquid ratio, and time to be 80 wt%, 0.012 g mL^{-1}, and 16.46 min, respectively, with the estimated maximum extracted amounts of 2.26, 2.43, 34.53, and 20.99 mg g^{-1} for aloe-emodin, emodin, chrysophanol and physcion, respectively. These conditions were used to extract anthraquinones to test the predictions from the model. Under these conditions, 2.29±0.09, 2.32±0.15, 35.44±0.71 and 20.80±0.09 mg g^{-1} of aloe-emodin, emodin, chrysophanol and physcion were extracted, respectively, confirming that the response model is suitable for optimization.

5.3.4 Comparison of different extraction solvents and methods

Anthraquinones in *rheum palmatum* were extracted using ethyl acetate, acetone, methanol, ethanol, and cyclohexane as extraction solvents, under the same conditions, and the results

obtained were compared with those for DES-8 (Figure D-10). DES-8 aqueous solution showed the best extraction efficiency because of its unique extraction performance under microwave irradiation. Furthermore, several traditional methods, including heat reflux extraction (HRE) and ultrasound-assisted extraction (UAE), were used for the extraction of anthraquinones from *rheum palmatum* using DES-8 (80%) and methanol. Results are listed in Table D-5. For HRE and UAE, the extraction yields with methanol were higher than those with 80% DES-8 solution. However, combined with MAE, excellent extraction efficiencies of the target compounds were obtained with DES-8. Table D-5 shows that the MAE methodology is more efficient than the other methods.

5.3.5 Recovery of anthraquinones from extract

Recovery of target compounds from DES extracts has always been a focus and a challenge in DES extraction research. Although our previous studies investigated the overall recovery strategy, few studies have been conducted on acid-based DESs and the effect of sorbent functional groups on recovery. Therefore, silica sorbents modified by three functional groups were synthesized to recover anthraquinones from DES-8. After destruction of the hydrogen bonds in DES-8 by addition of water, the three materials were added into the extracts to adsorb the target compounds. The results in Figure 5.7 (sorbent/liquid ratio=10 mg mL^{-1} and 15 mg mL^{-1}) show that the adsorption capacity of PHE-SIL was the highest, while that of C_8-SIL was higher than that of NH_2-SIL. This may be because the acidity of citric acid inhibits the ionization of phenolic hydroxyl groups of anthraquinones after adding water to DES-8, thus causing anthraquinones to be present in their neutral state. Therefore, hydrophobic functional groups can provide a strong force for adsorption, and thus anthraquinones with stronger hydrophobicity have higher adsorption on PHE-SIL and C_8-SIL. Compared with C_8-SIL, PHE-SIL had a higher adsorption capacity. Because

anthraquinones contain several benzene rings, the adsorption capacity of anthraquinones can be increased by π-π interactions. NH_2-SIL can form hydrogen bonds with anthraquinones, but citric acid destroys the interaction between anthraquinones and amino groups, thus reducing the adsorption capacity of anthraquinones on NH_2-SIL. Of these three sorbents, PHE-SIL was selected for subsequent optimization as the sorbent that exhibited the best adsorption behavior.

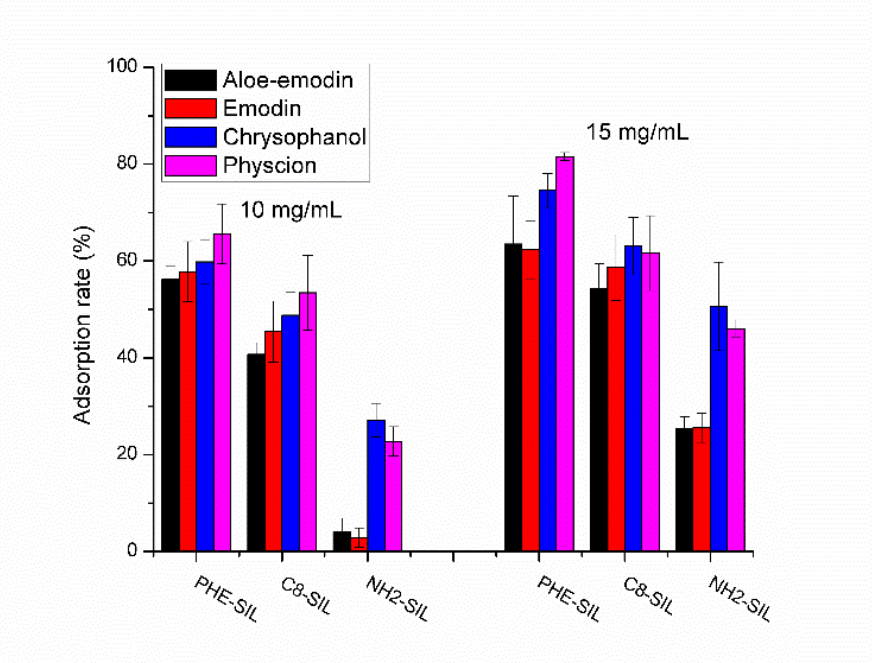

Figure 5.6 Adsorption rates of anthraquinones on three sorbents

In general, increasing the salinity (NaCl) in DES solutions increases the polarity of the solution and weakens the hydrogen bonding effect. In addition, chloride generates hydrogen bonds with HBD, further reducing hydrogen bond interaction with HBA. Moreover, the addition of NaCl can provide a salting-out effect, which can decrease the solubility of the target substances in the solutions and increase adsorption of the anthraquinones. However, the disadvantage is that too much salt will increase the viscosity of the solution and reduce the rate of diffusion of the target substance, thus reducing the adsorption efficiency. As shown in Figure D-11A, the adsorption

capacity increases with an increase in the salinity of the solution, reaching its maximum at 5 % (*w/v*) concentration of NaCl. The adsorption capacity decreases again with further increases in salinity. The amount of sorbent used for adsorption is also a significant factor because too small an amount of sorbent leads to incomplete adsorption of the targets, whereas too high an amount results in waste of the resource. Thus, the sorbent/liquid ratio was varied from 5 to 25 mg mL^{-1}, and the efficacy was evaluated based on the adsorption rate (the amount of target compounds adsorbed divided by the total content of target compounds in the extract). Figure D-11B shows that the adsorption rate tended to become constant after a sorbent/liquid ratio of 20 mg mL^{-1}. Therefore, 20 mg mL^{-1} was sufficient for adsorption of anthraquinones from the extract. The last and most important step after adsorption of the anthraquinones from the extract was to elute the adsorbed target compounds. Seven solvents (200 μL) were tested, and a comparison of their results is shown in Figure D-12. The highest recovery was obtained with acetonitrile, proving that the lower the polarity of the solvent, the better the elution effect. It was also shown that the hydrophobic interaction plays a major role in adsorption. Ethanol and methanol had similar elution abilities to acetonitrile. Considering that ethanol is safer and more environmentally friendly, ethanol was chosen as an alternative to acetonitrile. The volume of ethanol was then optimized as this may influence the elution efficiency. Increasing the eluent volume over a range of 200−600 μL resulted in an increase in the recovery. Further increases in the eluent volume did not further affect the recovery. Considering that the increase from 400 to 600 μL did not effectively improve the recovery, 400 μL was chosen as the most appropriate elution volume. Under these conditions, the recoveries of aloe-emodin, emodin, chrysophanol, and physcion were 74.05%, 74.86%, 85.92%, and 90.76 %, respectively. It can also be seen that water cannot elute anthraquinones from the

sorbent. Therefore, the residual DESs and water-soluble impurities present on the material surface can be eluted by water.

5.4 Conclusion

DES-MAE was successfully applied to the extract anthraquinones from *rheum palmatum*. It was also shown that, in most cases, addition of water reduced the heating efficiency of DES under microwave irradiation, and DESs containing carboxylic acid may react with cellulose, hemicellulose, and lignin to promote cell wall destruction. This study is helpful for the application of DES-MAE in laboratory and industrial extraction of natural products from plants. Moreover, in the recovery of anthraquinones from acid-based DES extracts, materials with phenyl functional groups on their surface exhibit a satisfactory adsorption and separation effect, which indicates that similar target natural products may be recovered from acid-based DES extracts by using phenyl-containing silica, polymer, or organic-inorganic composite materials. These studies provide guidance for further development of green DES-based extraction and recovery protocols. However, more efforts are required to unveil the interactions in DESs-based extractions and the mechanisms of reactions between acid-based DESs and cell wall. And our next research objective in the near future is to achieve an efficient high-throughput analysis of DESs extract in this chapter by DART-MS both qualitatively and quantitively.

Chapter 6: Concluding remarks and future work

6.1 Concluding remarks

The need for sensitive and accurate analysis of samples has been increasing very rapidly for decades, with the development of human societies. Nonetheless, the complicated matrix of samples, low abundance of target analytes, and limited capability of instruments all make the analysis process problematic. Therefore, the development of novel efficient analytical methods is paramount not only in the field of analytical chemistry, but for the whole research community. In this thesis, the work presented provides strategies for the development of new analytical methods involving DART-MS and insights into studies of the principle in analytical process.

The direct coupling of DMSPE to DART-MS was successfully established for the first time, synergizing the merits of the two analytical techniques. Coupling DMSPE to DART-MS with a newly developed metal iron probe enables high-throughput, sensitive detection of herbicides such as triazine in environmental waters. The iron probe, which is designed to fit into the moving trail of the DART interface, served as the sorbent collector as well as the support for the magnetic graphene oxide after DMSPE, and was put directly into the DART system. Magnetic graphene oxide was selected as the proper sorbent in this method, and the content of graphene oxide in the sorbent was also optimized in addition to other key factors in the proposed method. A high-throughput analysis of six triazine herbicides in environmental water samples was accomplished with good sensitivity. Obviously, this new analytical platform shows huge potential in achieving a sensitive high-throughput analysis of low-abundance compounds in aqueous real-world samples.

The systematic study of the effect of sorbent morphology and the type of organic solvent used on DART-MS analysis was performed using two sorbents with different morphologies and six commonly used solvents. The use of sorbent for preconcentration and solvents for assisting

desorption and ionization synergistically enhanced the signals from the trace pollutants detected by DART-MS. Based on the finding that the synergistic effect of sorbent and solvent could greatly enhance the sensitivity of DART-MS, we developed another novel analytical method named SSE-DART-MS. After the optimizations of key parameters in SSE-DART-MS, the effectiveness of this method was evaluated by the determination of trace PAEs in liquid samples, and the sensitivity was significantly improved. This work not only provides a reliable method for the coupling of solid phase extraction technique with DART-MS, but also presents valuable information for conducting other DART-MS analyses.

Inspired by the research work on SSE-DART-MS, a project was carried out to investigate the effect of sorbent hydrophobicity on SPME-DART-MS analysis. Nine custom-designed Si-ILs with different hydrophobicity were used as sorbents for the analysis of four PAEs in aqueous samples by SPME-DART-MS. The nine synthesized Si-ILs were divided into six groups according to their comparability, and the analytical performances of Si-ILs in SPME-DART-MS were compared within each group to study this effect. Based on the experimental results in this research, the effect of sorbent hydrophobicity on SPME-DART-MS remains obscure, and more efforts are expected to bring to light this effect.

In addition, we investigated a sample preparation technique using DES as green efficient extracting phase in MAE. The study revealed that the heating rate of most DESs under microwave irradiation decreased with increasing water content, and DESs containing carboxylic acids could react with hydroxyl groups of sugar and choline chloride so that they can easily destroy cell walls, thus leading to better extraction performance. This principle was demonstrated by extracting anthraquinones from *rheum palmatum* by the DES-MAE method with optimizing extraction conditions. The recovery experiments showed that the material containing a phenyl group is

beneficial to the recovery of anthraquinones in acid-based DESs because it can facilitate strong hydrophobic and π-π interactions. This study should serve as a reference for the laboratory or industrial green application of DES-MAE and allow for the recovery of natural products from DES extracts. The study also provides valuable information for environmentally friendly green extraction, modification, and comprehensive applications of cellulose, hemicellulose and lignin.

6.2 Future work

6.2.1 Applications of DMSPE-DART-MS and SSE-DART-MS in other analysis.

In this thesis, we demonstrated only one application of DMSPE-DART-MS and SSE-DART-MS in the analysis of contaminants in aqueous samples. Of course, the applications of these two novel analytical methods are not limited to the two presented cases, and we hope to analyze more analytes employing these two methods. More importantly, the additional application of these methods to trace analysis of analytes in other matrix, such as soil, plant and medical samples (urine, blood, or body fluid) is of our intense interest, and new challenges are undoubtedly waiting for us to solve. Additionally, for SSE-DART-MS, we plan to incorporate headspace mode of SPME into SSE-DART-MS for the high-throughput analysis of volatile organic compounds in various sample matrix.

6.2.2 Effect of sorbent hydrophobicity on SPME-DART-MS.

In Chapter 4, an attempt to systematically investigate the effect of sorbent hydrophobicity on SPME-DART-MS was exhibited, and no consolidated conclusion was made. So far, we have been thoroughly reevaluating and modifying our experimental scheme. We will be adapting more strategies to unveil this effect if no substantial progress is made using current scheme.

6.2.3 High-throughput analysis of DES-MAE extract by DART-MS

As was previously reported by our group,[84] the extract of artemisinins from A. annua plants using DES as extracting phase after MCE were qualitatively and quantitively analyzed by DART-MS. So far, we have completed the study of principle of DES-MAE, however this is not the end of this project. The next plan for our research work presented in Chapter 5 is to analyze the bioactive extract from rheum palmatum by DART-MS, which could further shorten the total analysis time and provide more valuable information. Moreover, more efforts will be devoted to unveiling the interactions in DESs-based extractions and the mechanisms of reactions between acid-based DESs and cell walls.

Bibliography

(1) Cooks, R. G.; Ouyang, Z.; Takats, Z.; Wiseman, J. M. *Science* **2006**, *311*, 1566.
(2) Clendinen, C. S.; Monge, M. E.; Fernández, F. M. *Analyst* **2017**, *142*, 3101-3117.
(3) Yang, Y.; Deng, J. *Trends Anal. Chem.* **2016**, *82*, 68-88.
(4) Chen, R.; Deng, J.; Fang, L.; Yao, Y.; Chen, B.; Wang, X.; Luan, T. *Trends Environ. Anal. Chem.* **2017**, *15*, 1-11.
(5) Domin, M.; Cody, R. *Ambient Ionization Mass Spectrometry*; Royal Society of Chemistry: London, England, 2015.
(6) Cody, R. B.; Laramée, J. A.; Durst, H. D. *Anal. Chem.* **2005**, *77*, 2297-2302.
(7) Hajslova, J.; Cajka, T.; Vaclavik, L. *Trends Anal. Chem.* **2011**, *30*, 204-218.
(8) Zhu, H.; Wang, C.; Qi, Y.; Song, F.; Liu, Z.; Liu, S. *Anal. Chim. Acta* **2012**, *752*, 69-77.
(9) Subbaraj, A. K.; Barrett, B. A.; Wakelin, S. A.; Fraser, K. *Anal. Bioanal. Chem.* **2015**, *407*, 8047-8058.
(10) Pavlovich, M. J.; Musselman, B.; Hall, A. B. *Mass Spectrom. Rev.* **2018**, *37*, 171-187.
(11) Green, F. M.; Salter, T. L.; Stokes, P.; Gilmore, I. S.; O'Connor, G. *Surf. Interface Anal.* **2010**, *42*, 347-357.
(12) Srbek, J.; Klejdus, B.; Douša, M.; Břicháč, J.; Stasiak, P.; Reitmajer, J.; Nováková, L. *Talanta* **2014**, *130*, 518-526.
(13) Gross, J. H. *Anal. Bioanal. Chem.* **2014**, *406*, 63-80.
(14) Baldwin, K. *Contemp. Phys.* **2005**, *46*, 105-120.
(15) Cody, R. B. *Anal. Chem.* **2009**, *81*, 1101-1107.
(16) Song, L.; Gibson, S. C.; Bhandari, D.; Cook, K. D.; Bartmess, J. E. *Anal. Chem.* **2009**, *81*, 10080-10088.
(17) Song, L.; Dykstra, A. B.; Yao, H.; Bartmess, J. E. *J. Am. Soc. Mass. Spectrom.* **2009**, *20*, 42-50.
(18) Schurek, J.; Vaclavik, L.; Hooijerink, H.; Lacina, O.; Poustka, J.; Sharman, M.; Caldow, M.; Nielen, M. W. F.; Hajslova, J. *Anal. Chem.* **2008**, *80*, 9567-9575.
(19) Crawford, E.; Musselman, B. *Anal. Bioanal. Chem.* **2012**, *403*, 2807-2812.
(20) Gómez-Ríos, G. A.; Gionfriddo, E.; Poole, J.; Pawliszyn, J. *Anal. Chem.* **2017**, *89*, 7240-7248.
(21) Farré, M.; Picó, Y.; Barceló, D. *Anal. Chem.* **2013**, *85*, 2638-2644.
(22) Guo, T.; Fang, P.; Jiang, J.; Zhang, F.; Yong, W.; Liu, J.; Dong, Y. *J. Chromatogr. A* **2016**, *1471*, 27-33.
(23) Lara, F. J.; Chan, D.; Dickinson, M.; Lloyd, A. S.; Adams, S. J. *J. Chromatogr. A* **2017**, *1496*, 37-44.
(24) Vaclavik, L.; Rosmus, J.; Popping, B.; Hajslova, J. *J. Chromatogr. A* **2010**, *1217*, 4204-4211.
(25) Dane, A. J.; Cody, R. B. *Analyst* **2010**, *135*, 696-699.
(26) Vaclavik, L.; Zachariasova, M.; Hrbek, V.; Hajslova, J. *Talanta* **2010**, *82*, 1950-1957.
(27) Busman, M.; Bobell, J. R.; Maragos, C. M. *Food Control* **2015**, *47*, 592-598.
(28) Busman, M.; Liu, J.; Zhong, H.; Bobell, J. R.; Maragos, C. M. *Food Addit. Contam. : Part A* **2014**, *31*, 932-939.
(29) Kubec, R.; Cody, R. B.; Dane, A. J.; Musah, R. A.; Schraml, J.; Vattekkatte, A.; Block, E. *J. Agric. Food. Chem.* **2010**, *58*, 1121-1128.

(30) Block, E.; Dane, A. J.; Thomas, S.; Cody, R. B. *J. Agric. Food. Chem.* **2010**, *58*, 4617-4625.
(31) Alberici, R. M.; Fernandes, G. D.; Porcari, A. M.; Eberlin, M. N.; Barrera-Arellano, D.; Fernández, F. M. *Food Chem.* **2016**, *211*, 661-668.
(32) Vaclavik, L.; Cajka, T.; Hrbek, V.; Hajslova, J. *Anal. Chim. Acta* **2009**, *645*, 56-63.
(33) Fiorino, G. M.; Losito, I.; De Angelis, E.; Arlorio, M.; Logrieco, A. F.; Monaci, L. *Food Res. Int.* **2019**, *116*, 1258-1265.
(34) Li, X. Q.; Li, H. M.; Xu, S.; Gao, Y.; Zhang, Q. H.; Zhang, Y.; Feng, M. Y. *Food Chem.* **2019**, *276*, 50-56.
(35) Jagerdeo, E.; Abdel-Rehim, M. *J. Am. Soc. Mass. Spectrom.* **2009**, *20*, 891-899.
(36) Steiner, R. R.; Larson, R. L. *J. Forensic. Sci* **2009**, *54*, 617-622.
(37) Lesiak, A. D.; Musah, R. A.; Cody, R. B.; Domin, M. A.; Dane, A. J.; Shepard, J. R. E. *Analyst* **2013**, *138*, 3424-3432.
(38) Sisco, E.; Forbes, T. P.; Staymates, M. E.; Gillen, G. *Anal. Methods* **2016**, *8*, 6494-6499.
(39) Nilles, J. M.; Connell, T. R.; Durst, H. D. *Anal. Chem.* **2009**, *81*, 6744-6749.
(40) Rummel, J. L.; Steill, J. D.; Oomens, J.; Contreras, C. S.; Pearson, W. L.; Szczepanski, J.; Powell, D. H.; Eyler, J. R. *Anal. Chem.* **2011**, *83*, 4045-4052.
(41) Harris, G. A.; Falcone, C. E.; Fernández, F. M. *J. Am. Soc. Mass. Spectrom.* **2012**, *23*, 153-161.
(42) Nilles, J. M.; Connell, T. R.; Stokes, S. T.; Dupont Durst, H. *Propellants Explos. Pyrotech.* **2010**, *35*, 446-451.
(43) Rowell, F.; Seviour, J.; Lim, A. Y.; Elumbaring-Salazar, C. G.; Loke, J.; Ma, J. *Forensic Sci.Int.* **2012**, *221*, 84-91.
(44) Sisco, E.; Dake, J.; Bridge, C. *Forensic Sci.Int.* **2013**, *232*, 160-168.
(45) Black, O.; Cody, R.; Edwards, D.; Cizdziel, J. V. *Forensic Chem.* **2017**, *5*, 26-32.
(46) Musah, R. A.; Cody, R. B.; Dane, A. J.; Vuong, A. L.; Shepard, J. R. E. *Rapid Commun. Mass Spectrom.* **2012**, *26*, 1039-1046.
(47) Jones, R. W.; Cody, R. B.; McClelland, J. F. *J. Forensic. Sci* **2006**, *51*, 915-918.
(48) Drury, N.; Ramotowski, R.; Moini, M. *Forensic Sci.Int.* **2018**, *289*, 27-32.
(49) Williamson, R.; Raeva, A.; Almirall, J. R. *J. Forensic. Sci* **2016**, *61*, 706-714.
(50) Jones, R. W.; McClelland, J. F. *Forensic Sci.Int.* **2013**, *231*, 73-81.
(51) Musah, R. A.; Domin, M. A.; Cody, R. B.; Lesiak, A. D.; John Dane, A.; Shepard, J. R. E. *Rapid Commun. Mass Spectrom.* **2012**, *26*, 2335-2342.
(52) Brown, H.; Oktem, B.; Windom, A.; Doroshenko, V.; Evans-Nguyen, K. *Forensic Chem.* **2016**, *1*, 66-73.
(53) Lei, Y. T.; Lu, Y.; Zhang, T. C.; Qi, Y.; Lu, Y. F. *Environ. Earth Sci.* **2016**, *75*, 1005.
(54) Grange, A. H. *Rapid Commun. Mass Spectrom.* **2013**, *27*, 305-318.
(55) Chan, M. N.; Nah, T.; Wilson, K. R. *Analyst* **2013**, *138*, 3749-3757.
(56) Wang, J.; Zhu, J.; Si, L.; Du, Q.; Li, H.; Bi, W.; Chen, D. D. Y. *Anal. Chim. Acta* **2017**, *996*, 20-28.
(57) Bridoux, M. C.; Malandain, H.; Leprince, F.; Progent, F.; Machuron-Mandard, X. *Anal. Chim. Acta* **2015**, *869*, 1-10.
(58) Wang, J.; Du, Q.; You, X.; Lv, Y.; Bi, W.; Li, H.; Chen, D. D. Y. *Anal. Chim. Acta* **2019**, *1071*, 8-16.
(59) Wang, L.; Zeng, S.; Qu, H. *J. Pharm. Biomed. Anal.* **2016**, *121*, 30-38.
(60) He, Y.; Liu, W.; Su, R.; Xiu, Y.; Pei, J. *Chem. Res. Chin. Univ.* **2017**, *33*, 172-178.

(61) Ma, H.; Zhang, K.; Jiang, Q.; Dai, D.; Li, H.; Bi, W.; Chen, D. D. Y. *J. Chromatogr. A* **2018**, *1547*, 29-36.
(62) Chen, Z.; Wang, M.; Yang, Y.; Du, X.; Zhang, Z.; Li, Y. *Phytochem. Anal* **2019**, *30*, 311-319.
(63) Liu, W.; He, Y.; Li, L.; Liu, S. *Rapid Commun. Mass Spectrom.* **2016**, *30*, 111-115.
(64) Ma, H.; Jiang, Q.; Dai, D.; Li, H.; Bi, W.; Da Yong Chen, D. *Anal. Chem.* **2018**, *90*, 3628-3636.
(65) Wang, Y.; Li, C.; Huang, L.; Liu, L.; Guo, Y.; Ma, L.; Liu, S. *Anal. Chim. Acta* **2014**, *845*, 70-76.
(66) Pena-Pereira, F.; Lavilla, I.; Bendicho, C. *Trends Anal. Chem.* **2010**, *29*, 617-628.
(67) Spietelun, A.; Marcinkowski, Ł.; de la Guardia, M.; Namieśnik, J. *Talanta* **2014**, *119*, 34-45.
(68) Sajid, M. *Trends Anal. Chem.* **2018**, *106*, 169-182.
(69) Mousavi, L.; Tamiji, Z.; Khoshayand, M. R. *Talanta* **2018**, *190*, 335-356.
(70) Risticevic, S.; Niri, V. H.; Vuckovic, D.; Pawliszyn, J. *Anal. Bioanal. Chem.* **2009**, *393*, 781-795.
(71) Ho, T. D.; Canestraro, A. J.; Anderson, J. L. *Anal. Chim. Acta* **2011**, *695*, 18-43.
(72) Reyes-Gallardo, E. M.; Lucena, R.; Cárdenas, S.; Valcárcel, M. *Microchem. J.* **2016**, *124*, 751-756.
(73) Moliner-Martinez, Y.; Vitta, Y.; Prima-Garcia, H.; González-Fuenzalida, R. A.; Ribera, A.; Campíns-Falcó, P.; Coronado, E. *Anal. Bioanal. Chem.* **2014**, *406*, 2211-2215.
(74) Zheng, H.-B.; Mo, J.-Z.; Zhang, Y.; Gao, Q.; Ding, J.; Yu, Q.-W.; Feng, Y.-Q. *J. Chromatogr. A* **2014**, *1329*, 17-23.
(75) Han, Q.; Wang, Z.; Xia, J.; Chen, S.; Zhang, X.; Ding, M. *Talanta* **2012**, *101*, 388-395.
(76) Wang, Y.; Wang, L.; Tian, T.; Hu, X.; Yang, C.; Xu, Q. *Analyst* **2012**, *137*, 2400-2405.
(77) Tang, S.; Chia, G. H.; Chang, Y.; Lee, H. K. *Anal. Chem.* **2014**, *86*, 11070-11076.
(78) Maya, F.; Palomino Cabello, C.; Estela, J. M.; Cerdà, V.; Turnes Palomino, G. *Anal. Chem.* **2015**, *87*, 7545-7549.
(79) Hu, C.; Deng, J.; Zhao, Y.; Xia, L.; Huang, K.; Ju, S.; Xiao, N. *Food Chem.* **2014**, *158*, 366-373.
(80) García, A.; Rodríguez-Juan, E.; Rodríguez-Gutiérrez, G.; Rios, J. J.; Fernández-Bolaños, J. *Food Chem.* **2016**, *197*, 554-561.
(81) Huang, Y.; Wang, Y.; Pan, Q.; Wang, Y.; Ding, X.; Xu, K.; Li, N.; Wen, Q. *Anal. Chim. Acta* **2015**, *877*, 90-99.
(82) Yilmaz, E.; Soylak, M. *Talanta* **2015**, *136*, 170-173.
(83) Chen, J.; Liu, M.; Wang, Q.; Du, H.; Zhang, L. *Molecules* **2016**, *21*.
(84) Wang, J.; Zhou, Y.; Wang, M.; Bi, W.; Li, H.; Chen, D. D. Y. *Anal. Chem.* **2018**, *90*, 3109-3117.
(85) Bai, Y.; Zhang, J.; Bai, Y.; Liu, H. *Anal. Bioanal. Chem.* **2012**, *403*, 2307-2314.
(86) Li, X.; Xing, J.; Chang, C.; Wang, X.; Bai, Y.; Yan, X.; Liu, H. *J. Sep. Sci.* **2014**, *37*, 1489-1495.
(87) LaPointe, J.; Musselman, B.; O'Neill, T.; Shepard, J. R. E. *J. Am. Soc. Mass. Spectrom.* **2015**, *26*, 159-165.
(88) Wang, X.; Li, X.; Li, Z.; Zhang, Y.; Bai, Y.; Liu, H. *Anal. Chem.* **2014**, *86*, 4739-4747.
(89) Jastrzembski, J. A.; Sacks, G. L. *Anal. Chem.* **2016**, *88*, 8617-8623.

(90) Monia, B.; Cristina, B.; Yolanda, P. *J. Sep. Sci.* **2015**, *33*, 1-10.
(91) Meritxell, G.; Mira, P.; Damiá, B. *Talanta* **2006**, *70*, 678-690.
(92) Fife, P. C.; Mcleod, J. B. *J. Sep. Sci.* **2015**, *32*, 314-320.
(93) Huang, M. Z.; Cheng, S. C.; Cho, Y. T.; Shiea, J. *Anal. Chim. Acta* **2011**, *702*, 1-15.
(94) Cooks, R. G.; Ouyang, Z.; Takats, Z.; Wiseman, J. M. *Science* **2006**, *311*, 1566-1570.
(95) Alberici, R. M.; Simas, R. C.; Sanvido, G. B.; Wanderson, R. O.; Lalli, P. M.; Mario, B.; Cunha, I. B. S.; Eberlin, M. N. *Anal. Bioanal. Chem.* **2010**, *398*, 265-294.
(96) Yao, Z. P. *Mass Spectrom. Rev.* **2012**, *31*, 437-447.
(97) Wang, X.; Li, X.; Li, Z.; Zhang, Y.; Bai, Y.; Liu, H. *Anal. Chem.* **2014**, *86*, 4739-4747.
(98) Rodriguez-Lafuente, A.; Mirnaghi, F. S.; Pawliszyn, J. *Anal. Bioanal. Chem.* **2013**, *405*, 9723-9727.
(99) Eshwar, J.; Mohamed, A. R. *J. Am. Soc. Mass. Spectrom.* **2009**, *20*, 891-899.
(100) Gómez-Ríos, G. A.; Pawliszyn, J. *Chem. Commun.* **2014**, *50*, 12937-12940.
(101) Li, N.; Jiang, H.-L.; Wang, X.; Wang, X.; Xu, G.; Zhang, B.; Wang, L.; Zhao, R.-S.; Lin, J.-M. *Trends Anal. Chem.* **2018**, *102*, 60-74.
(102) Herrero-Latorre, C.; Barciela-García, J.; García-Martín, S.; Peña-Crecente, R. M.; Otárola-Jiménez, J. *Anal. Chim. Acta* **2015**, *892*, 10-26.
(103) Wierucka, M.; Biziuk, M. *Trends Anal. Chem.* **2014**, *59*, 50-58.
(104) Dreyer, D. R.; Park, S.; Bielawski, C. W.; Ruoff, R. S. *Chem. Soc. Rev.* **2010**, *39*, 228-240.
(105) Wang, L.; Bao, J.; Wang, L.; Zhang, F.; Li, Y. *Chem. Eur. J.* **2006**, *12*, 6341-6347.
(106) He, F.; Fan, J.; Ma, D.; Zhang, L.; Leung, C.; Chan, H. L. *Carbon* **2010**, *48*, 3139-3144.
(107) Wells, G.; Prest, H.; Russ, C. W. *Signal, Noise, and Detection Limits in Mass Spectrometry;* Technical note for Agilent Technologies, Inc.: Wilmington, DE, May 2011.
(108) Stobinski, L.; Lesiak, B.; Malolepszy, A.; Mazurkiewicz, M.; Mierzwa, B.; Zemek, J.; Jiricek, P.; Bieloshapka, I. *J. Electron. Spectrosc. Relat. Phenom.* **2014**, *195*, 145-154.
(109) Zhou, Q.; Wang, Y.; Xiao, J.; Fan, H. *Sci. Rep.* **2017**, *7*, 11316.
(110) Maliyekkal, S. M.; Sreeprasad, T. S.; Deepti, K.; Summayya, K.; Abhishek Kumar, M.; Waghmare, U. V.; Pradeep, T., . *Small* **2013**, *9*, 273-283.
(111) Xin, X.; Qin, W.; Jian, Y.; Yan, L.; Rui, F.; Chen, G.; Du, B.; He, L. *Chem. Eng. J.* **2012**, *184*, 132-140.
(112) Li, D.; Zhu, J.; Man, W.; Bi, W.; Huang, X.; Chen, D. D. Y. *J. Chromatogr. A* **2017**, *1491*, 27-35.
(113) Xin, W.; Xianjiang, L.; Ze, L.; Yiding, Z.; Yu, B.; Huwei, L. *Anal. Chem.* **2014**, *86*, 4739-4747.
(114) Qiu, Z.; Ping, S.; Yao, Z.; Wang, R.; Yi, Y. *Microchim. Acta* **2012**, *178*, 341-347.
(115) Li, X.; Xing, J.; Chang, C.; Wang, X.; Bai, Y.; Yan, X.; Liu, H. *J. Sep. Sci.* **2014**, *37*, 1489-1495.
(116) Zhao, G.; Song, S.; Wang, C.; Wu, Q.; Wang, Z. *Anal. Chim. Acta* **2011**, *708*, 155-159.
(117) Zhang, H.; Yuan, Y.; Sun, Y.; Niu, C.; Qiao, F.; Yan, H. *Analyst* **2017**, *143*, 175-181.
(118) Jiménez-Soto, J. M.; Cárdenas, S.; Valcárcel, M. *Anal. Bioanal. Chem.* **2013**, *405*, 2661-2669.
(119) Djozan, D.; Sorouraddin, S. M.; Baheri, T.; Norouzi, J. *Chromatographia* **2012**, *75*, 139-148.
(120) Wang, J.; Zhou, Y.; Wang, M.; Bi, W.; Li, H.; Chen, D. D. Y. *Anal. Chem.* **2018**, *90*, 3109-3117.

(121) Lesiak, A. D.; Musah, R. A.; Cody, R. B.; Domin, M. A.; Dane, A. J.; Shepard, J. R. E. *Analyst* **2013**, *138*, 3424-3432.
(122) Kubec, R.; Cody, R. B.; Dane, A. J.; Musah, R. A.; Schraml, J.; Vattekkatte, A.; Block, E. *J. Agric. Food. Chem.* **2010**, *58*, 1121-1128.
(123) Gomez-Rios, G. A.; Gionfriddo, E.; Poole, J.; Pawliszyn, J. *Anal. Chem.* **2017**, *89*, 7240-7248.
(124) Ackerman, L. K.; Noonan, G. O.; Begley, T. H.; Theobald, A. *Food Addit. Contam.* **2009**, *26*, 1611-1618.
(125) Li, X.; Wang, X.; Li, L.; Bai, Y.; Liu, H. *Mass Spectrom. Lett.* **2015**, *6*, 1-6.
(126) Gómez-Ríos, G. A.; Pawliszyn, J. *Chem Commun (Camb)* **2014**, *50*, 12937-12940.
(127) Fang, L.; Deng, J.; Yang, Y.; Wang, X.; Chen, B.; Liu, H.; Zhou, H.; Ouyang, G.; Luan, T. *Trends Anal. Chem.* **2016**, *85*, 61-72.
(128) Jing, W.; Zhou, Y.; Wang, J.; Ni, M.; Bi, W.; Chen, D. D. Y. *Anal. Chem.* **2019**, *91*, 11240-11246.
(129) Kenessov, B. N.; Koziel, J. A.; Grotenhuis, T.; Carlsen, L. *Anal. Chim. Acta* **2010**, *674*, 32-39.
(130) Bonansea, R. I.; Amé, M. V.; Wunderlin, D. A. *Chemosphere* **2013**, *90*, 1860-1869.
(131) Mirnaghi, F. S.; Pawliszyn, J. *Anal. Chem.* **2012**, *84*, 8301-8309.
(132) Martinis, B. S. D.; Ruzzene, M. A. M.; Martin, C. C. S. *Anal. Chim. Acta* **2004**, *522*, 163-168.
(133) Moreira, M. A.; André, L. C.; Cardeal, Z. d. L. *Food Chem.* **2015**, *178*, 195-200.
(134) Innocente, N.; Marchesini, G.; Biasutti, M. *Food Chem.* **2011**, *124*, 1249-1257.
(135) Kataoka, H.; Ehara, K.; Yasuhara, R.; Saito, K. *Anal. Bioanal. Chem.* **2013**, *405*, 331-340.
(136) Ahmad, S.; Tucker, M.; Spooner, N.; Murnane, D.; Gerhard, U. *Anal. Chem.* **2014**, *87*.
(137) Vuckovic, D.; Cudjoe, E.; Hein, D.; Pawliszyn, J. *Anal. Chem.* **2008**, *80*, 6870-6880.
(138) Olszowy, P.; Szultka, M.; Buszewski, B. *Anal. Bioanal. Chem.* **2011**, *401*, 1377.
(139) Piri-Moghadam, H.; Ahmadi, F.; Pawliszyn, J. *Trends Anal. Chem.* **2016**, *85*, 133-143.
(140) Zhang, S.; Yang, Q.; Wang, W.; Wang, C.; Wang, Z. *J. Agric. Food. Chem.* **2016**, *64*, 2792-2801.
(141) Mehdinia, A.; Khani, H.; Mozaffari, S. *Microchim. Acta* **2014**, *181*, 89-95.
(142) Rocío-Bautista, P.; Pacheco-Fernández, I.; Pasán, J.; Pino, V. *Anal. Chim. Acta* **2016**, *939*, 26-41.
(143) Zhang, N.; Gao, J.; Huang, C.; Liu, W.; Tong, P.; Zhang, L. *Anal. Chim. Acta* **2016**, *934*, 122-131.
(144) Pandey, S. K.; Kim, K.-H.; Brown, R. J. C. *Trends Anal. Chem.* **2011**, *30*, 1716-1739.
(145) Gunatilake, S. R.; Munasinghe, V. K.; Ranaweera, R.; Mlsna, T. E.; Xia, K. *Anal. Methods* **2016**, *8*, 5556-5568.
(146) Hajslová, J. *Anal. Chim. Acta* **2007**, *582*, 24-33.
(147) Fu, X.; Hu, X.; Yan, Z.; Lei, K.; Li, F.; Cheng, F.; Chen, J. *Chem. Commun.* **2016**, *52*, 1725-1728.
(148) Wang, M.; Cui, S.; Yang, X.; Bi, W. *Talanta* **2015**, *132*, 922-928.
(149) Yan, S. C.; Li, Z. S.; Zou, Z. G. *Langmuir* **2009**, *25*, 10397-10401.
(150) Fan, S.; Zhu, J.; Ren, L.; Wang, M.; Bi, W.; Li, H.; Huang, X.; Chen, D. D. Y. *Anal. Chim. Acta* **2017**, *960*, 63-71.

(151) Xiaoyan, T.; Suyu, W.; Yang, Y.; Ran, T.; Yunv, D.; Dan, A.; Li, L. *Chem. Eng. J.* **2015**, *275*, 198-205.
(152) Wang, M.; Yang, X.; Bi, W. *J. Sep. Sci.* **2015**, *38*, 445-452.
(153) Chen, W. S.; Chiang, W. C.; Wei, K. M. *J. Hazard. Mater.* **2007**, *147*, 197.
(154) Sun, M.; Tang, R.; Wu, Q.; Wang, C.; Wang, Z. *Anal. Methods* **2013**, *5*.
(155) Zhang, M.; Huang, J.; Zeng, J.; Zhang, C. *RSC Advances* **2014**, *4*.
(156) Russo, M. V.; Notardonato, I.; Avino, P.; Cinelli, G. *Anal. Methods* **2014**, *6*.
(157) Cajka, T.; Riddellova, K.; Tomaniova, M.; Hajslova, J. *J. Chromatogr. A* **2010**, *1217*, 4195-4203.
(158) Vasiljevic, T.; Pawliszyn, J. *Anal. Methods* **2019**, *11*, 3882-3889.
(159) Wang, J.-H.; Li, M.; Li, D. *Chem. Eur. J.* **2014**, *20*, 12004-12008.
(160) Damon, D. E.; Davis, K. M.; Moreira, C. R.; Capone, P.; Cruttenden, R.; Badu-Tawiah, A. K. *Anal. Chem.* **2016**, *88*, 1878-1884.
(161) Bi, W.; Zhou, J.; Row, K. H. *Talanta* **2011**, *83*, 974-979.
(162) Li, M.; Pham, P. J.; Wang, T.; Pittman, C. U.; Li, T. *Sep. Purif. Technol.* **2009**, *66*, 1-8.
(163) Wang, Z.; Ye, C.; Li, J.; Wang, H.; Zhang, H. *J. Hazard. Mater.* **2013**, *260*, 955-966.
(164) da Silva, M. R.; Mauro Lanças, F. *J. Sep. Sci.* **2018**, *41*, 2237-2244.
(165) Nakamoto, K. In *Handbook of Vibrational Spectroscopy*, Chalmers, J. M.; Griffiths, P. R., Eds., 2006.
(166) Liu, J.-f.; Jiang, G.-b.; Liu, J.-f.; Jönsson, J. Å. *Trends Anal. Chem.* **2005**, *24*, 20-27.
(167) Seddon Kenneth, R.; Stark, A.; Torres, M.-J. In *Pure Appl. Chem.*, 2000, p 2275.
(168) Francesco, F. D.; Calisi, N.; Creatini, M.; Melai, B.; Salvo, P.; Chiappe, C. *Green Chem.* **2011**, *13*, 1712-1717.
(169) Cao, Y.; Chen, Y.; Sun, X.; Zhang, Z.; Mu, T. *PCCP* **2012**, *14*, 12252-12262.
(170) Chen, S.; Zeng, Z.; Hu, N.; Bai, B.; Wang, H.; Suo, Y. *Food Chem.* **2018**, *242*, 1-8.
(171) Stekolshchikova, E.; Turova, P.; Shpigun, O.; Rodin, I.; Stavrianidi, A. *J. Chromatogr. A* **2018**, *1574*, 82-90.
(172) Zhao, B.-Y.; Xu, P.; Yang, F.-X.; Wu, H.; Zong, M.-H.; Lou, W.-Y. *ACS Sustainable Chem. Eng.* **2015**, *3*, 2746-2755.
(173) Parhiz, H.; Roohbakhsh, A.; Soltani, F.; Rezaee, R.; Iranshahi, M. *Phytother. Res.* **2015**, *29*, 323-331.
(174) Ventura, S. P. M.; e Silva, F. A.; Quental, M. V.; Mondal, D.; Freire, M. G.; Coutinho, J. A. P. *Chem. Rev.* **2017**, *117*, 6984-7052.
(175) Azmir, J.; Zaidul, I. S. M.; Rahman, M. M.; Sharif, K. M.; Mohamed, A.; Sahena, F.; Jahurul, M. H. A.; Ghafoor, K.; Norulaini, N. A. N.; Omar, A. K. M. *J. Food Eng.* **2013**, *117*, 426-436.
(176) Paiva, A.; Craveiro, R.; Aroso, I.; Martins, M.; Reis, R. L.; Duarte, A. R. C. *ACS Sustainable Chem. Eng.* **2014**, *2*, 1063-1071.
(177) Wagle, D. V.; Zhao, H.; Baker, G. A. *Acc. Chem. Res.* **2014**, *47*, 2299-2308.
(178) Tang, B.; Zhang, H.; Row, K. H. *J. Sep. Sci.* **2015**, *38*, 1053-1064.
(179) Duan, L.; Dou, L.-L.; Guo, L.; Li, P.; Liu, E. H. *ACS Sustainable Chem. Eng.* **2016**, *4*, 2405-2411.
(180) Nam, M. W.; Zhao, J.; Lee, M. S.; Jeong, J. H.; Lee, J. *Green Chem.* **2015**, *17*, 1718-1727.
(181) Dai, Y.; Rozema, E.; Verpoorte, R.; Choi, Y. H. *J. Chromatogr. A* **2016**, *1434*, 50-56.

(182) Cao, J.; Yang, M.; Cao, F.; Wang, J.; Su, E. *ACS Sustainable Chem. Eng.* **2017**, *5*, 3270-3278.
(183) Cui, Q.; Peng, X.; Yao, X.-H.; Wei, Z.-F.; Luo, M.; Wang, W.; Zhao, C.-J.; Fu, Y.-J.; Zu, Y.-G. *Sep. Purif. Technol.* **2015**, *150*, 63-72.
(184) Liu, Y.; Chen, W.; Xia, Q.; Guo, B.; Wang, Q.; Liu, S.; Liu, Y.; Li, J.; Yu, H. *ChemSusChem* **2017**, *10*, 1692-1700.
(185) Peng, X.; Duan, M.-H.; Yao, X.-H.; Zhang, Y.-H.; Zhao, C.-J.; Zu, Y.-G.; Fu, Y.-J. *Sep. Purif. Technol.* **2016**, *157*, 249-257.
(186) Flórez, N.; Conde, E.; Domínguez, H. *J. Chem. Technol. Biotechnol.* **2015**, *90*, 590-607.
(187) Yunpu, W.; Leilei, D. A. I.; Liangliang, F. A. N.; Shaoqi, S.; Yuhuan, L. I. U.; Roger, R. *J. Anal. Appl. Pyrolysis* **2016**, *119*, 104-113.
(188) Tian, H.; Wang, J.; Li, Y.; Bi, W.; Chen, D. D. Y. *ACS Sustainable Chem. Eng.* **2019**, *7*, 9976-9983.
(189) Wang, M.; Wang, J.; Zhou, Y.; Zhang, M.; Xia, Q.; Bi, W.; Chen, D. D. Y. *ACS Sustainable Chem. Eng.* **2017**, *5*, 6297-6303.
(190) Aichner, D.; Ganzera, M. *Talanta* **2015**, *144*, 1239-1244.
(191) Dong, X.; Fu, J.; Yin, X.; Cao, S.; Li, X.; Lin, L.; Huyiligeqi; Ni, J. *Phytother. Res.* **2016**, *30*, 1207-1218.
(192) Ma, Y.-S.; Hsiao, Y.-P.; Lin, J.-H.; Hsu, S.-C.; Chueh, F.-S.; Weng, S.-W.; Lai, K.-C.; Lin, J.-G.; Chung, J.-G. *Environ. Toxicol.* **2015**, *30*, 852-863.
(193) Leron, R. B.; Li, M.-H. *Thermochim. Acta* **2012**, *530*, 52-57.
(194) Dugoni, G. C.; Di Pietro, M. E.; Ferro, M.; Castiglione, F.; Ruellan, S.; Moufawad, T.; Moura, L.; Costa Gomes, M. F.; Fourmentin, S.; Mele, A. *ACS Sustainable Chem. Eng.* **2019**, *7*, 7277-7285.
(195) Pal, M.; Rai, R.; Yadav, A.; Khanna, R.; Baker, G. A.; Pandey, S. *Langmuir* **2014**, *30*, 13191-13198.
(196) Sanchez-Fernandez, A.; Arnold, T.; Jackson, A. J.; Fussell, S. L.; Heenan, R. K.; Campbell, R. A.; Edler, K. J. *PCCP* **2016**, *18*, 33240-33249.
(197) Pal, M.; Singh, R. K.; Pandey, S. *ChemPhysChem* **2015**, *16*, 2538-2542.

Appendices

Appendix A Supplemental information for Chapter 2

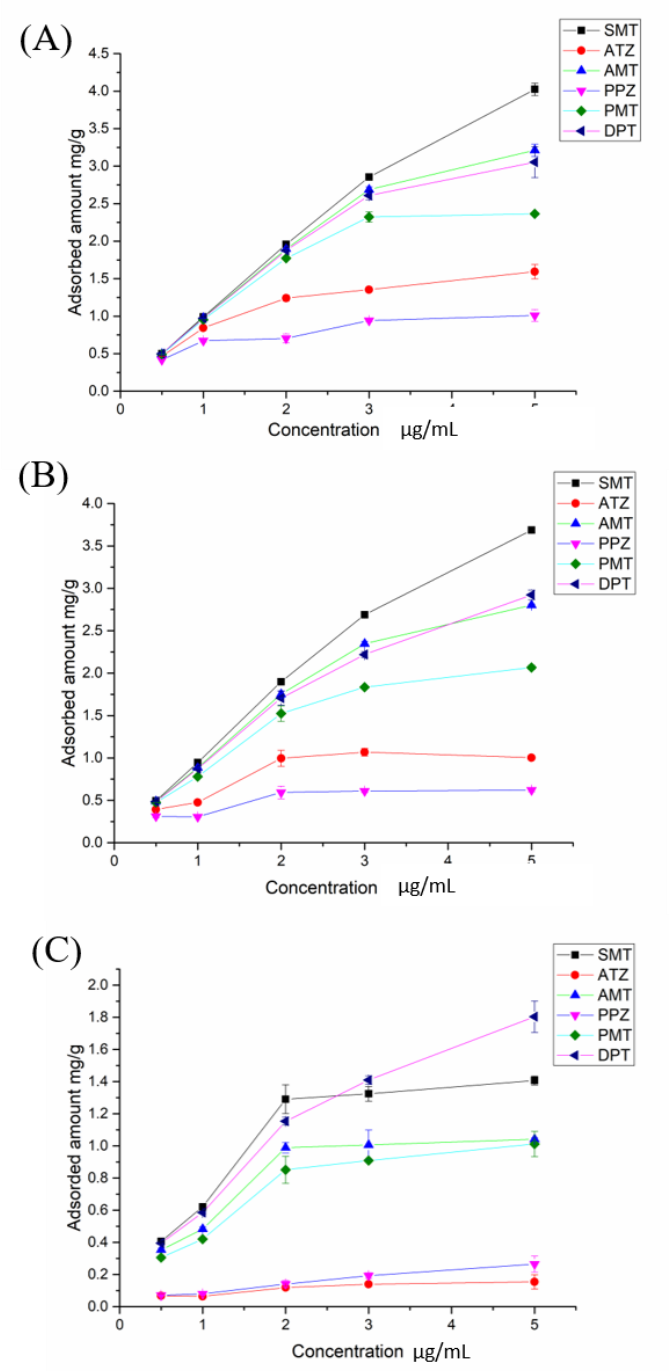

Figure A-1 Effect of initial concentrations of triazine herbicides standard solutions on DMSPE process: (A) M2GO; (B) M3GO; (C) M4GO.

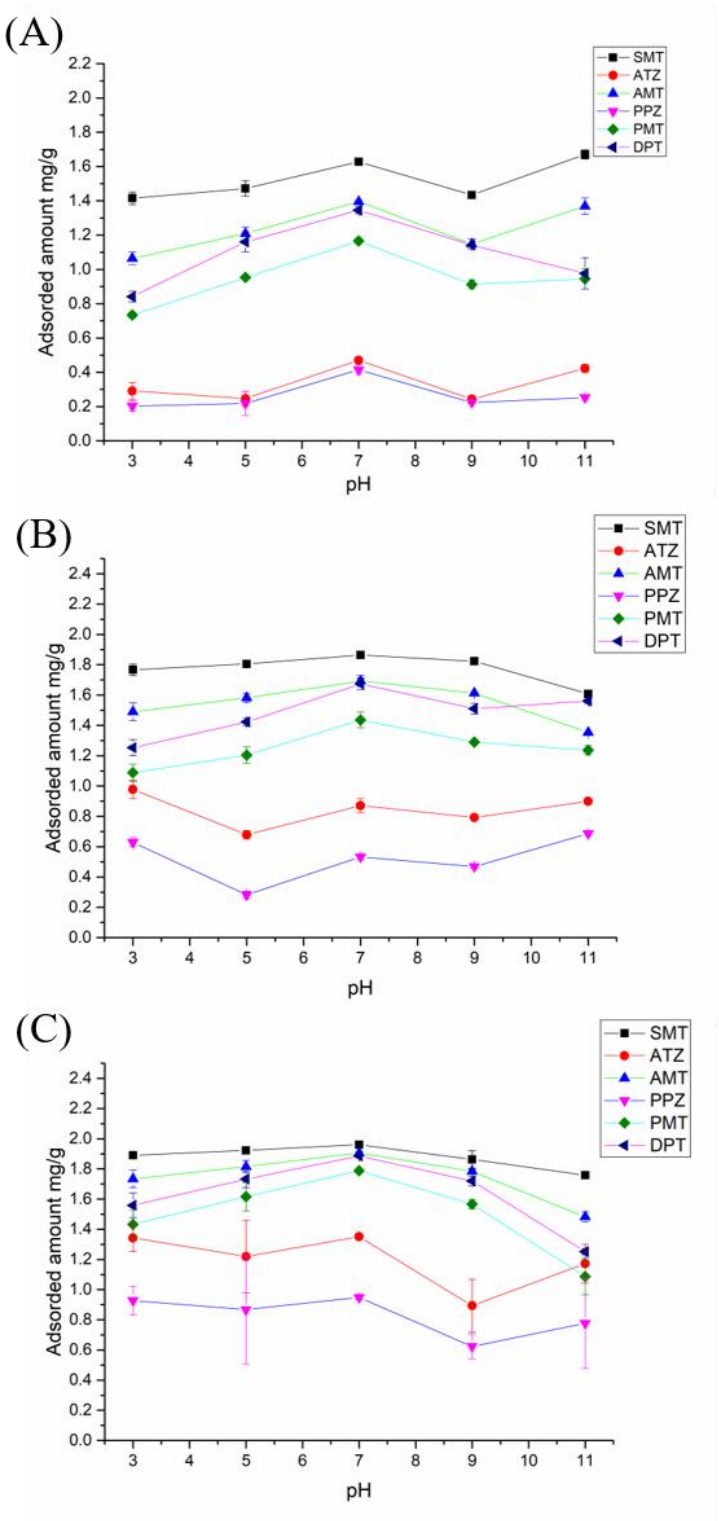

Figure A-2 Effect of pH on DMSPE process: (A) M2GO; (B) M3GO; (C) M4GO.

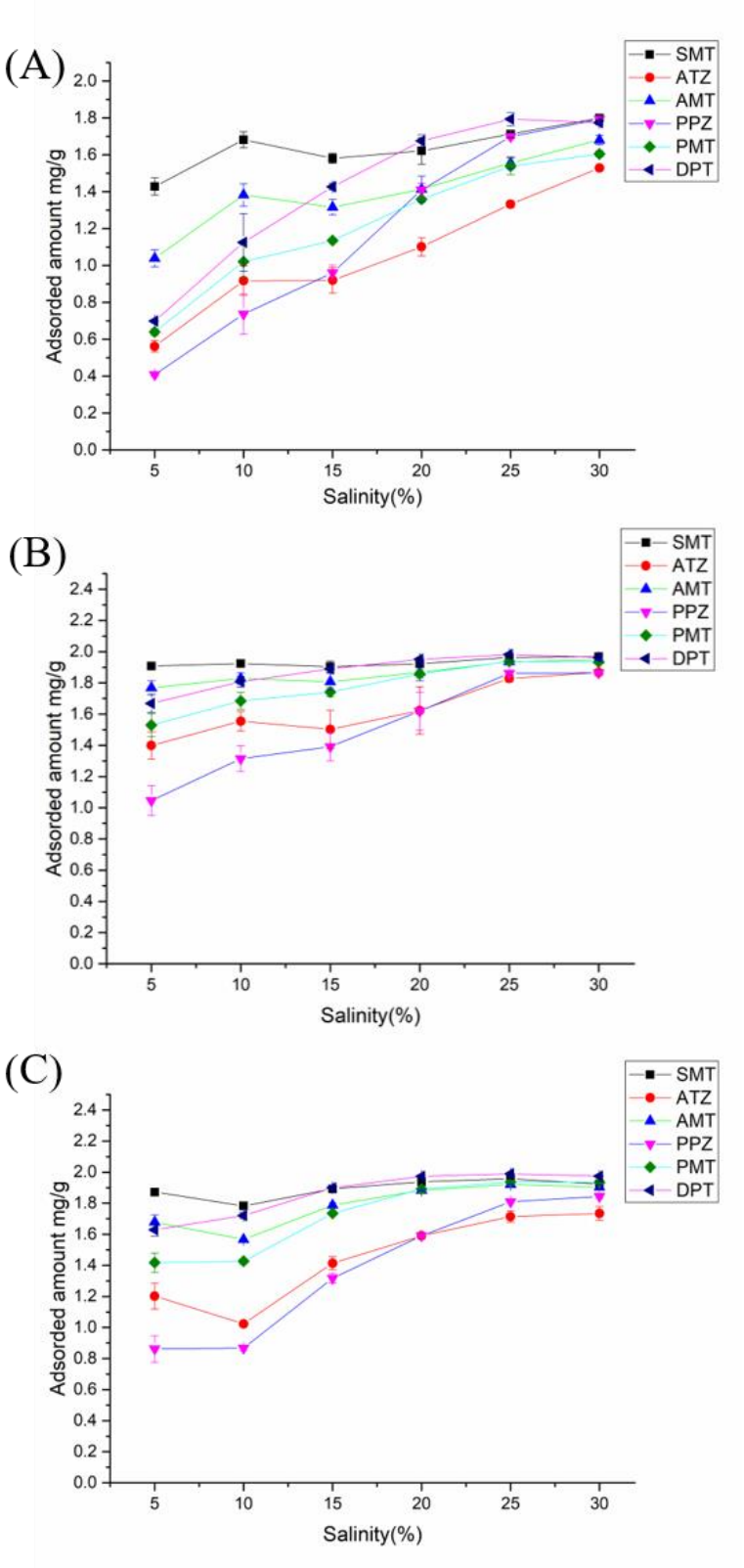

Figure A-3 Effect of salinity on DMSPE process: (A) M2GO; (B) M3GO; (C) M4GO.

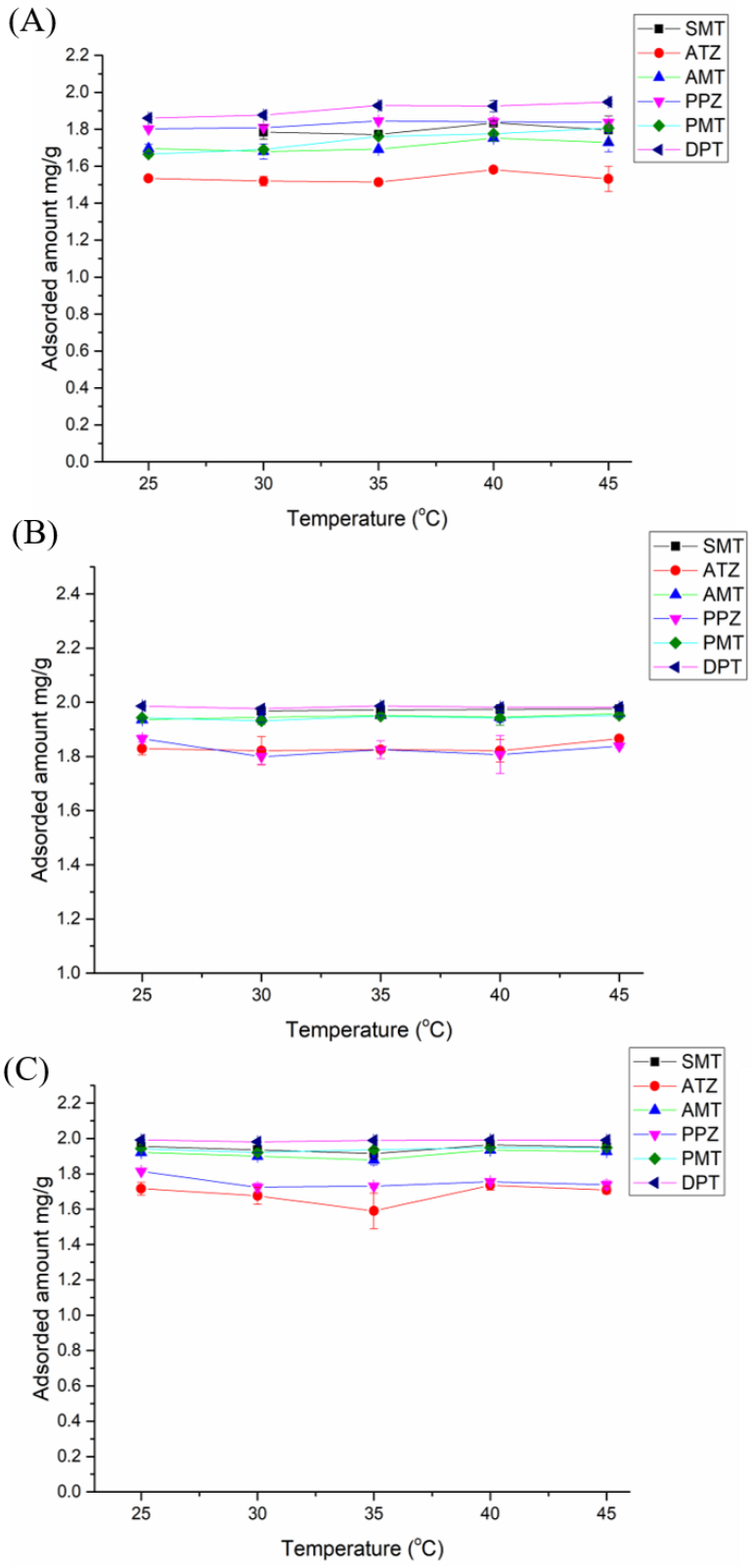

Figure A-4 Effect of temperature on DMSPE process: (A) M2GO; (B) M3GO; (C) M4GO.

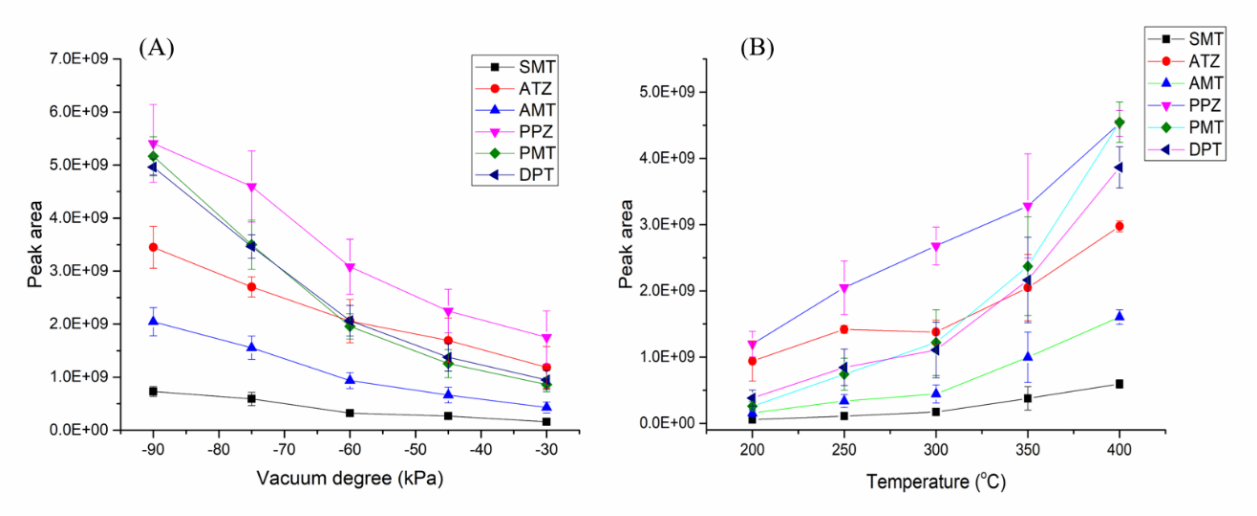

Figure A-5 Effect of vacuum degree (A) and of temperature of DART gas (B) on DART-MS analysis using M2GO as sorbents.

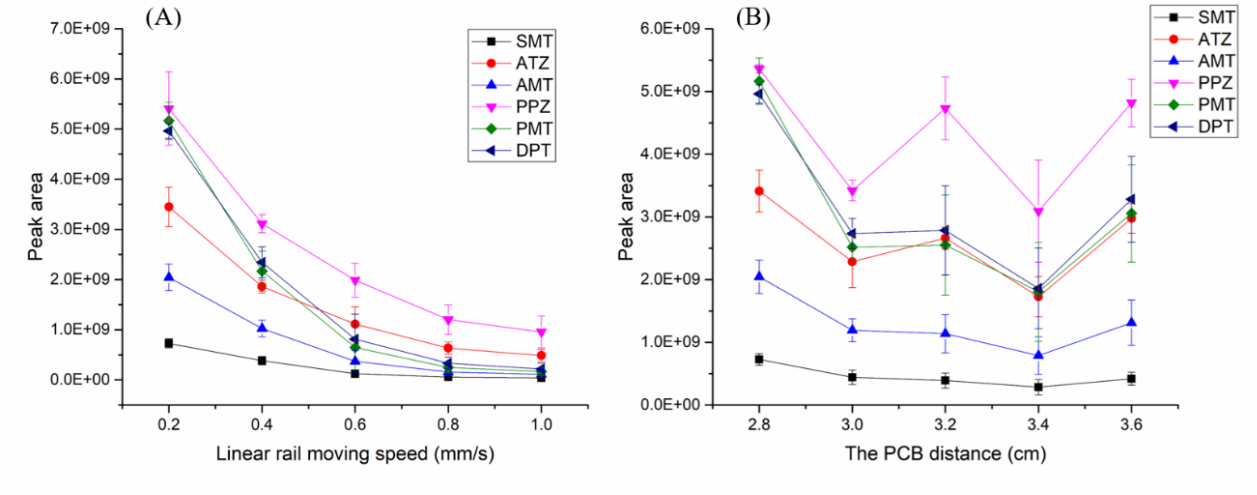

Figure A-6 Effect of moving speed of linear rail 12-Dip-It module (A) and the PCB rail distance (B) on DART-MS analysis using M2GO as sorbents.

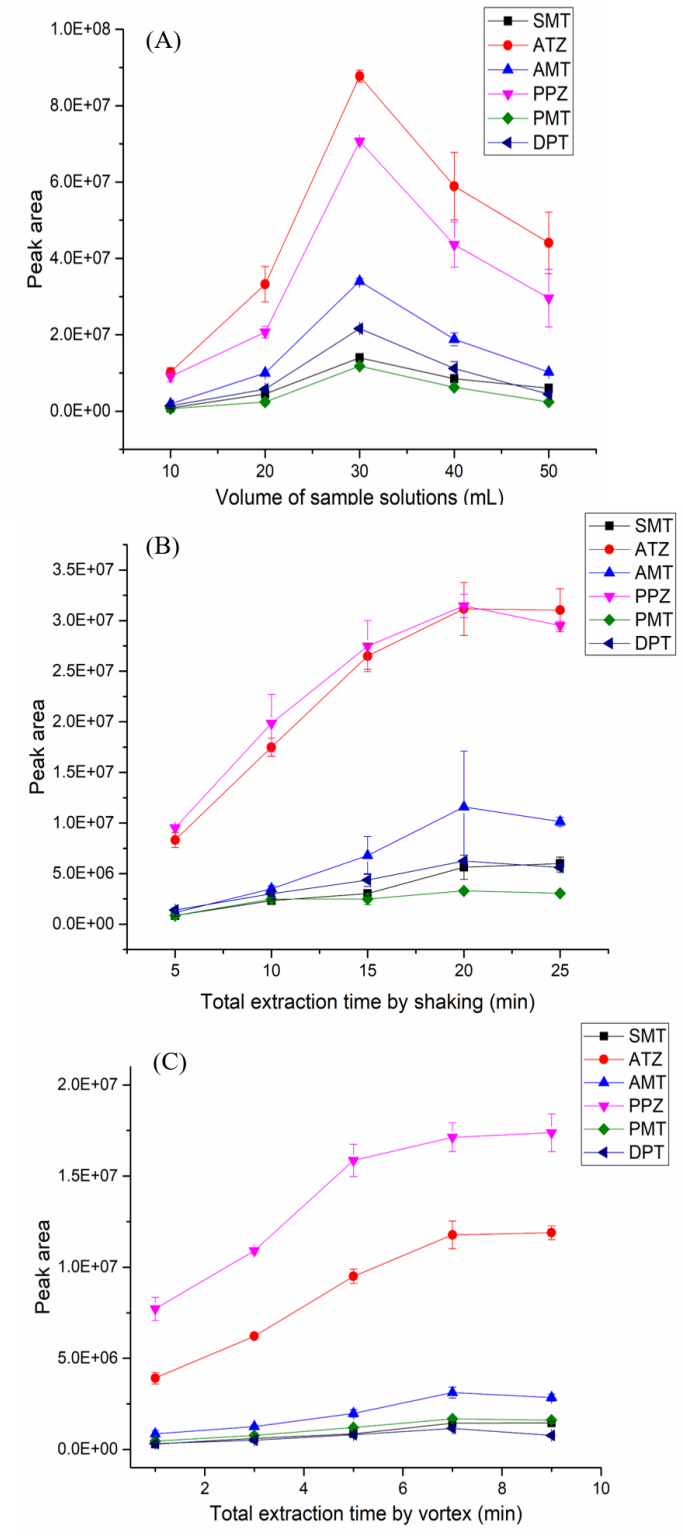

Figure A-7 Effect of sorbent/liquid ratio (A), total extraction time by shaking (B), and total extraction time by vortex (C) on DART-MS analysis using 1.0 mg M2GO as sorbents.

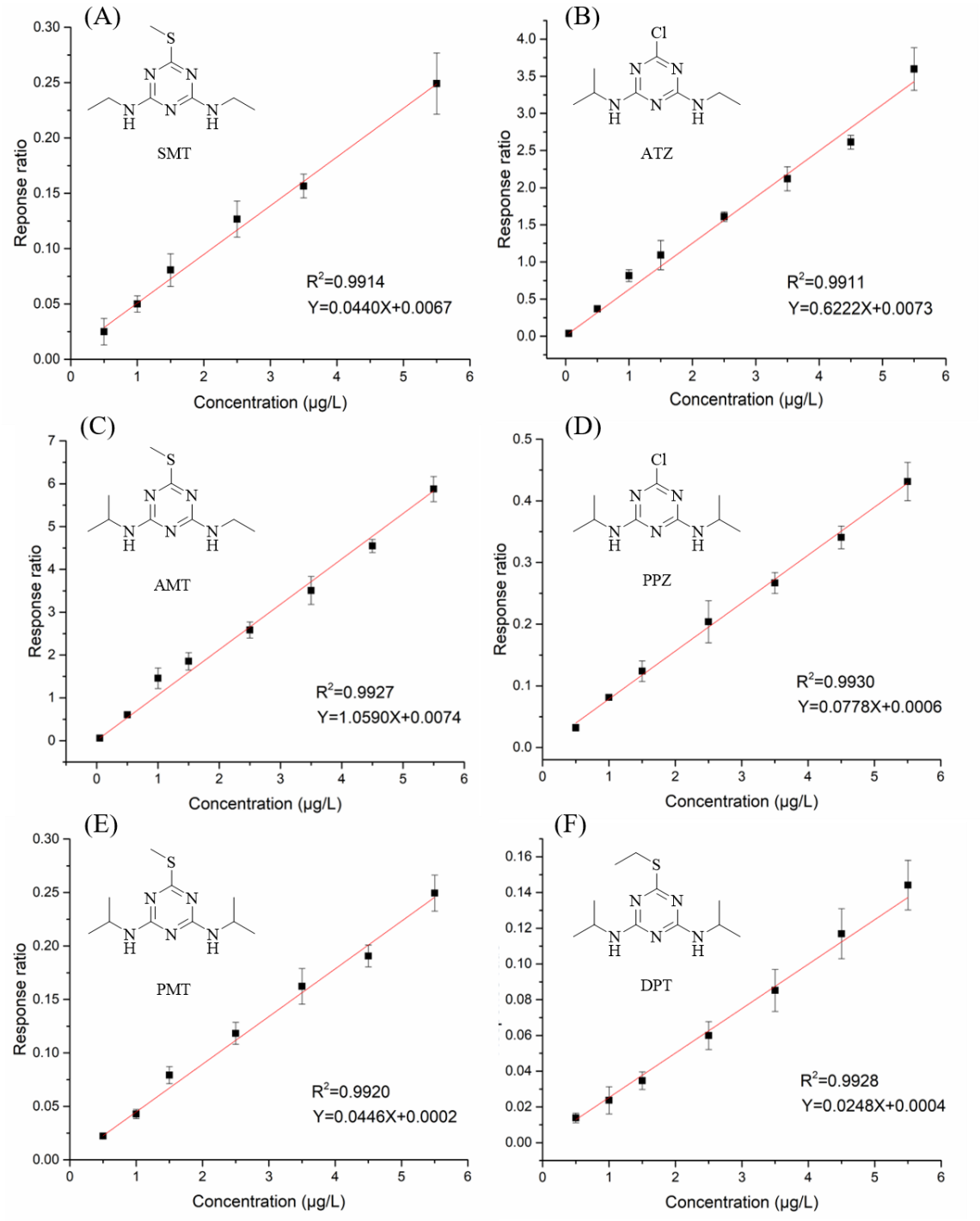

Figure A-8 Calibration curves of six triazine herbicides established by DMSPE-DART-MS method: (A) SMT; (B) ATZ; (C) AMT; (D) PPZ; (E) PMT; (F) DPT.

Table A-1Determination of LODs for six triazine herbicides by DMSPE-DART-MS method.

Analytes	Amount standard (ng/L)	RSD (%)	LOD (ng/L)
SMT	400	12.1	152.1
ATZ	4	12.9	1.6
AMT	24	11.5	8.7
PPZ	4	13.6	1.7
PMT	400	11.4	143.3
DPT	400	10.5	132.0

Note: The LOD value for each analyte was performed with 7 replicates. For the 7 replicate measurements (6 degrees of freedom, n=6) and a 99% confidence interval, the value of the test statistic t_α is 3.143. LOD= t_α*RSD*(amount standard)/100%.[108]

Appendix B Supplemental information for Chapter 3.

In the present study, the synthesized nanoparticles were directly pasted on the ss bar with red silicone sealant. SEM images of the surface of the (A) ss bar;(B) ss bar with red silicone sealant; (C) g-C_3N_4 coated ss bar and (D) g-C_3N_4/C coated ss bar were shown in Figure B-1 indicated the surface of the ss bar was well-covered. The bar surfaces became porous after coating, and the morphologies of the g-C_3N_4 and g-C_3N_4/C coatings on the bars were relatively homogeneous and dense morphological.

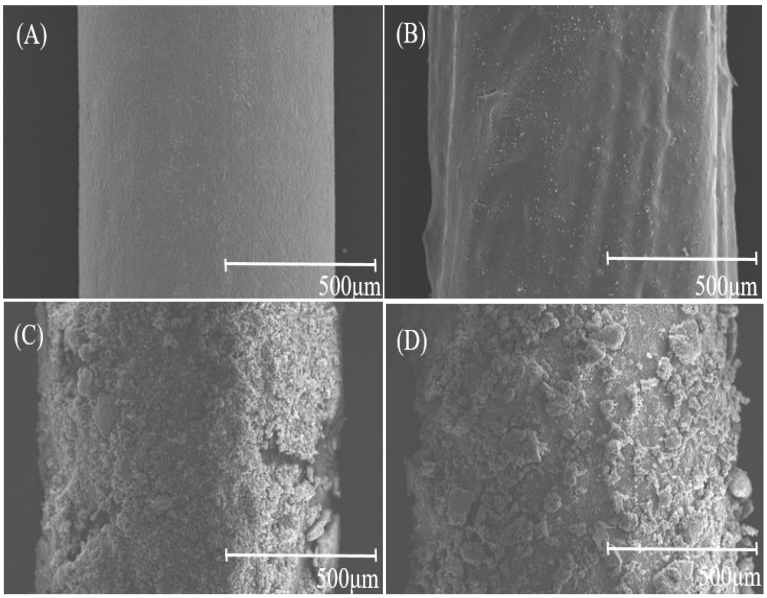

Figure B-1 Scanning electron micrographs of the surface of the sorbent-coated ss bars. (A) ss bar;(B) ss bar with red silicone sealant; (C) g-C_3N_4 coated ss bar and (D) g-C_3N_4/C coated ss bar. The images are at a magnification of 100.

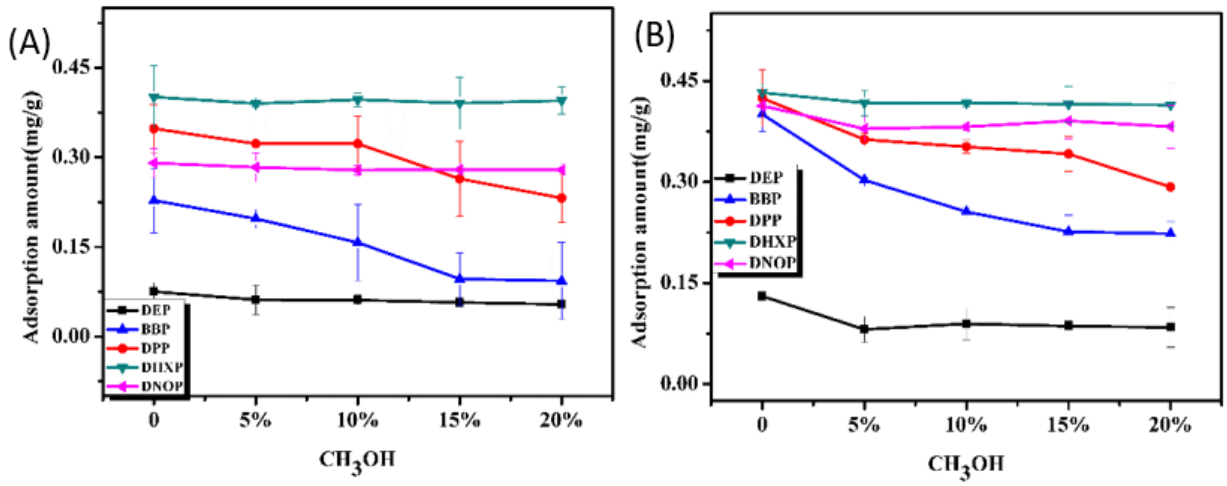

Figure B-2 Effect of the addition of methanol (0, 5%, 10 %, 15 %, 20 %) for (A) g-C_3N_4 and (B) g-C_3N_4/C on UPLC-UV. The error bars are standard deviations.

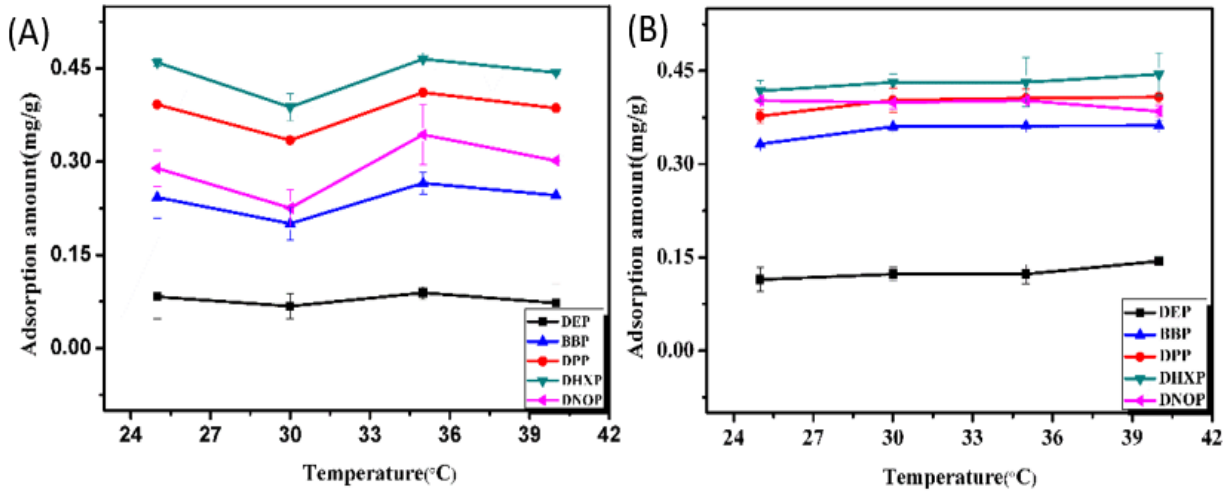

Figure B-3 Effect of temperature (25 ºC, 30 ºC, 35 ºC, 40 ºC) for (A) g-C_3N_4 and (B) g-C_3N_4/C on UPLC-UV. The error bars are standard deviations.

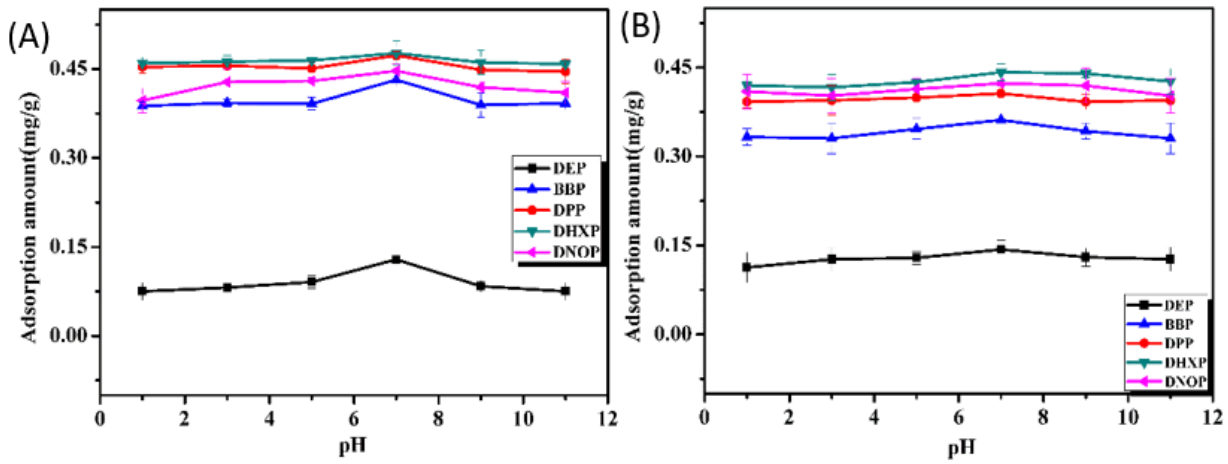

Figure B-4 Effect of pH (1, 3, 5, 7, 9, 11) for (A) g-C_3N_4 and (B) g-C_3N_4/C on UPLC-UV. The error bars are standard deviations.

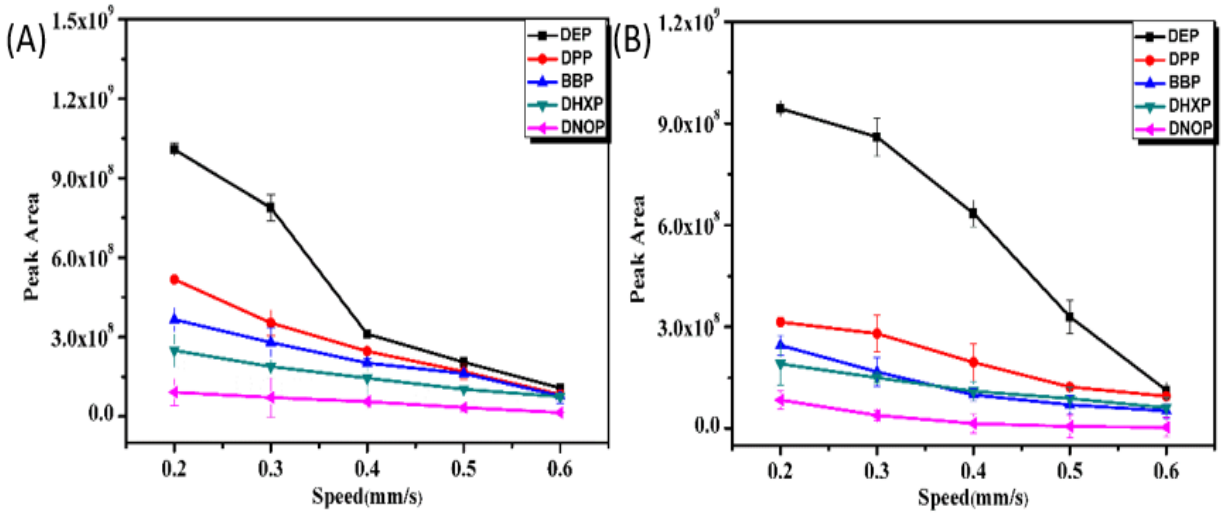

Figure B-5 Effect of linear rail moving speed (0.2, 0.3, 0.4, 0.5, 0.6 mm s^{-1}) for (A) g-C_3N_4 and (B) g-C_3N_4/C on DART source. The error bars are standard deviations.

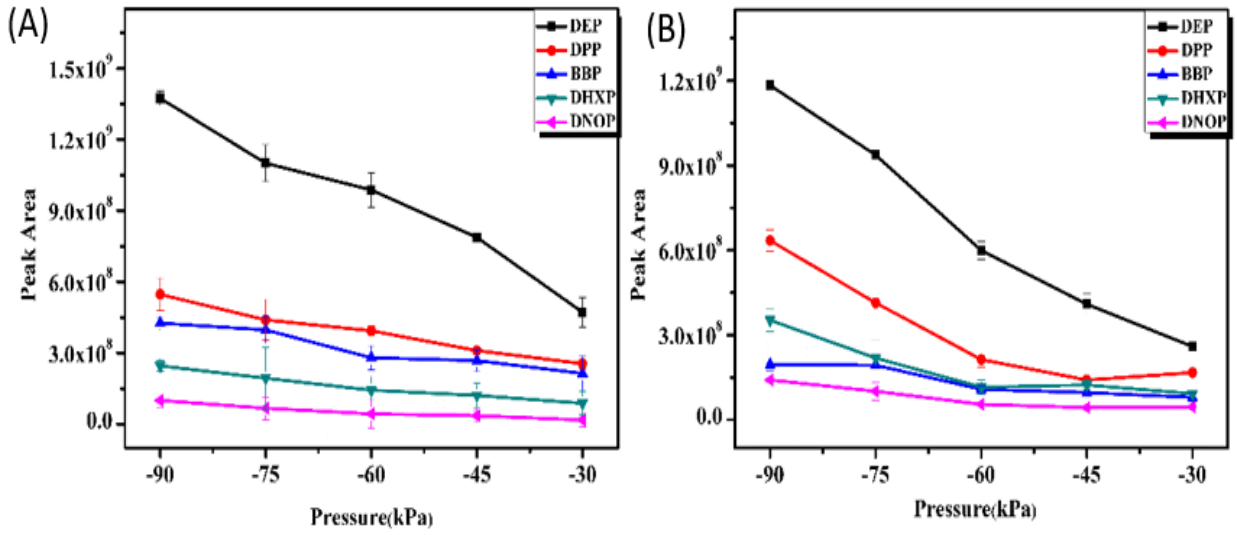

Figure B-6 Effect of pressure at Vapur™ interface (-90, -75, -60, -45, -30 kPa) for (A) g-C_3N_4 and (B) g-C_3N_4/C on DART source. The error bars are standard deviations.

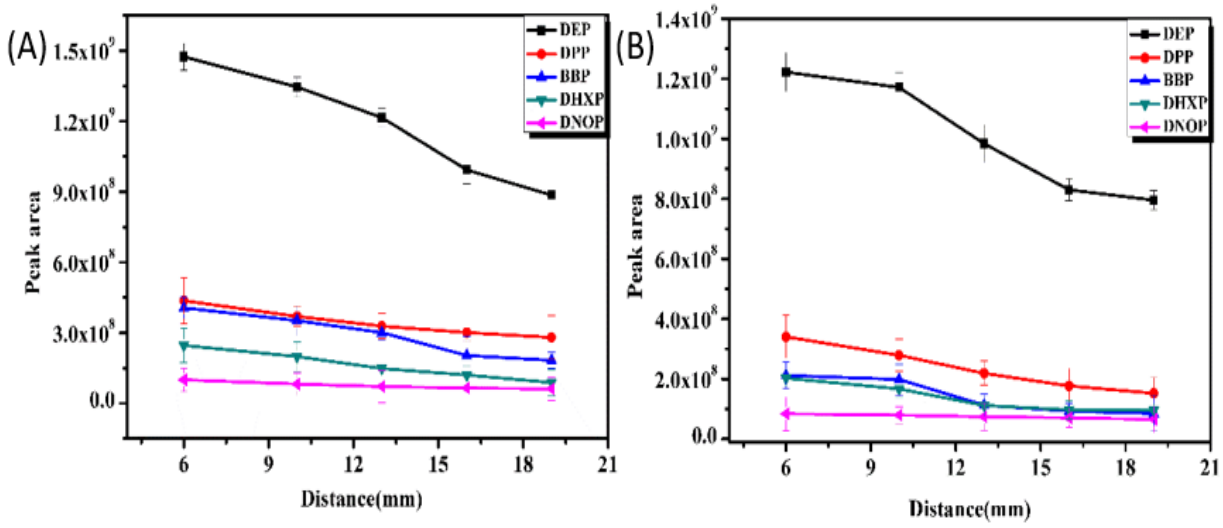

Figure B-7 Effect of the distance (6, 10, 13, 16, 19 mm) from samples to DART ion source for (A) g-C_3N_4 and (B) g-C_3N_4/C. The error bars are standard deviations.

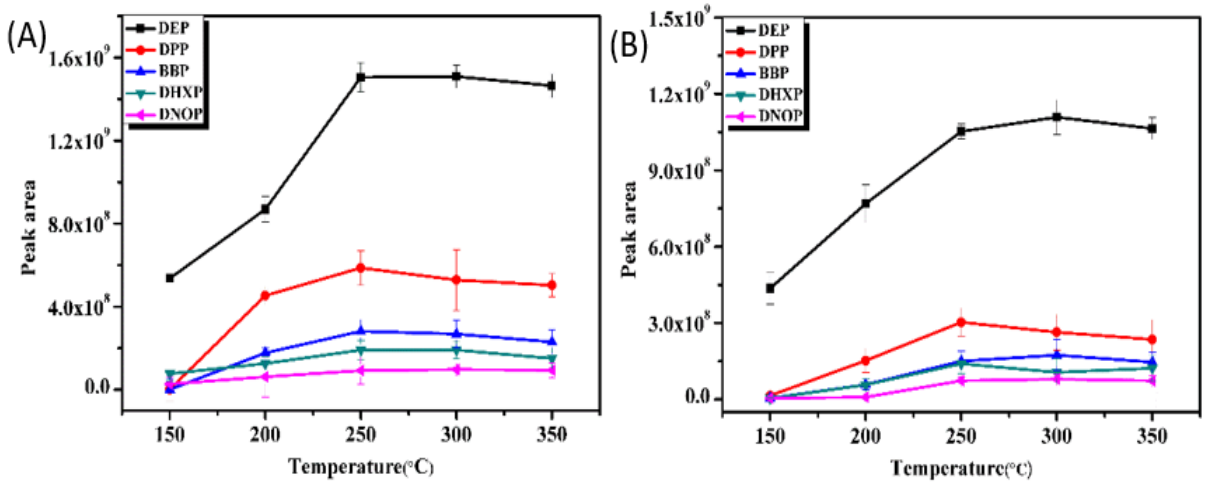

Figure B-8 Effect of gas temperature (150 ºC, 200 ºC, 250 ºC, 300 ºC, 350 ºC) for (A) g-C_3N_4 and (B) g-C_3N_4/C on DART source. The error bars are standard deviations.

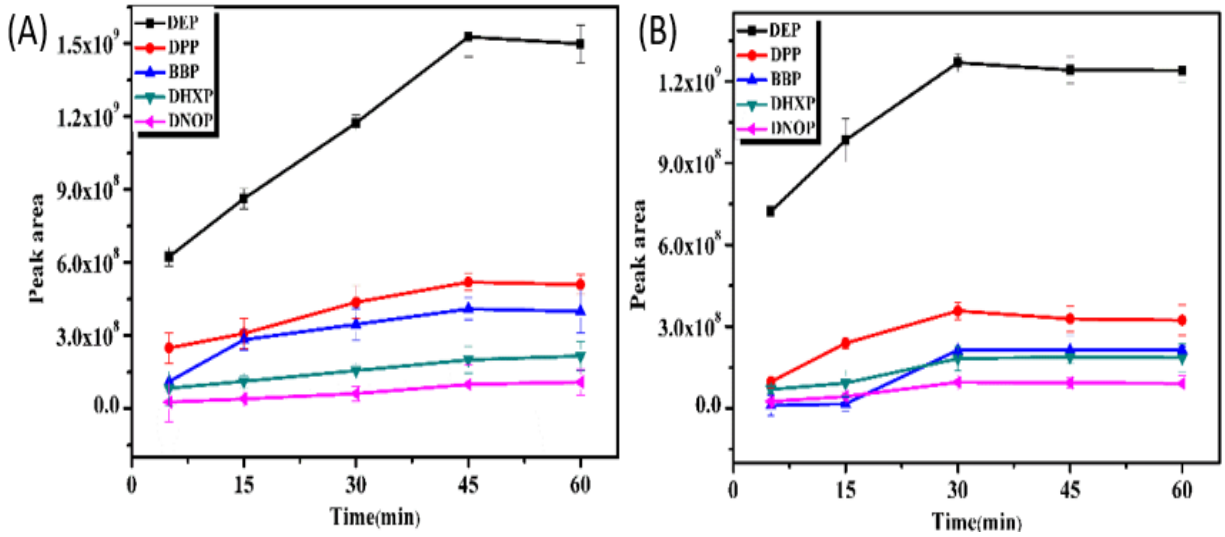

Figure B-9 Effect of the extraction time (5, 15, 30, 45, 60 min) in SPME process for (A) g-C_3N_4 and (B) g-C_3N_4/C on DART source. The error bars are standard deviations.

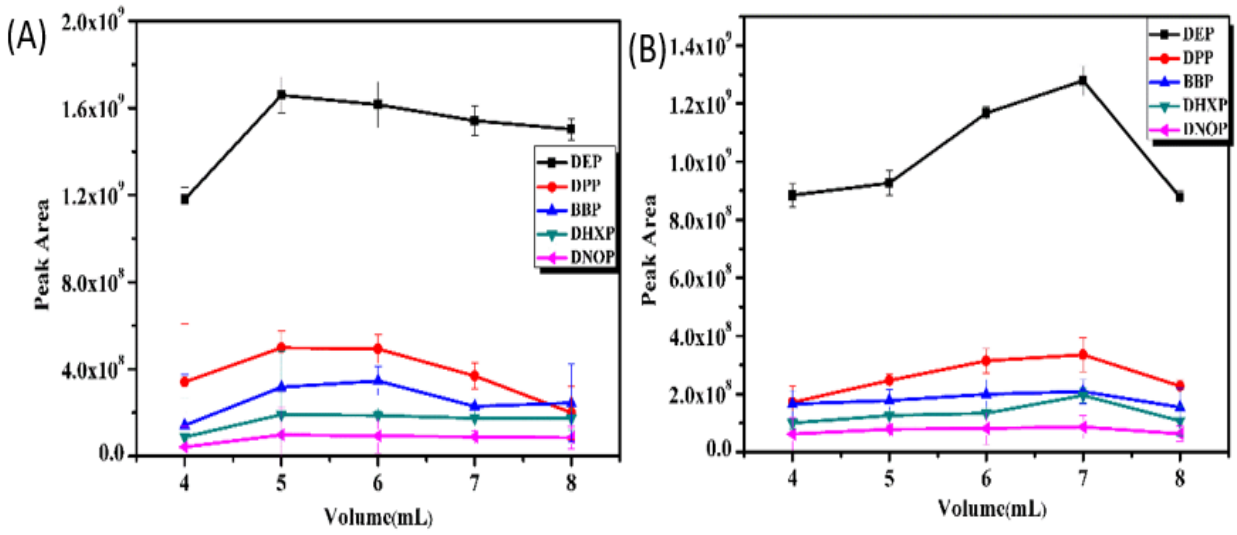

Figure B-10 Effect of the amount of organic solvents (4, 5, 6, 7, 8 µL) for (A) g-C_3N_4 and (B) g-C_3N_4/C on DART source. The error bars are standard deviations.

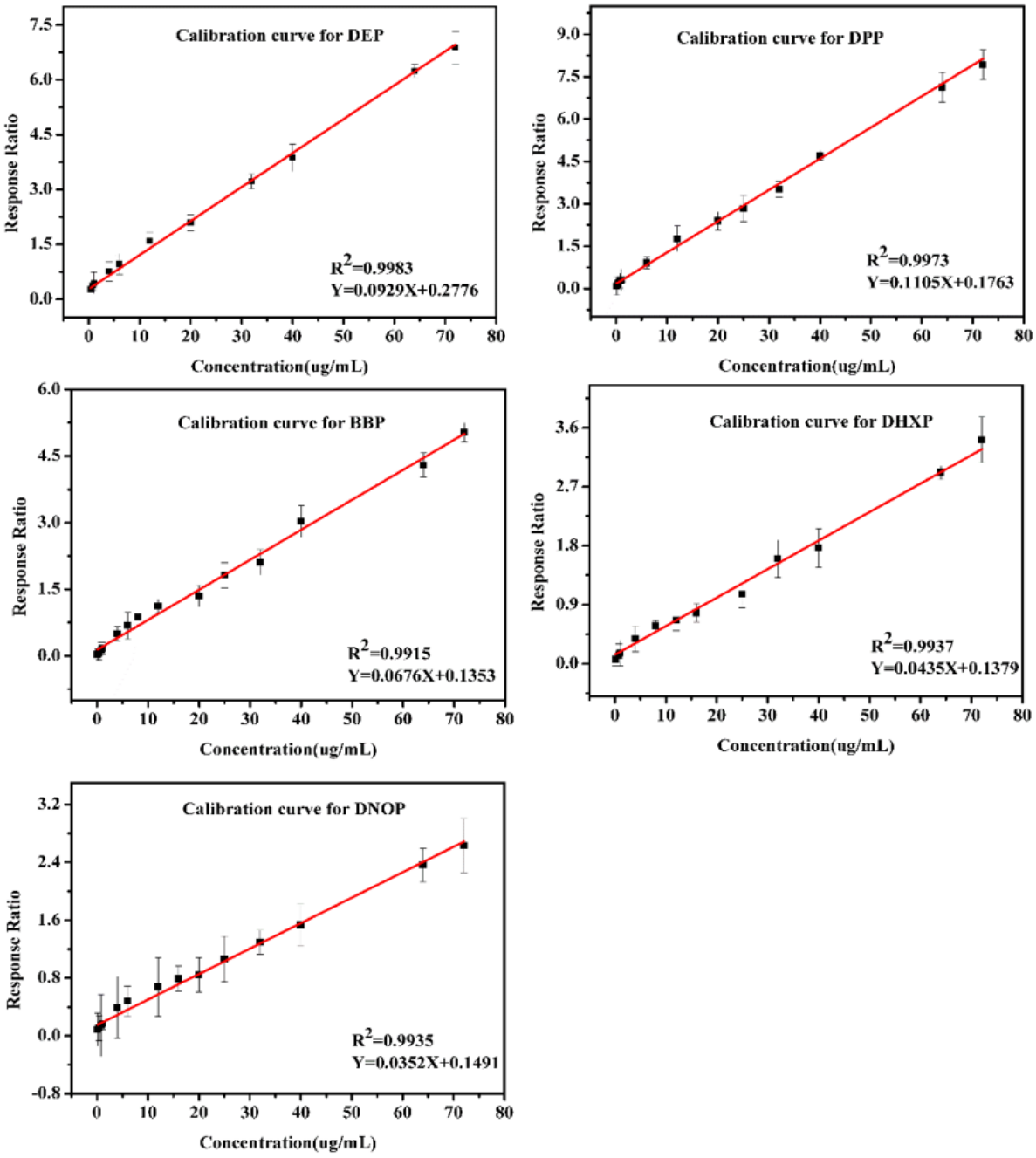

Figure B-11 Respective calibration curves for DEP, DPP, BBP, DHXP and DNOP on g-C_3N_4 using DART-MS. The concentrations in the curves are in the range of 0.1-72 µg L^{-1}. The limit of detection (LOD) were for 0.94 ng L^{-1} for BBP, 0.11 ng L^{-1} for DEP and DPP, 0.09 ng L^{-1} for DHXP, and 0.07 ng L^{-1} for DNOP, respectively. The error bars in presented calibration curves refer to standard deviations.

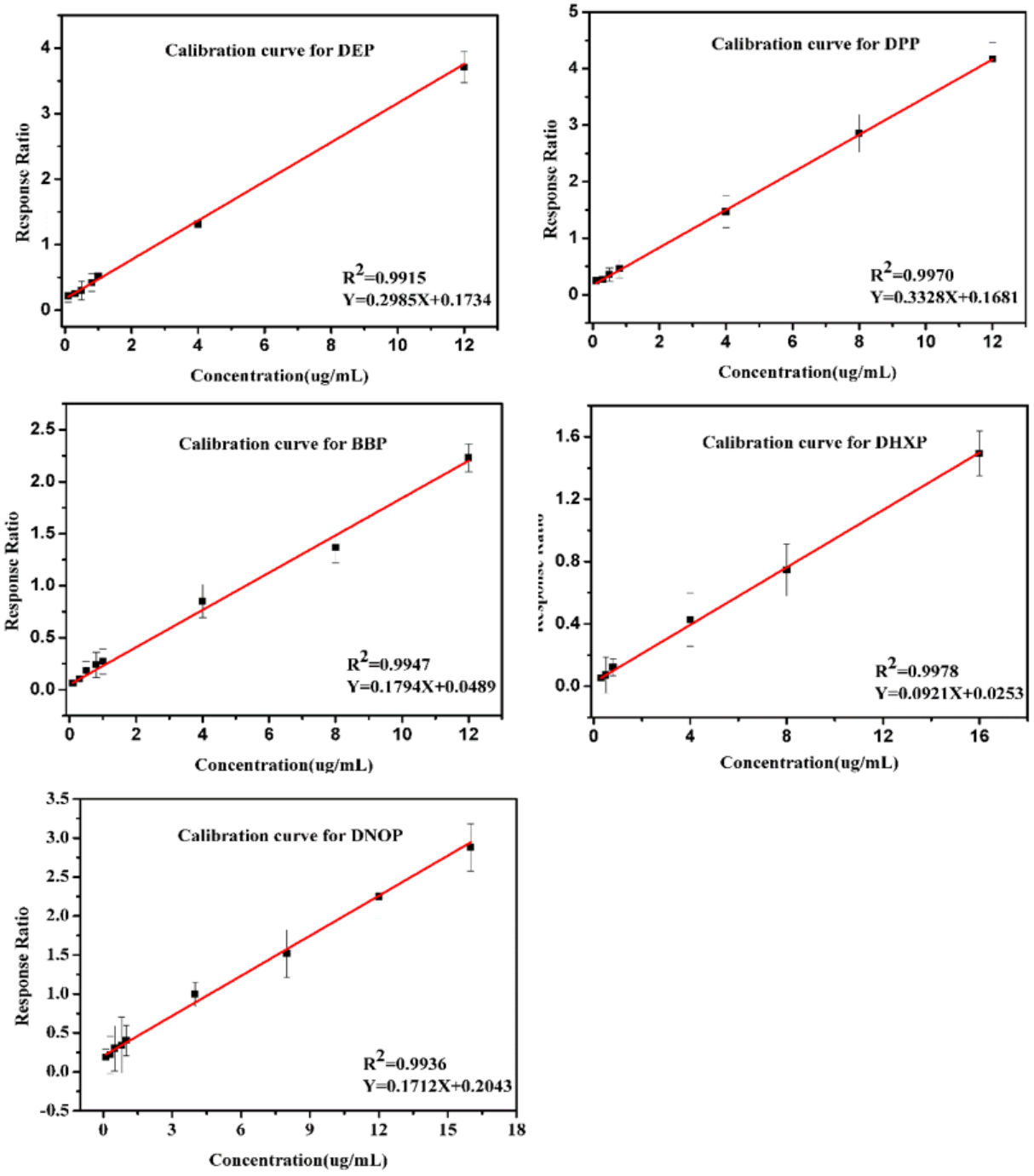

Figure B-12 Respective calibration curves for DEP, DPP, BBP, DHXP and DNOP on g-C_3N_4/C using DART-MS. The concentrations in the curves are in the range of 0.1-16 μg L^{-1}. The limit of detection (LOD) were 9.19 ng L^{-1} for BBP, 5.23 ng L^{-1} for DEP, 10.29 ng L^{-1} for DPP, 9.66 ng L^{-1} for DHXP, and 6.84 ng L^{-1} for DNOP respectively. The error bars in presented calibration curves refer to standard deviations.

Table B-1 Determination of LODs for five PAEs by SSE-DART-MS method using g-C_3N_4

Analytes	Amount standard (ng/L)	RSD (%)	LOD (ng/L)
BBP	2.5	12.0	0.94
DEP	0.25	14.3	0.11
DPP	0.25	13.5	0.11
DHXP	0.25	10.9	0.09
DNOP	0.25	8.4	0.07

Table B-2 Determination of LODs for five PAEs by SSE-DART-MS method using g-C_3N_4/C

Analytes	Amount standard (ng/L)	RSD (%)	LOD (ng/L)
BBP	25	11.7	9.19
DEP	15	11.1	5.23
DPP	25	13.1	10.29
DHXP	25	12.3	9.66
DNOP	15	14.5	6.84

Note: The LOD value for each analyte was performed with 7 replicates. For the 7 replicate measurements (6 degrees of freedom, n=6) and a 99% confidence interval, the value of the test statistic t_α is 3.143. LOD= t_α*RSD*(amount standard)/100%.[108]

Appendix C Supplemental information for Chapter 4

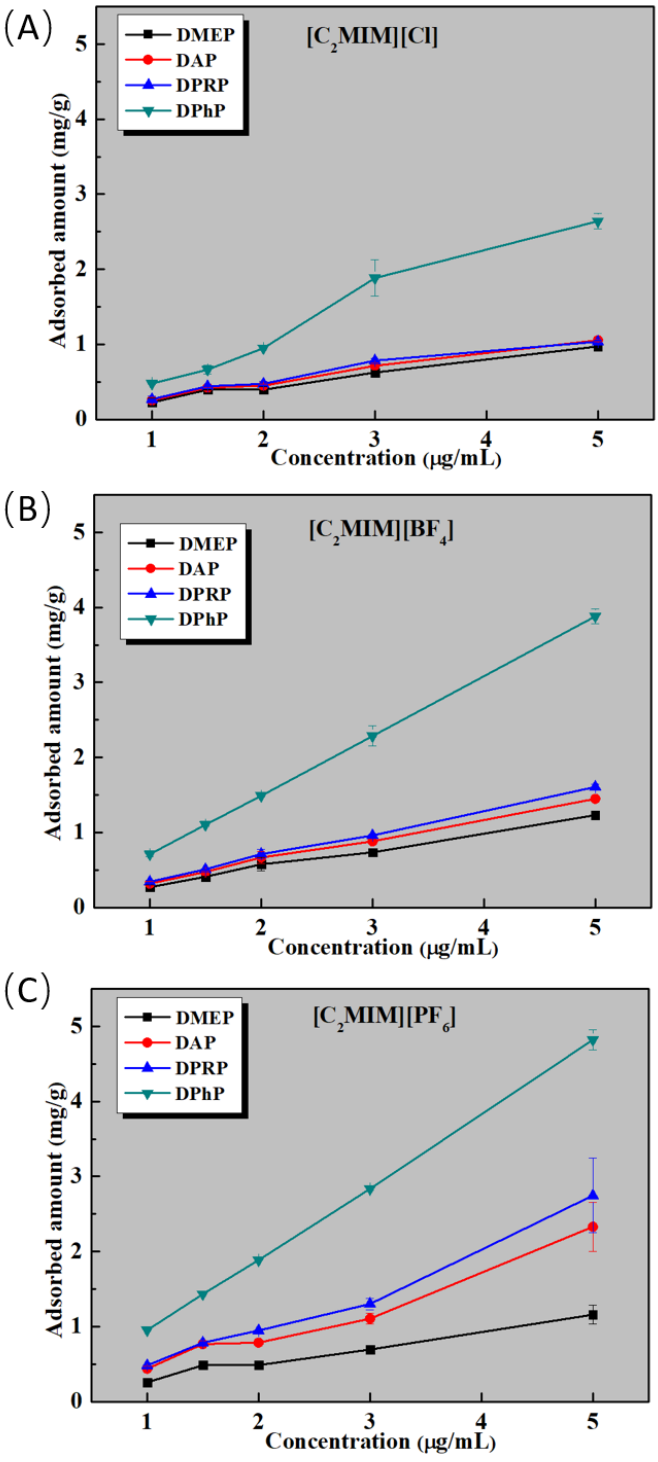

Figure C-1 Effect of initial concentrations of PAEs standard solutions on SPME process: (A) [C_2MIM][Cl]; (B) [C_2MIM][BF_4]; (C) [C_2MIM][PF_6].

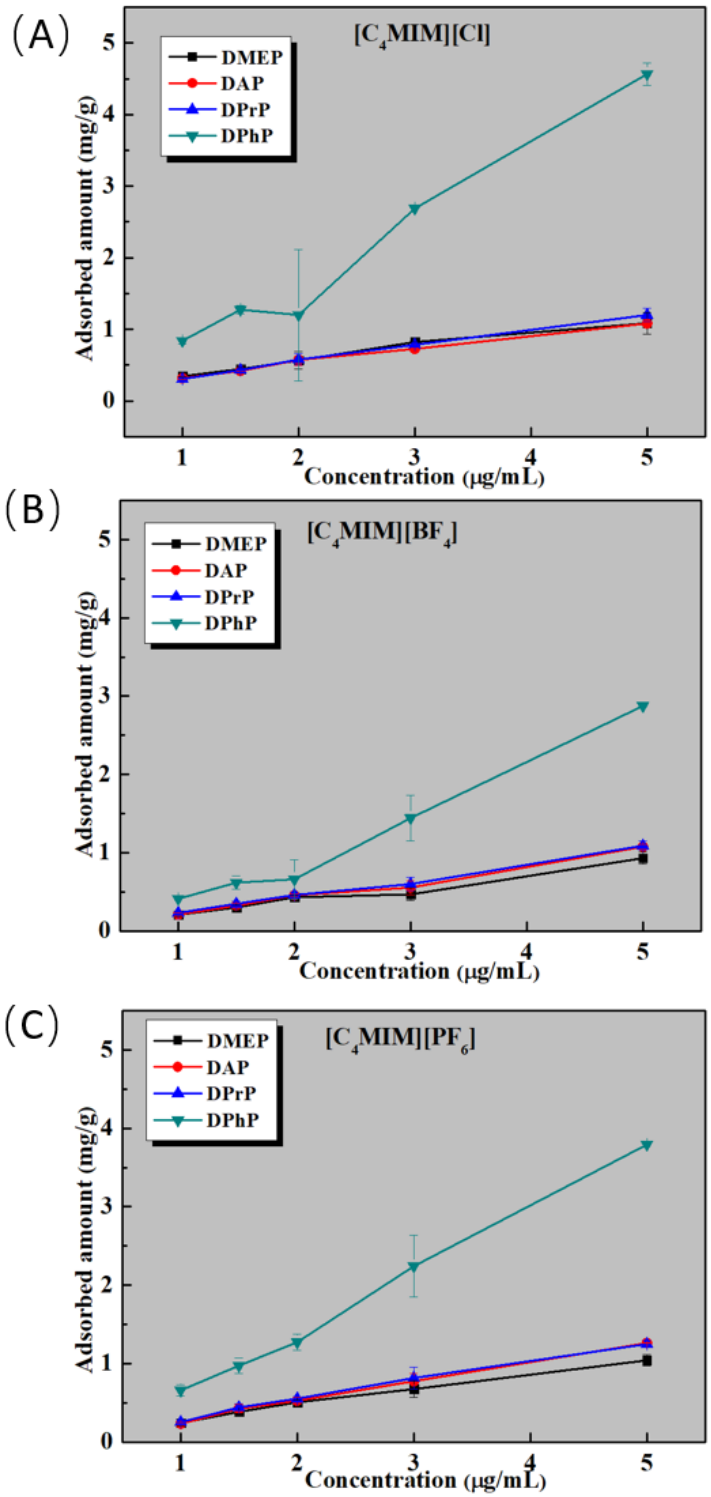

Figure C-2 Effect of initial concentrations of PAEs standard solutions on SPME process: (A) [C_4MIM][Cl]; (B) [C_4MIM][BF_4]; (C) [C_4MIM][PF_6].

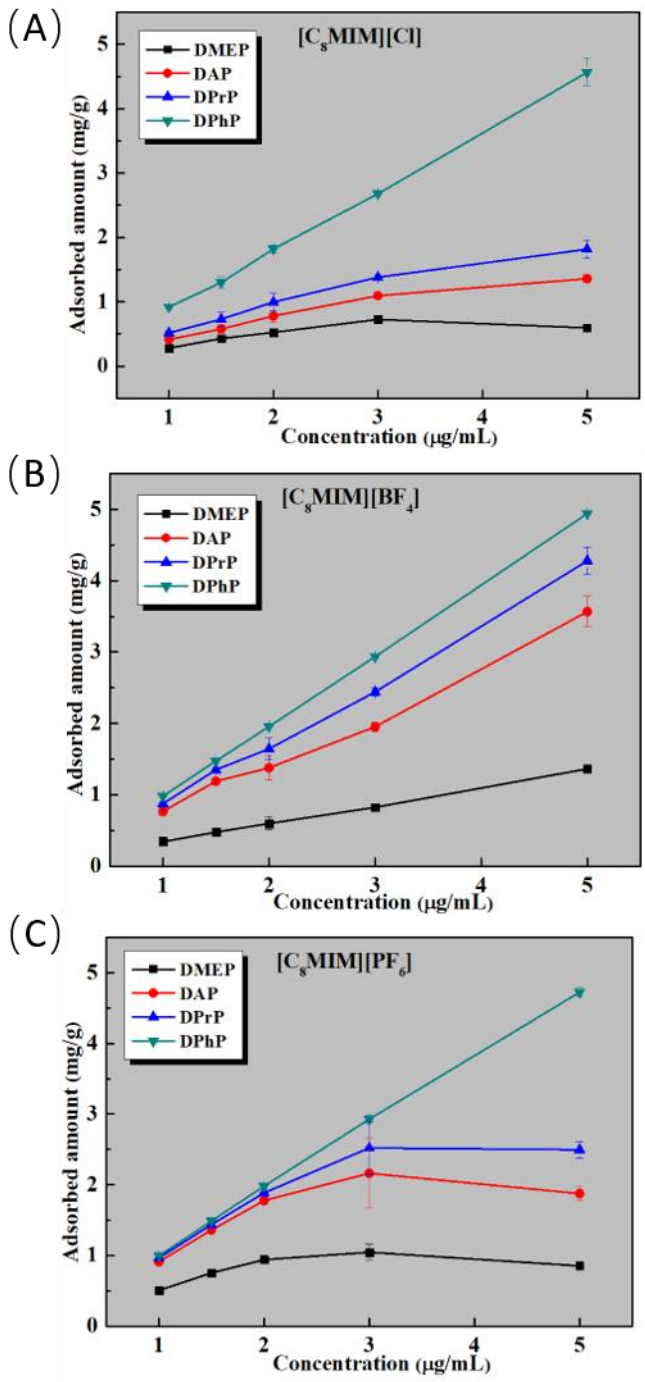

Figure C-3 Effect of initial concentrations of PAEs standard solutions on SPME process: (A) [C_8MIM][Cl]; (B) [C_8MIM][BF_4]; (C) [C_8MIM][PF_6].

Appendix D Supplemental information for Chapter 5

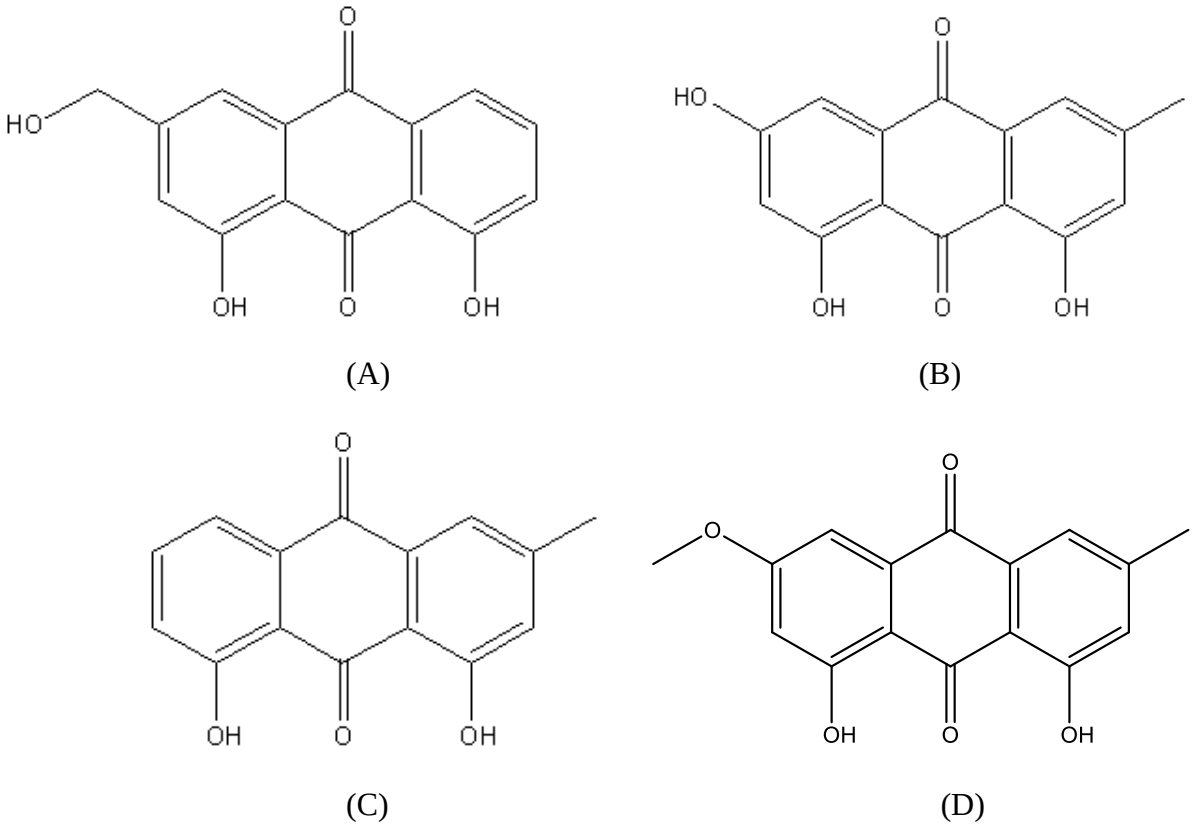

Figure D-1 Chemical structures of aloe-emodin (A), emodin (B), chrysophanol (C) and physcion (D)

Instruments

Thermo gravimetric analysis (TGA; simultaneous thermal analyser, STA 449 F3 Jupiter, NETZSCH, German) was tested at a heating rate of 10.0 °C min^{-1} in air. Fourier transform infrared (FT-IR, Bruker Tensor 27) spectrometry was operated between 400 and 4000 cm^{-1} at a scan rate of 20 scans min^{-1}. JSM-7600F (JEOL Ltd., Japan) instrument was used for the scanning electronic microscopy (SEM) analysis. Thermo Evolution 201 UV-Visible spectrophotometer was used to analyse the interaction between glucose and DESs.

Ultimate 3000 UPLC (Thermo Scientific, Jose, CA, USA) system equipped with an HPG-3400RS pump, WPS-3000TRS autosampler, diode array, and multiple wavelength detectors was used for the analysis of samples. For the optimization of extraction parameters. A commercial C_{18} column (Thermo Fisher Scientific Inc., 4.5× 150 mm, 5.0 μm, China) was used for the separation of compounds. The chromatographic separation was achieved using a solvent gradient employing the solvents of water (A) and methanol (B) at a flow rate of 1.0 mL min^{-1}. The gradient programs were as follows: 0-5 min, 50% B; 5-20 min, 50-100% B; 20-22.5 min, 100% B; 22.5-25 min, 100-50 % B; 25-30 min, 50% B. The detection wavelength was set at 254 nm, the injection volume was 20 μL and column temperature was set at 30 ℃. Data processing was performed using Chromeleon 7 (Thermo Scientific, Jose, CA, USA). All samples were analyzed in triplicates.

The liquid chromatography-mass spectrometry (LC-MS) analysis were carried out with an Agilent 1290 Infinity LC (Agilent Technologies, CA, USA) equipped with an Agilent 6460 Triple Quadrupole MS system (Agilent Technologies, CA, USA) using a commercial Zorbax Eclipse XDB-C18 column (Agilent Technologies, 4.6 mm × 250 mm, 5 μm). The chromatographic separation was performed using an isocratic elution of 90% water (A) and 10% acetonitrile (B) at a flow rate of 0.6 mL min^{-1}. The UV detection wavelengths were set at 250 nm and 300 nm. The injection volume was 10 μL. The MS system was operated in the following settings: electrospray ionization; ion spray voltage 3500 V; nebulizer pressure 40 psi; gas temperature 300 ℃; full scan mode in the range of m/z 50-1000.

Experimental design of response surface methodology (RSM)

Design Expert 8.05b, (Stat-Ease Inc., Minneapolis, MN, USA) was used for Box-Behnken design in this work. The purpose was to investigate the best combination of extraction parameters,

including the DES content (X_1), the solid/liquid ratio (X_2) and the extraction time (X_3) on the basis of limited experimental optimization steps. Single factor, one level design was used to determine the appropriate ranges of these three variables. The experimental data were fitted using multiple regression to the quadratic equation which is given by

$$Y = \beta_0 + \sum_{j=1}^{k} \beta_j X_j + \sum_{j=1}^{k} \beta_{jj} X_j^2 + \sum \sum_{i<j}^{k} \beta_{ij} X_i Y_j$$

where Y is the output variable (extracted amounts of anthraquinones); β_0 is the constant coefficient; β_j, β_{jj}, and β_{ij} are interaction coefficients of linear, quadratic, and the second-order terms, respectively; k is the number of independent variables. Analysis of variance (ANOVA) was carried out to evaluate the model.

Characterization of three sorbents

The carbon, hydrogen, and nitrogen contents of the three sorbents were determined by elemental analysis. The element contents of PHE-SIL, C_8-SIL, and NH_2-SIL were listed on Table D-1. The C and H elements on sorbents PHE-SIL and C_8-SIL were from phenyl and octyl functional groups, respectively. The unique N element on sorbent NH_2-SIL was from its amino functional group. Thermogravimetry was used to determine the thermal stability of the chemically modified silica (Fig. D-2A). The weight of the three sorbents decreased between 0 and 200 ^oC, which was due to the evaporation of adsorbed water. NH_2-SIL reduced more water than the other two sorbents because of its stronger absorptivity of water. The weight loss observed between 300 ^oC and 800 ^oC was found to be associated with the loss of the organic groups attached to the surface. As shown in Fig. D-2B, the bands of PHE-SIL at 1600, 1500 and 1450 cm^{-1} in FT-IR spectra were ascribed to the skeleton stretching vibration of aromatic rings. With respect to the

spectra of C_8-SIL, the bands in the range of 2975-2845 cm^{-1} were assigned to the symmetric and asymmetric stretching vibration of methyl, methylene and methylene groups. The band at 1460 cm^{-1} was the characteristic absorption of methyl group. The band of NH_2-SIL at 698 cm^{-1} was assigned to the vibration of NH_2 group.

Table D-1 Elemental analysis of three sorbents.

Sorbent	N(%)	C(%)	H(%)
PHE-SIL	ND	10.65	1.344
C_8-SIL	ND	12.01	2.518
NH_2-SIL	3.444	8.664	2.290

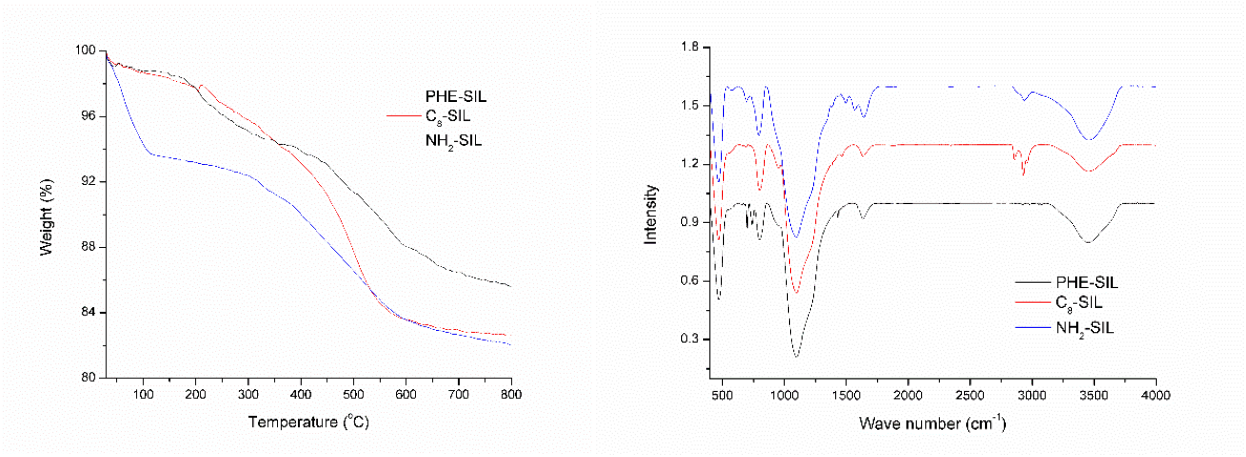

(A) (B)

Figure D-2 TGA (A) and FT-IR (B) data of three sorbents.

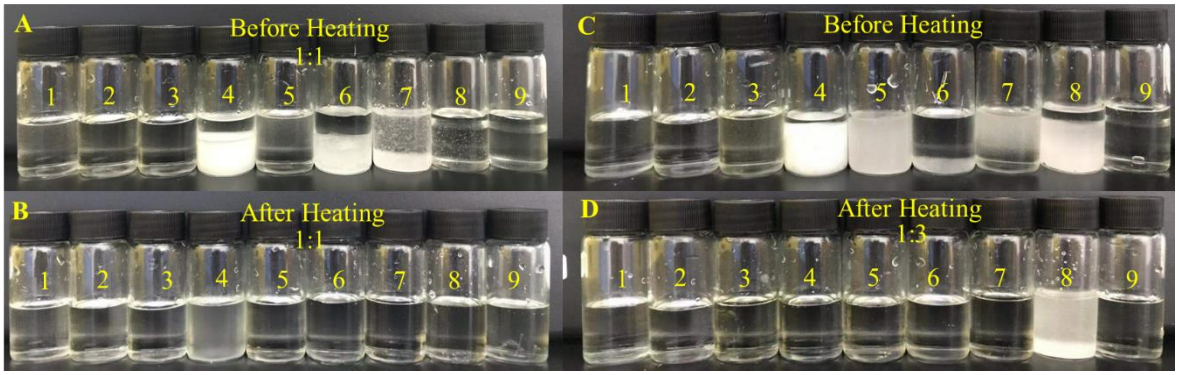

Figure D-3 Photographs of DES-1 to DES-9 (HBA/HBD=1/1, mol/mol) in 20 wt% water before (A) and after heating (B), and DES-1 to 9 (HBA/HBD=1/3, mol/mol) in 20 wt% water before (C) and after heating (D).

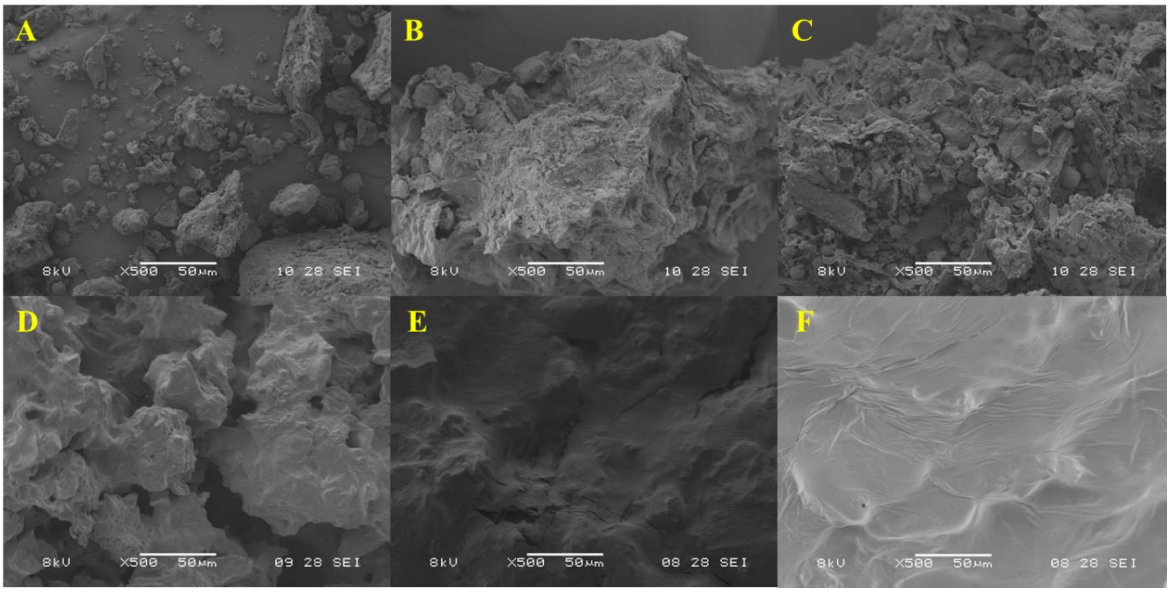

Figure D-4 SEM images of plant residues before and after MAE with different solvents: (A) without MAE; (B) water; (C) methanol; (D) 80 wt% DES-2 (HBA/HBD=1/1, mol/mol); (E) 80 wt% DES-6 (HBA/HBD=1/1, mol/mol); (F) 80 wt% DES-8 (HBA/HBD=1/1, mol/mol).

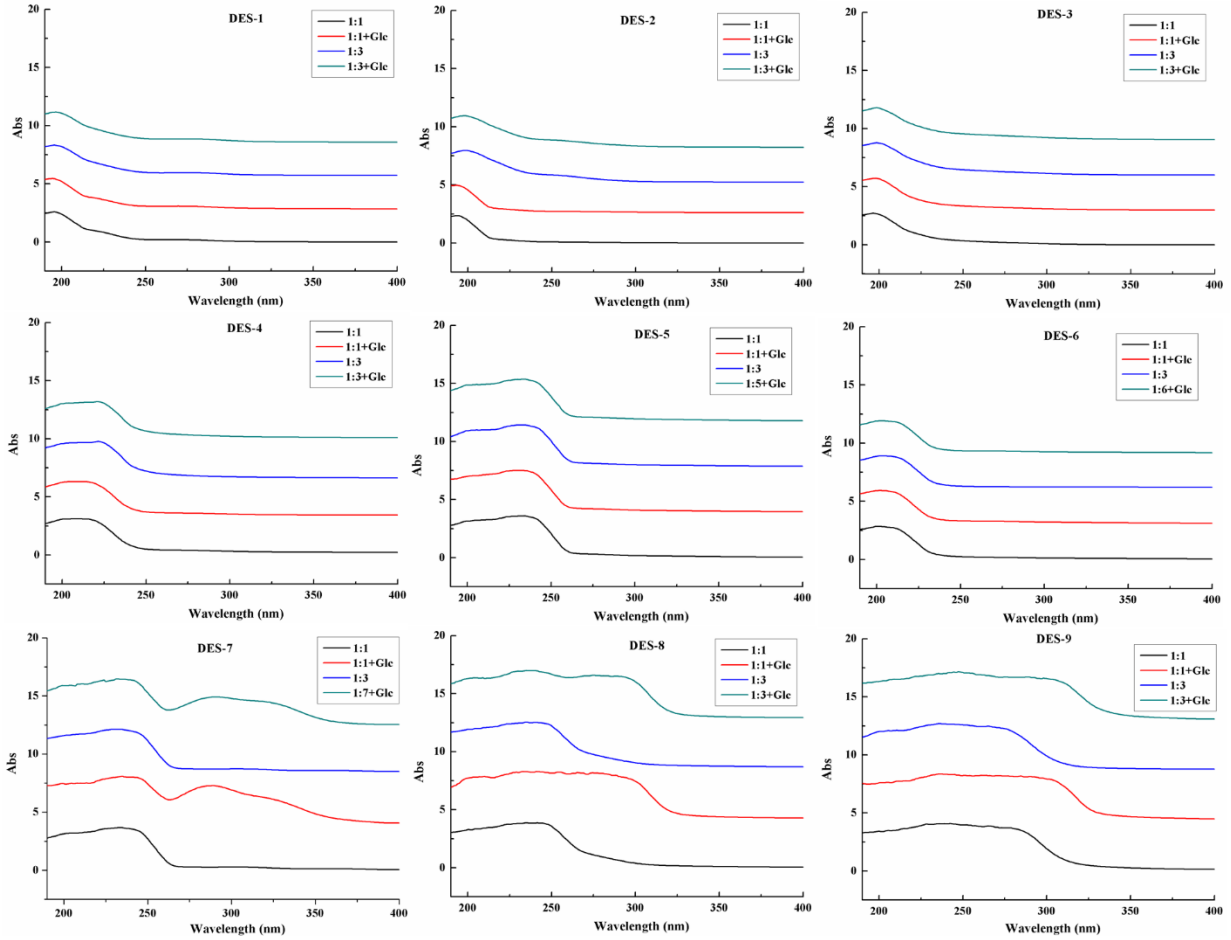

Figure D-5 UV-Vis data of 80 wt% DES-1 to 9 (HBA/HBD=1/1, mol/mol) aqueous solutions with glucose after heating by microwave irradiation.

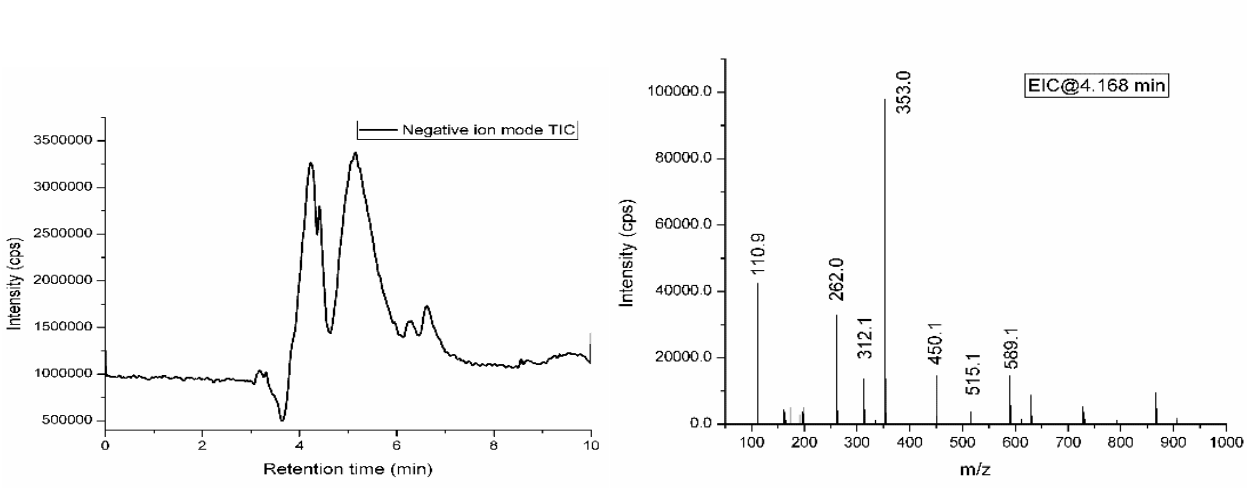

(A) (B)

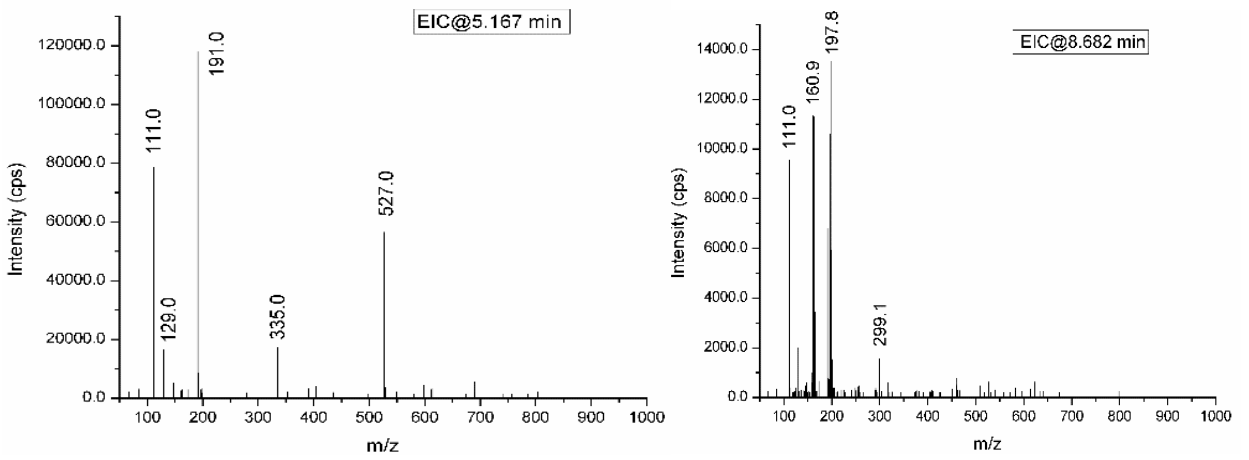

(C) (D)

Figure D-6 Total ion chromatogram (TIC) (A) and extracted ion chromatogram (EIC) (B, C, and D) of LC-MS (negative ion mode) of 80 wt% DES-8 (HBA/HBD=1/1, mol/mol) aqueous solutions with glucose after heating by microwave irradiation.

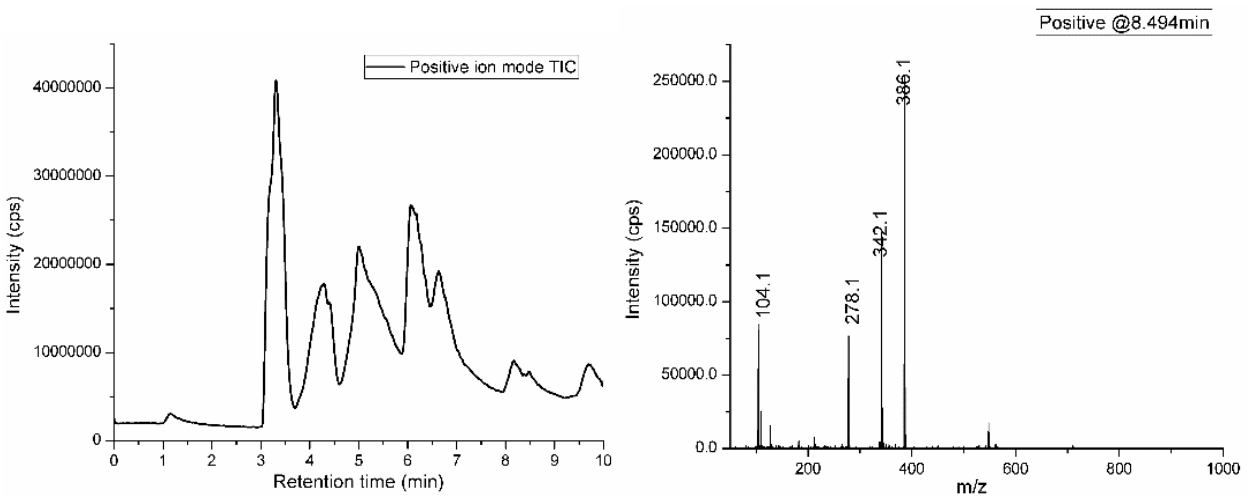

(A) (B)

Figure D-7 Total ion chromatogram (TIC) (A) and extracted ion chromatogram (EIC) (B) of LC-MS (positive ion mode) of 80 wt% DES-8 (HBA/HBD=1/1, mol/mol) aqueous solutions with glucose after heating by microwave irradiation.

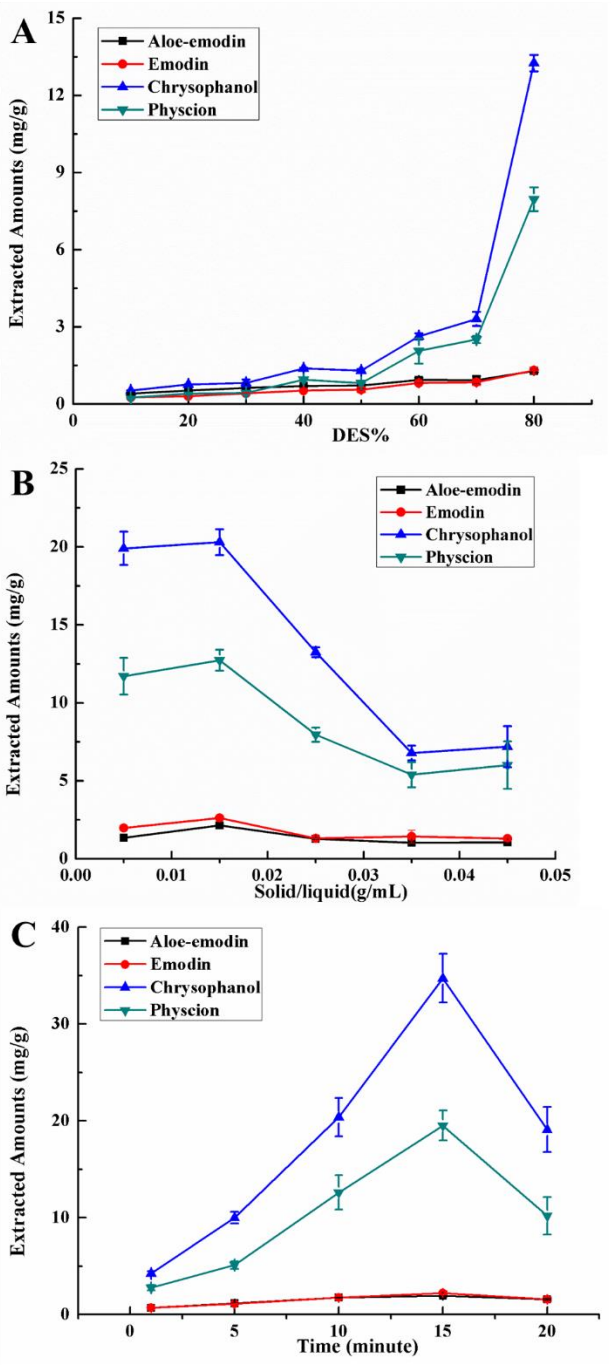

Figure D-8 Effect of the concentration of DES (A); solid/liquid ratio (B); extraction time (C) on extracted amounts of anthraquinones.

Table D-2 Box–Behnken experiment design with the independent variables.

RUN	X_1	X_2	X_3	Extracted amount of anthraquinones (mg g^{-1})			
				Aloe-emodin	Emodin	Chrysophanol	Physcion
1	70.00	0.015	15.00	1.94	2.15	15.30	12.38
2	70.00	0.020	10.00	1.47	1.18	3.62	1.77
3	80.00	0.015	10.00	2.07	1.64	20.64	12.67
4	70.00	0.015	15.00	1.93	2.13	17.65	12.78
5	70.00	0.015	15.00	1.95	2.13	17.23	12.36
6	70.00	0.010	10.00	1.51	1.35	8.52	5.35
7	80.00	0.020	15.00	1.91	1.89	27.18	15.46
8	70.00	0.020	20.00	1.46	1.42	4.94	3.38
9	70.00	0.015	15.00	1.90	2.13	15.70	11.35
10	60.00	0.015	10.00	1.38	1.04	1.81	2.13
11	60.00	0.020	15.00	1.41	1.24	2.49	1.88
12	80.00	0.015	20.00	2.08	2.19	31.64	19.32
13	70.00	0.010	20.00	1.61	1.51	8.31	7.21
14	60.00	0.010	15.00	1.61	1.42	9.63	9.29
15	70.00	0.015	15.00	1.87	2.06	17.16	11.95
16	80.00	0.010	15.00	2.21	2.30	34.44	18.80
17	60.00	0.015	20.00	1.50	1.18	2.46	1.81

Table D-3 Analysis of variance for the fitted quadratic polynomial model of extracted amounts of target compounds.

Source	BRFs	Sum of squares	Degree of freedom	Mean square	*F*-value	Probability>*F*
Model	Aloe-emodin	1.15	9	0.13	46.58	< 0.0001
	Emodin	3.01		0.33	73.56	< 0.0001
	Chrysophanol	1647.76		183.08	55.31	< 0.0001
	Physcion	549.53		61.06	63.90	< 0.0001
Residual	Aloe-emodin	0.019	7	2.747E-003		
	Emodin	0.31		4.430E-003		
	Chrysophanol	23.17		3.31		
	Physcion	6.69		0.96		
Lack of Fit	Aloe-emodin	0.015	3	5.157E-003	5.49	0.0668
	Emodin	0.025		8.477E-003	6.08	0.0569
	Chrysophanol	18.86		6.29	5.83	0.0607
	Physcion	5.51		1.84	6.24	0.0546
Experimental error	Aloe-emodin	3.758E-003	4	9.395E-004		
	Emodin	5.575E-003		1.394E-003		
	Chrysophanol	4.31		1.08		
	Physcion	1.18		0.29		

Table D-4 Estimated regression model of relationship between response variables and independent variables (X1, X2, X3).

PCAs	Variables	Sum of squares	Degree of freedom	Mean squares	F-value	p-value
Aloe-emodin	X_1	0.70	1	0.70	256.41	< 0.0001
	X_2	0.056	1	0.056	20.49	0.0027
	X_3	5.390E-003	1	5.390E-003	1.96	0.2040
	X_1X_2	2.330E-003	1	2.330E-003	0.85	0.3877
	X_1X_3	3.268E-003	1	3.268E-003	1.19	0.3115
	X_2X_3	3.354E-003	1	3.354E-003	1.22	0.3057
	X_1^2	0.013	1	0.013	4.85	0.0636
	X_2^2	0.15	1	0.15	55.31	0.0001
	X_3^2	0.20	1	0.20	72.99	< 0.0001
Emodin	X_1	1.24	1	1.24	279.30	< 0.0001
	X_2	0.090	1	0.090	20.33	0.0028
	X_3	0.15	1	0.15	34.00	0.0006
	X_1X_2	0.012	1	0.012	2.77	0.1399
	X_1X_3	0.043	1	0.043	9.80	0.0166
	X_2X_3	2.045E-003	1	2.045E-003	0.46	0.5186
	X_1^2	0.072	1	0.072	16.18	0.0050
	X_2^2	0.33	1	0.33	74.23	< 0.0001
	X_3^2	0.96	1	0.96	216.48	< 0.0001

Chrysophanol	X_1	1188.69	1	1188.69	359.13	< 0.0001
	X_2	64.28	1	64.28	19.42	0.0031
	X_3	20.35	1	20.35	6.15	0.0423
	X_1X_2	3.240E-003	1	3.240E-003	9.788E-004	0.9759
	X_1X_3	26.73	1	26.73	8.08	0.0250
	X_2X_3	0.59	1	0.59	0.18	0.6867
	X_1^2	97.38	1	97.38	29.42	0.0010
	X_2^2	37.44	1	37.44	11.31	0.0120
	X_3^2	223.21	1	223.21	67.44	< 0.0001
Physcion	X_1	326.97	1	326.97	342.16	< 0.0001
	X_2	41.22	1	41.22	43.14	0.0003
	X_3	12.02	1	12.02	12.57	0.0094
	X_1X_2	4.13	1	4.13	4.33	0.0761
	X_1X_3	12.14	1	12.14	12.70	0.0092
	X_2X_3	0.015	1	0.015	0.016	0.9035
	X_1^2	14.81	1	14.81	15.50	0.0056
	X_2^2	30.23	1	30.23	31.64	0.0008
	X_3^2	107.55	1	107.55	112.55	< 0.0001

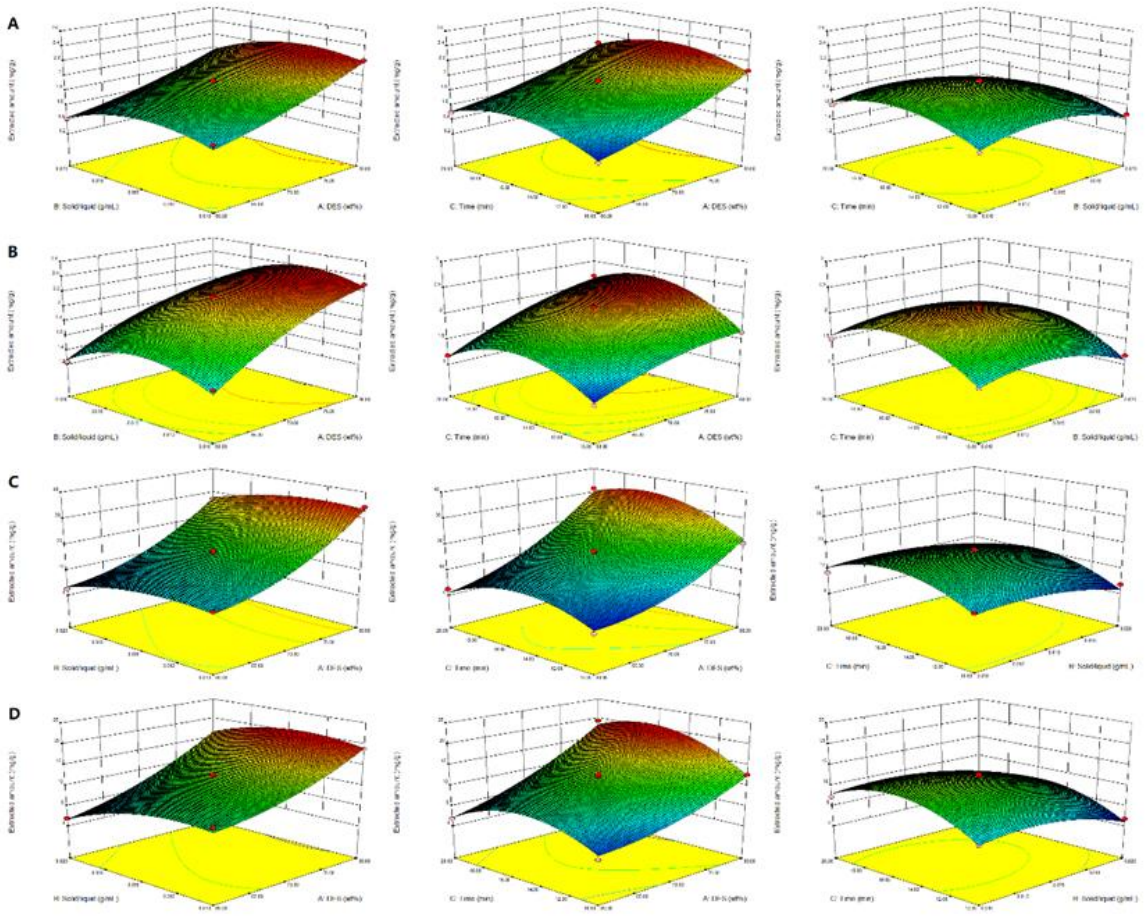

Figure D-9 Response surface plots showing the effect of the concentration of DES content (X1), solid/liquid ratio (X2) and time (X3) on the extracted amounts of aloe-emodin (A), emodin (B), chrysophanol (C), physcion (D).

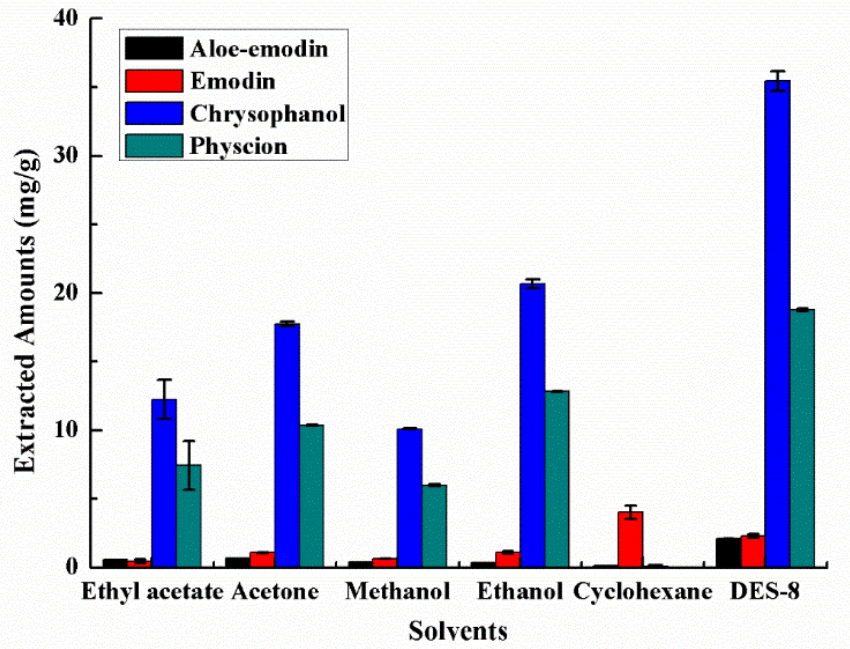

Figure D-10 Comparison of the extracted amounts of anthraquinones by MAE with different organic solvents and 80 wt% DES-8 aqueous solution (solid/liquid ratio=0.012 g mL-1, time=16.5 min).

Table D-5 Comparison of MAE method with UAE and HRE methods (solid/liquid ratio=0.012g mL-1).

Method	Solvent	Time	Extracted amount (mg g^{-1})			
			Aloe-emodin	Emodin	Chrysophanol	Physcion
HRE	DES-8 (80%)	16.5 min	0.96±0.06	0.97±0.06	16.00±1.00	8.06±0.28
	Methanol	16.5 min	0.82±0.02	1.13±0.03	20.67±0.50	12.16±0.35
UAE	DES-8 (80%)	16.5 min	0.49±0.04	0.45±0.01	7.31±0.05	3.86±0.78
	Methanol	16.5 min	0.86±0.02	1.26±0.05	20.03±0.09	11.65±0.32
MAE	DES-5 (80%)	16.5 min	2.09±0.09	2.30±0.15	35.44±0.71	18.80±0.09

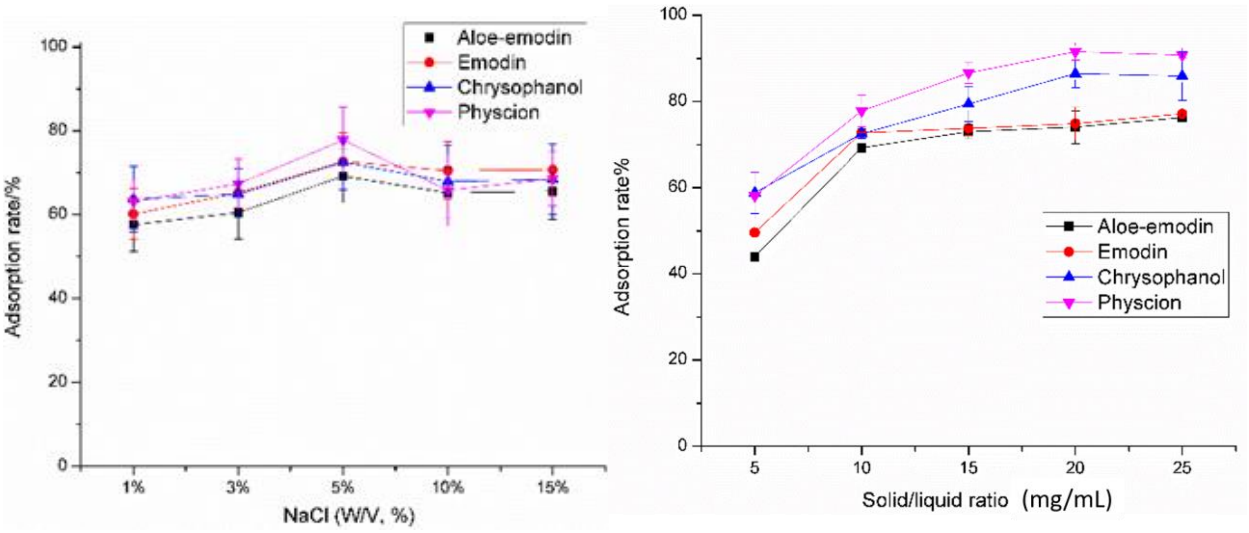

(A) (B)

Figure D-11 Effect of NaCl concentration (w/v, %) (A), and solid/liquid ratio (sorbent/extract, mg/mL) (B) on adsorption rate of anthraquinones.

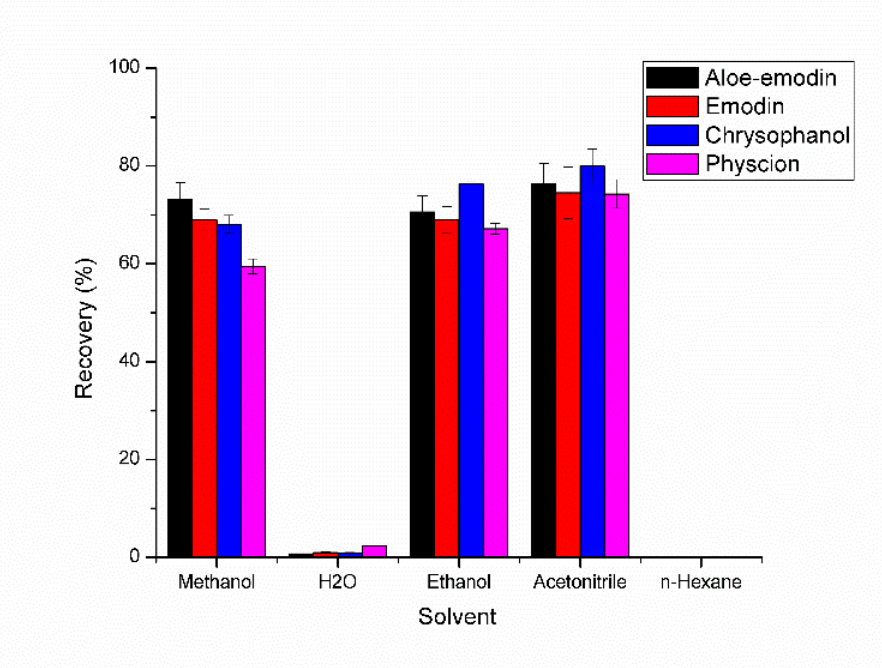

Figure D-12 Effect of solvents on recovery of anthraquinones.